2 mp

NASA CR-112314

A THEORETICAL AND EXPERIMENTAL STUDY OF WOOD PLANER NOISE AND ITS CONTROL

by
John S. Stewart

Center for Acoustical Studies
Department of Mechanical and Aerospace Engineering
North Carolina State University
Raleigh, North Carolina

August 1972

NGR 34-002-035

N. C.
STATE
UNIVERSITY

ABSTRACT

STEWART, JOHN STEDMAN. A Theoretical and Experimental Study of Wood Planer Noise and Its Control. (Under the direction of FRANKLIN DELANO HART and LARRY HERBERT ROYSTER).

A combined analytical and experimental study of wood planer noise is made and the results applied to the development of practical noise control techniques. The investigation entails identification of the dominant mechanisms of sound generation and an analysis is presented which accurately predicts the governing levels of noise emission. Both the experimental and theoretical studies are concerned with planing operations in which the length of the board is much greater than the width. The study thus applies to workpieces which can structurally be characterized as beams as opposed to plates.

The dominant source of planer noise is identified as the board being surfaced, which is set into vibration by the impact of cutterhead knives. This is determined from studies made both in the laboratory and in the field concerning the effect of board width on the resulting noise, which indicate a six decibel increase in noise level for each doubling of board width.

The theoretical development of a model for board vibration defines the vibrational field set up in the board and serves as a guide for cutterhead redesign. The relationships governing structural vibration and the resulting radiation of sound are presented in which the phase cell concept of beam vibration is combined with classical sound radiation expressions for rectangular pistons. The analytical study consolidates previous work on beam radiation and the results are presented in a unified form. The unified theory is valid over a wide frequency

range and has general applicability. The trends deduced from the sound radiation formulations elucidate the important parameters governing the radiation of sound and serve as an aid in the design of quieter machinery.

An extensive experimental program identifies noise sources and the effect of various parameters on planer noise. Techniques of noise reduction are presented along with a discussion of research into several areas of noise control. The experimental study, in addition to bearing out the theory, identifies the importance of operational and maintenance variables and has led to the development of practical noise control techniques which have been implemented on production line machinery.

TABLE OF CONTENTS

	Page
LIST OF TABLES	vii
LIST OF FIGURES	viii
1. INTRODUCTION	1
2. REVIEW OF LITERATURE	4
3. DEFINITION OF THE NOISE PROBLEM IN WOOD PLANERS	6
3.1 Introduction	6
3.2 The Planing Operation	6
3.2.1 Sources of Planer Noise	9
3.2.2 Energy Considerations	10
3.2.3 Identification of the Dominant Noise Source	10
4. THEORETICAL DEVELOPMENT OF A MODEL FOR BOARD VIBRATION	18
4.1 Introduction	18
4.2 The Governing Differential Equation of Motion	18
4.3 Consideration of Boundary Conditions	19
4.4 The Modal Solution Technique	23
4.4.1 Fourier Transform Representation	27
4.4.2 Power Spectral Density	33
4.4.3 The Special Case of Periodic Signals	34
4.5 Application to Wood Planers	40
5. THEORETICAL DEVELOPMENT OF A MODEL FOR BOARD RADIATION	42
5.1 Introduction	42
5.2 The Vibrational Field	43
5.2.1 The Structural Wavelength	43
5.2.2 Power and Energy Considerations	46
5.3 The Elementary Piston Model for Board Radiation	48
5.3.1 The Critical Frequency	49
5.3.2 The Phase Cell Concept	56

TABLE OF CONTENTS (continued)

		Page
5.4	Acoustic Power Radiation	56
5.4.1	Individual Piston Behavior	59
5.4.2	Application of the Piston Model to a Finite Beam	67
5.4.3	An Exact Solution for Beam Radiation	84
5.5	Theoretical Trends and Comparisons	91
5.5.1	A Comparison of the Radiation Characteristics of Wide and Narrow Beams	94
5.5.2	A Numerical Calculation of Radiated Sound Power	109
6.	EXPERIMENTAL INVESTIGATION OF WOOD PLANER NOISE	114
6.1	Introduction	114
6.2	Reiteration of the Sources of Planer Noise	114
6.3	Data Acquisition and Analysis	115
6.4	Factors Influencing Planer Noise	117
6.4.1	Board Width	119
6.4.2	Board Length	121
6.4.3	Board Species	126
6.4.4	Board Thickness	129
6.4.5	Depth of Cut	129
6.4.6	Sharpness of Knives	129
6.4.7	Pressure Bar Tightness	131
6.4.8	Machine Feed Speed	131
6.4.9	Chipbreaker Mechanism	133
6.4.10	Cutterhead Design	136
6.4.11	Dust Hoods	140
6.4.12	Electric Motors	143
6.4.13	Drive Train Systems	143
6.4.14	Machine Component Vibration	144
6.5	Techniques of Noise Reduction	146
6.5.1	Reduction of Noise Produced as a Result of Board Vibration	146
6.5.2	Reduction of Noise Produced as a Result of Anvil Vibration	147
6.5.3	Reduction of Noise Resulting from Other Sources	147

TABLE OF CONTENTS (continued)

	Page
6.6 Noise Control Study Areas	147
6.6.1 Cutterhead Redesign	148
6.6.2 Treatment of Vibrating Surfaces	154
6.6.3 Acoustic Enclosures	160
7. COMPARISON OF THEORETICAL AND EXPERIMENTAL RESULTS	169
8. SUMMARY AND CONCLUSIONS	172
9. RECOMMENDATIONS	176
10. LIST OF REFERENCES	177
11. LIST OF SYMBOLS	180

LIST OF TABLES

		Page
4.1	Values of the Coefficients β for Various Boundary Conditions	21
5.1	Radiation Resistance for Different Values of the Ka Factor for Each Frequency Range	85
5.2	Radiation Efficiency Parameter for Different Values of KW for Each Beam	95
5.3	Acoustic Loss Factor for Different Frequencies	95
5.4	Comparison of Radiation Parameters for Different Mathematical Models	96
5.5	Radiation Efficiency for Different KW Values of Each Beam	99
5.6	Radiation Efficiency Parameter for Several Values of the Fundamental Frequency Ratio	111
5.7	Sound Power Level for Each Beam	111
5.8	Sound Power and Sound Pressure Levels for Each Beam	113
6.1	Ratio of E/ρ_b for Different Wood Species	127
6.2	Noise Reduction for Acoustically Lined Plywood Enclosures with Untreated Openings	161

LIST OF FIGURES

		Page
3.1	Industrial Roughing Planer	7
3.2	Cabinet Type Single Surfacer	8
3.3	Diagram of Cutting Works for a Single Surfacer	11
3.4	Flow Diagram for Energy Input to the Board	12
3.5	Narrow Band Analysis of Sound Pressure Level	14
3.6	Narrow Band Analysis of Board Vibration	15
3.7	Variation in Sound Pressure Level with Board Width	16
4.1	Board Vibration Model	22
4.2	Simply Supported Beam	22
4.3	Fourier Transform of a Rectangular Pulse	28
4.4	Periodic Pulse Train	36
4.5	One Period of the Pulse Train	36
4.6	Fourier Transform of the Pulse Train	36
5.1	Structural Wavelength Parameter Versus Fundamental Frequency Ratio	45
5.2	Structural and Acoustic Wavelength Versus Critical Frequency Ratio	50
5.3	Acoustic and Structural Wavelength Versus Frequency	52
5.4	Board Thickness Versus Critical Frequency	53
5.5	Individual Piston Radiation Above the Critical Frequency	55
5.6	Individual Piston Radiation Near the Critical Frequency	55
5.7	Individual Piston Radiation Below the Critical Frequency	55
5.8	Structural Wavelength Illustration	57
5.9	Phase Cell Representation of Structural Wavelength	57
5.10	Individual Piston Element	60

LIST OF FIGURES (continued)

		Page
5.11	Simple Source Model for Piston Radiation	60
5.12	Radiation Efficiency for Baffled and Unbaffled Pistons at Low Ka	63
5.13	Radiation Efficiency Versus Ka for a Baffled Circular Piston (after [15])	64
5.14	Radiation Efficiency Versus Ka for a Baffled Rectangular Piston (after [24])	66
5.15	Radiation Efficiency Parameter Versus Ka for Baffled and Unbaffled Pistons	68
5.16	Different Views of the Phase Cell Representation of the Beam	70
5.17	Diagram of Beam Radiation Below the Critical Frequency . . .	80
5.18	Phase Cell Representation of Beam Radiation Below the Critical Frequency	80
5.19	Radiation Loss Factor Versus Ka Parameter (after [14]) . . .	87
5.20	Radiation Loss Factor Versus Frequency for Different Board Widths	89
5.21	Radiation Efficiency Versus Critical Frequency Ratio for the Piston Model and the Model of [14]	90
5.22	Radiation Parameter Versus Critical Frequency Ratio for the Piston Models and the Model of [14]	97
5.23	Radiation Efficiency Versus Frequency for the Eight and Four Inch Beam Widths	100
5.24	Response Ratios Versus Fundamental Frequency Ratio for Constant Acceleration	102
5.25	Mean-square Velocity Ratio Versus Beam Length for Constant $\langle \bar{v}^2/\bar{v}_o^2 \rangle_\ell$	104
5.26	Acoustic Power Parameter Versus Fundamental Frequency Ratio for the Eight and Four Inch Beam Widths	105
6.1	Diagram of Laboratory Test Positions	116

LIST OF FIGURES (continued)

		Page
6.2	Diagram of Experimental Apparatus	118
6.3	Increase in Sound Pressure Level with Board Width	120
6.4	Sound Pressure Level Versus Board Length	122
6.5	Relationship Between Sound Pressure Level, Acceleration, and Board Length for a Double Surfacer	123
6.6	Relationship Between Sound Pressure Level, Acceleration, and Board Length for a Single Surfacer	124
6.7	Decrease in Acceleration Level with Board Length	125
6.8	Comparison of Sound Pressure Spectra for Oak and Pine Boards	128
6.9	Variation in Sound Pressure Level with Board Thickness	130
6.10	Sound Pressure and Acceleration Levels for Operation with the Pressure Bar in the "Tight" and "Loose" Positions	132
6.11	Comparison of Sound Pressure Level for Operation with and without the Chipbreaker	134
6.12	Acceleration Spectrum for the Chipbreaker Mechanism	135
6.13	Oscilloscope Trace of Chipbreaker Acceleration Response Versus Time	137
6.14	Noise Spectra for Planers Idling with Four and Six Cutterhead Knives	139
6.15	Narrow Band Comparison of Sound and Vibration for Cutterhead with Six Knives	141
6.16	Narrow Band Comparison of Sound and Vibration for Cutterhead with Four Knives	142
6.17	Waveform of Force Delivered to the Board for the Standard Cutterhead	150
6.18	Force Delivered to the Board for the Ideal Case	150
6.19	Segmented Cutterhead	152

LIST OF FIGURES (continued)

Page

6.20 Comparison of Sound Pressure Spectra for Operation with Segmented (Helical) and Standard Cutterheads 153

6.21 Comparison of Sound Pressure Levels for Damping Treated and Untreated Boards 156

6.22 Effect of Damping Treatments on Anvil Vibration 158

6.23 Acoustic Enclosure for Single Surfacer 162

6.24 Sound Pressure Level Versus Board Length for Operation with and without an Acoustic Enclosure 164

6.25 Sound Pressure Level Versus Board Position with Respect to the Enclosure 165

6.26 Relative Importance of Different Sections of the Acoustic Enclosure 166

6.27 Directivity Characteristics for Operation with and without the Acoustic Enclosure 167

6.28 Directivity Characteristics for Different Board Widths . . . 168

1. INTRODUCTION

Noisy machinery has been a characteristic of the wood processing industry for generations. The noise levels in this industry have steadily increased as a result of added horsepower, accelerated cutterhead speeds, increased mechanization, and in general a stepped up production tempo. Also characteristic of the woodworking industry are the comparatively small size but numerous plants that produce and utilize woodworking machinery. The result is an industry with a tremendous noise problem but relatively few individual companies large enough to mount a full scale noise control program. This lack of support has caused researchers to shy away from the woodworking industry and its problems. A review of current literature on woodworking machinery noise reveals that while limited work has been done on the aerodynamic or rotational noise produced by rotating cutterheads, little if any serious effort has been made to determine the mechanisms of noise generation during machine operation. Since the more noisy woodworking machines, such as planers and moulders, are significantly louder when material is being processed, these studies are of limited value.

Through a cooperative effort between the Center for Acoustical Studies at North Carolina State University and Newman Machine Company, a major manufacturer of woodworking machinery, a research and development program was developed that has been directed towards uncovering ways to reduce noise emission from woodworking machinery. This close association with a machine manufacturer has unfolded an opportunity to define a meaningful and interesting problem of value to industry in the

area of noise control and machine design. Through such a liaison effort, an acoustics and vibration problem has been defined and carried to completion through a theoretical and experimental analysis. The concepts developed have been successfully designed and implemented into production line machines.

The type of study described, quite obviously, could not be conducted for all types of woodworking machinery. The type machine selected for detailed study was the industrial wood planer, generally recognized as a major noise source in the industry. The machine consists basically of a system for feeding lumber on a flat table past a rotating cutterhead which removes a layer of wood and leaves a smooth surface. The impacting of a cutterhead knife or tooth on wood stock is typical of a great number of woodworking machines. Thus, the planer is considered to be representative of many machines as are the results and conclusions of this study.

The research program was developed on the premise that a basic understanding of the noise generation mechanisms is the best way to arrive at noise control solutions. The theoretical goal of the program was to develop a mathematical model, in a simple usable form, for the radiation of sound from a wood planer. This model was to be used in identifying the dominant sources of noise as well as the critical parameters influencing the radiation. This information could then serve as a guideline for the development of practical noise control techniques. The practical goals were both short and long term in nature. The design of retrofit systems for existing machinery as well as major redesign with noise as an important factor were the objectives.

The analysis carried out in this study was both theoretical and analytical in nature, although the two study areas were not approached completely independently. A certain amount of insight was gained by operating the machine, conducting several preliminary measurements and making observations. This familiarization with the problem led to the development of several phases of study, with theory and experiment interrelated to varying degrees. Chapter 3 deals with the general familiarization with the problem and the identification of major noise sources, which served to define the theoretical aspect of the problem. Chapters 4 and 5 are theoretical in nature and constitute a definition and analysis of the sound radiation problem. Chapter 6 is essentially experimental in nature, dealing with the effect of various parameters on the noise generated as well as actual techniques of coping with the noise problem. Chapters 7 and 8 summarize the results and conclusions of this study. A discussion of noise reduction techniques now in use or in the final design stage is also presented along with plans for future study in this area.

2. REVIEW OF LITERATURE

Most of the previous work done on noise in the woodworking industry has been surveyed in a review by J. Howard Smith [28] and a contract report to the Ministry of Technology prepared by Sound Research Laboratories [4]. The object of both studies was to seek out and evaluate all current references on noise and vibration in woodworking machinery with special emphasis on planers and moulders. The literature reviewed deals primarily with aerodynamic (rotational) noise which results when a cutterhead is rotated near stationary surfaces. The noise produced when the machine is planing, which is usually significantly higher than the idling noise, has not been examined in detail.

The rotational noise was studied by Cox [7] in a report which identified the nearness of feed tables to the rotating cutterhead as a critical parameter. Pahlitzch [25] and Liegman [19] expanded on this work. Thunell [37] investigated the effect of slitting table lips near the cutterhead. Kuleshov and Grinkov [18] compared the noise levels produced by square and helical cutterhead knives and observed an appreciable reduction in the noise level for the helical cutterhead. Chizhevskij and Shkalenko [5] found that modifications of table lips reduced noise levels during machine idle but were ineffective during the cutting operation. Schmutzler [27] observed that the noise level for machine idle increased as the fourth power of cutterhead speed and indicated the importance of board vibration in the noise generated by planers. Several authors have reported a significant increase in the noise levels produced by planers when cutting as opposed to idling. Mazur and Kovtun [23] carried out a series of experiments on a planer,

dealing with numerous parameters including board geometry, and observed an increase in noise level with increasing board width. Kozyakov [17] made an experimental study of planer noise in which he identified the major noise source as rotational noise produced by the cutterheads.

The literature dealing with noise abatement is concentrated in the areas of acoustic enclosures and cutterhead redesign. Greenwood [10] suggested an enclosure design for a planer. Schmutzer [27] also suggested improvement in machine design to reduce noise at the source. Stewart and Hart [34] give an experimental evaluation of planer noise and its control. Details of enclosure construction for woodworking machinery are outlined by Stewart [33].

The modal analysis technique presented in Chapter 4 was applied to periodically excited beams by Barnoski [1] using Fourier transform techniques. Random excitations were also considered in the study. The phase cell concept of structural vibration has been considered by Smith [29], Lyon [20], Maidanik [22], and Lyon and Maidanik [21]. Smith and Lyon [30] address themselves to the overall problem of sound and structural vibration using approximate formulations.

The determination of sound power levels from a number of sound pressure level measurements is outlined for various environments by Hart and Stewart [11]. The effects of particular environments on sound pressure and sound power levels is also discussed in detail by Beranek [2].

3. DEFINITION OF THE NOISE PROBLEM IN WOOD PLANERS

3.1 Introduction

In order to define the noise problem for wood planers it was necessary to observe the operation of the machine, since a general understanding of the type of noise produced is required before designing an experimental procedure. The sources of planer noise are determined and the identification of dominant noise sources is accomplished through energy considerations. A correlation study is utilized to delineate board radiation as the probable dominant source. The board width is identified as the most important geometric parameter since noise levels are observed to increase as board width increases.

3.2 The Planing Operation

Planers typically fall into the broad categories of; (a) roughing type planers, Figure 3.1, which usually surface more than one face of the material, and (b) cabinet type planers, Figure 3.2, which usually surface only one face. For several reasons, including cost and laboratory space, a cabinet type planer was selected for a detailed study of planer noise generation. The roughing planer differs considerably from the single surfacer in appearance, but removes wood from the board in much the same manner. Thus, the basic mechanics of the planing operation are similar for both machines, the major differences being cutterhead geometry, number of knives and proximity of the cutterhead to stationary surfaces such as feed beds. The cutterhead geometry defines the nature of the impact of the cutterhead knives on the wood stock,

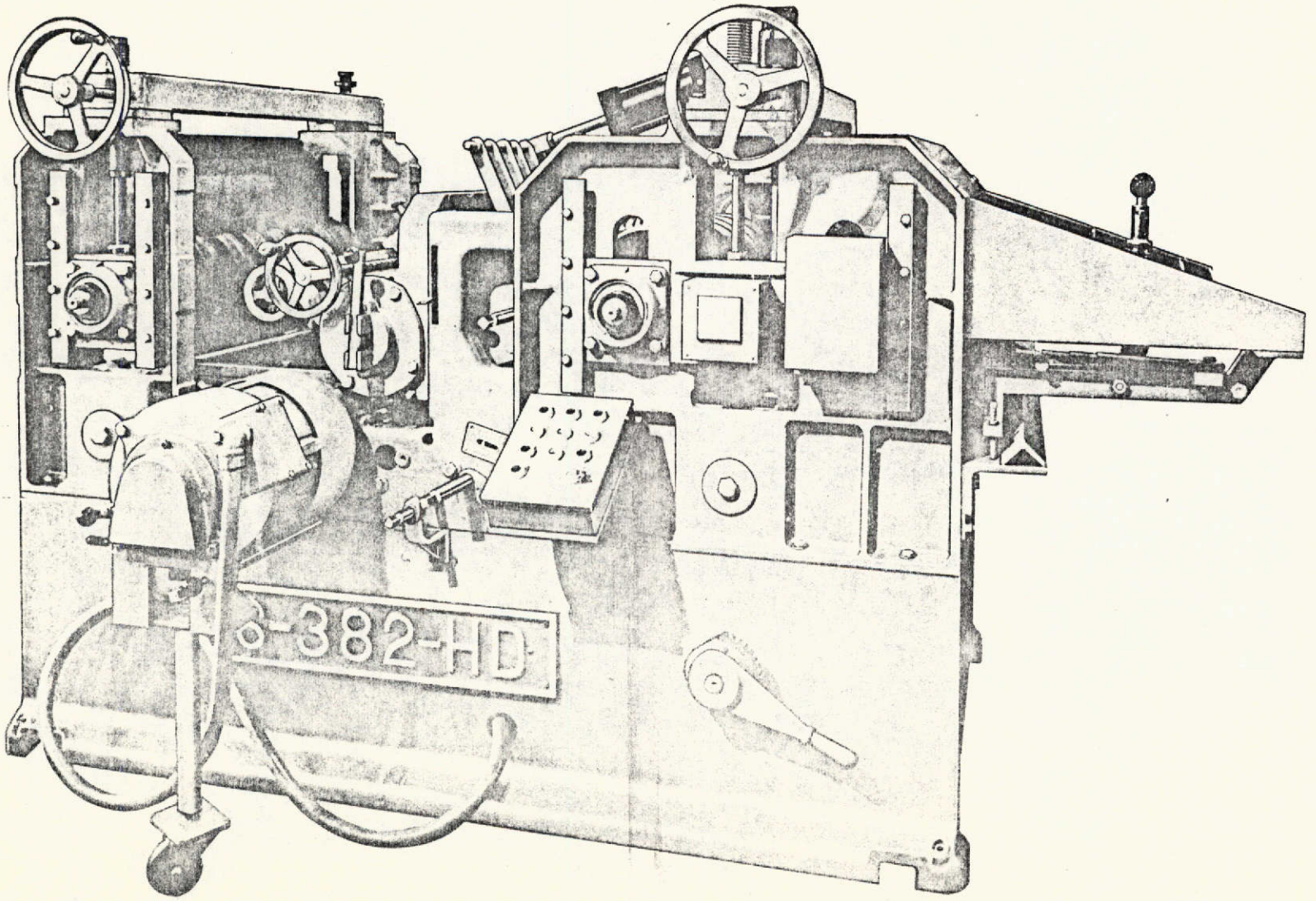

Figure 3.1 Industrial Roughing Planer

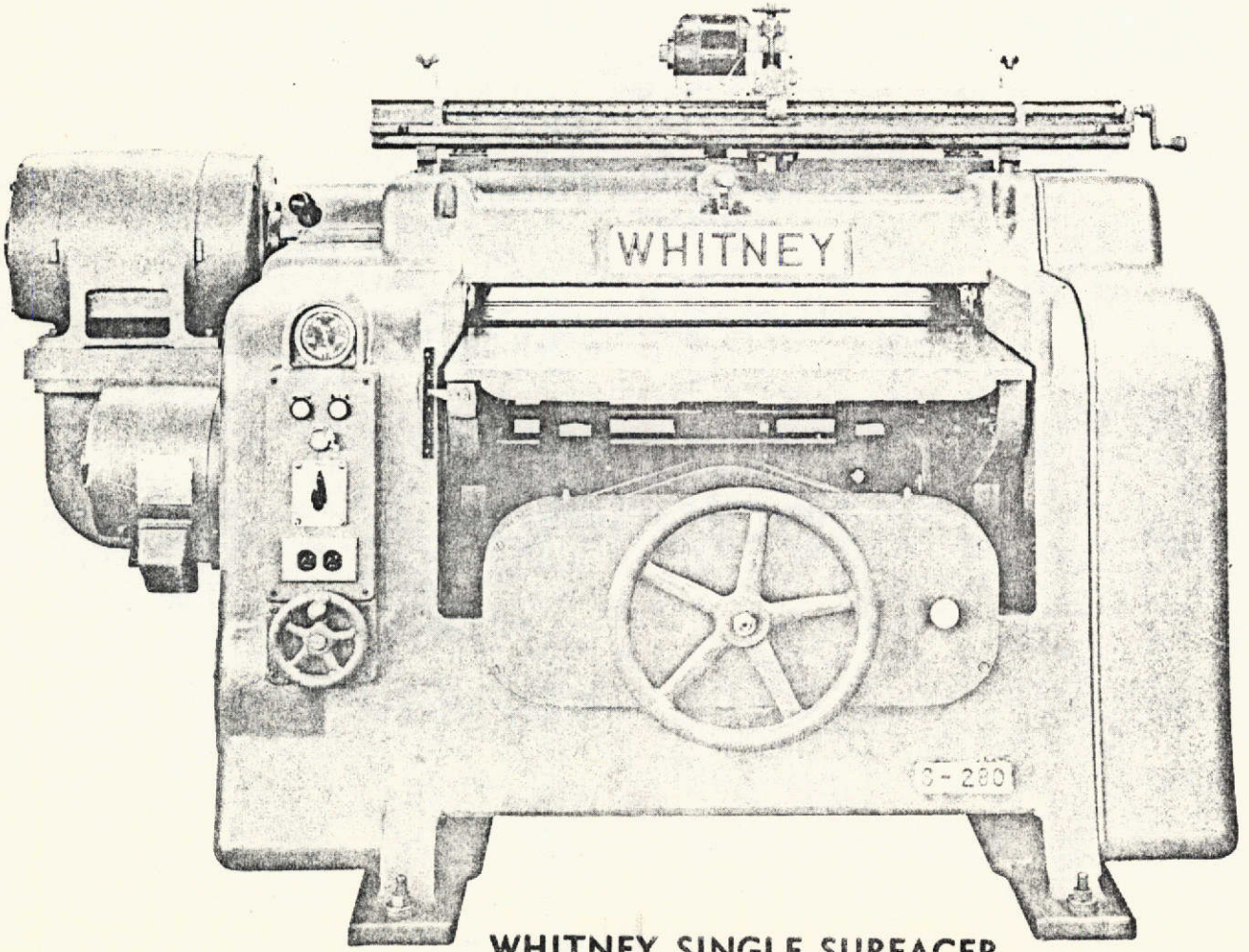

Figure 3.2 Cabinet Type Single Surfacer

while the location of the cutterhead would be expected to affect the rotational noise produced by the machine.

3.2.1 Sources of Planer Noise

From a basic consideration of the possible noise sources for the planer of Figure 3.2, the following emerge:

(1) Noise produced due to the high vibration level of the board being surfaced. The vibration is caused by the periodic impact of the cutterhead knives upon the surface of the board.

(2) Noise resulting from the vibration of the anvil structure directly opposite the cutterhead. Vibratory energy is transmitted directly through the board and into the anvil and is dissipated in the anvil or transmitted on to another component of the machine. The amount of radiation and the frequency characteristics are dependent upon the geometry of the anvil as well as the energy transmitted from the board to the anvil.

(3) Rotational noise resulting from the interaction of the cutterhead with the air in the proximity of stationary surfaces such as the anvil and feed beds. This is primarily responsible for machine idle noise and is typically referred to as "siren noise".

(4) Noise produced by the electric motors. This noise can dominate the idling noise in some machines (especially high frequency motors).

(5) Noise produced by the dust collection system. This includes sound radiated from the dust hood due to particle (chip) impact, cavity resonance, and vibration transmitted directly from the machine.

(6) Noise is also produced by other vibrating surfaces such as housings and feed beds. The means by which this vibratory energy spreads throughout the machine is (a) transmission from the anvil, and (b) transmission back through the cutterhead and subsequently throughout the machine.

(7) Noise produced by the drive train system.

3.2.2 Energy Considerations

In most cases the noise produced while the machine is operating is substantially greater than that produced while the machine is idling. This increase in noise level is related to the impact of the cutterhead knives on the material being surfaced. When a cutter knife makes contact with a board, a certain amount of energy is transferred from the cutterhead into the board. This energy is associated with the force required to remove a chip from the board and depends on a great number of parameters, including the hardness of the board being cut and the sharpness of the knives. A portion of this energy is distributed throughout the board causing vibration, while part is transmitted through the board and into the anvil structure below the cutterhead. The energy that is transferred into the board is transmitted internally throughout the board and is dissipated primarily by (1) internal damping, and (2) the generation of sound. Figure 3.4 is an energy flow diagram for the system depicted in Figure 3.3.

3.2.3 Identification of the Dominant Noise Source

To determine the dominant source of planer noise, a series of sound pressure level and vibration measurements were conducted. The

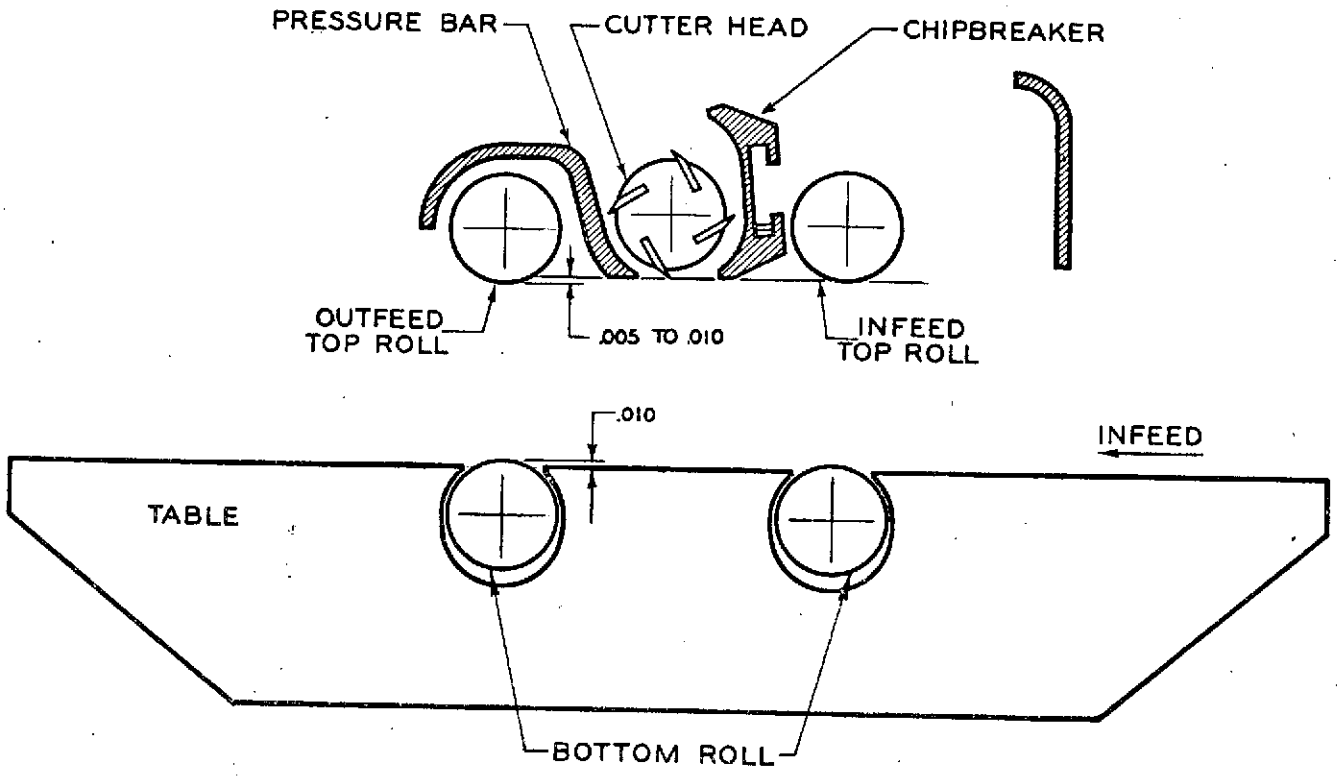

Figure 3.3 Diagram of Cutting Works for a Single Surfacer

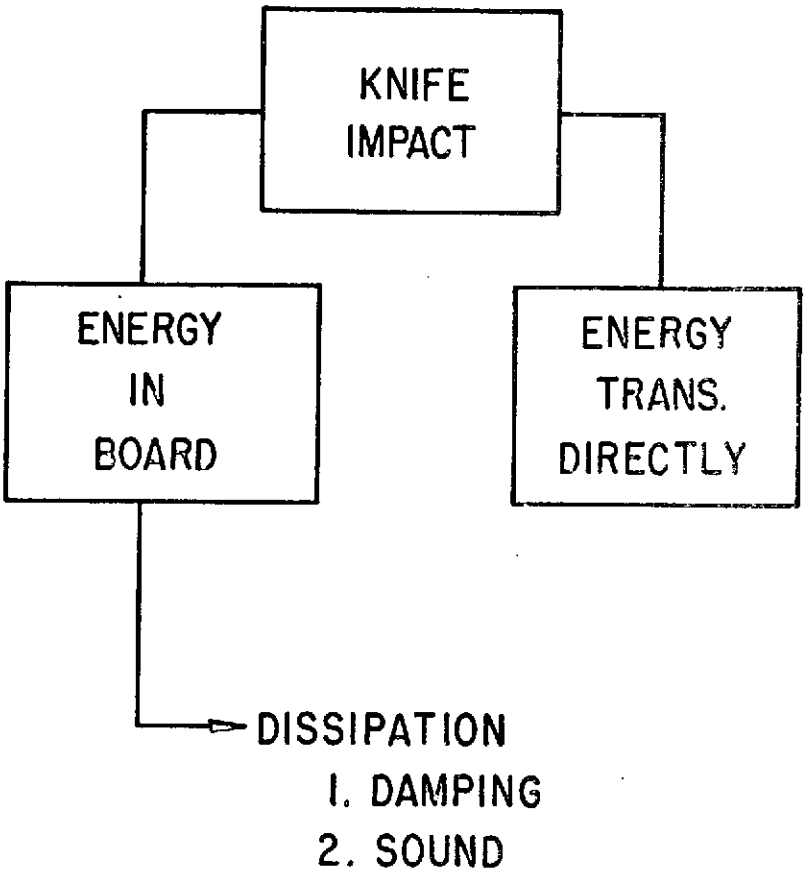

Figure 3.4 Flow Diagram for Energy Input to the Board

sound pressure level spectrum, shown in Figure 3.5, indicates the presence of a blade passage frequency of 240 Hz, which corresponds to a four knife cutterhead rotating at 3600 RPM. Harmonics of 240 Hz (240 times n, n=1,2,3...) are also present over an extended frequency range, indicative of sound produced by structural vibration as opposed to aerodynamically generated sound. From Figure 3.4 it is noted that considerable energy may be stored in the board being machined in the form of a reverberant vibrational field. Figure 3.6 shows the vibration (acceleration) spectrum obtained when a transducer is attached directly to the board during the planing operation. Again the blade passage frequency of 240 Hz and the harmonics are present. The excellent correlation between the sound and vibration narrow band spectra suggests that board radiation is a dominant noise generating mechanism. The dominance of board radiation as a noise source for the planer is evident experimentally from a study of the effect of various board parameters on the radiated noise. Of the numerous parameters that influence the radiation, board width was found to have the most direct effect on the noise levels produced. In general the efficiency of the board as a source of sound is related to the surface area and mean-square velocity of the board itself. This surface area increases with both board width and length. The length, however, governs the energy distribution in the board and consequently does not directly affect the resulting noise levels. This theoretical principle involving source strength for a vibrating surface was evident experimentally as shown in Figure 3.7. The sound pressure level at a particular point is observed to increase six decibels for each doubling of board width. This important result,

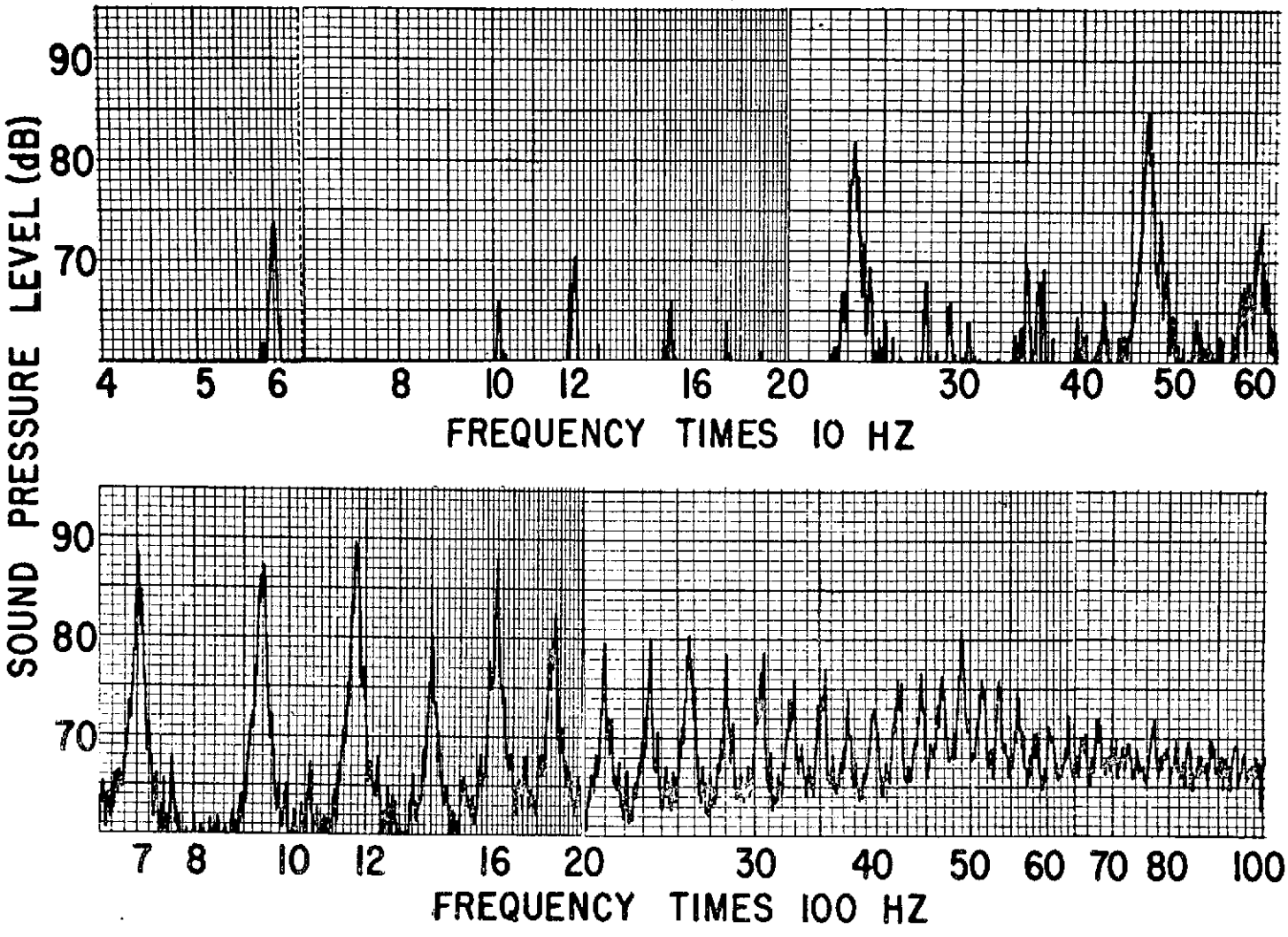

Figure 3.5 Narrow Band Analysis of

Sound Pressure Level

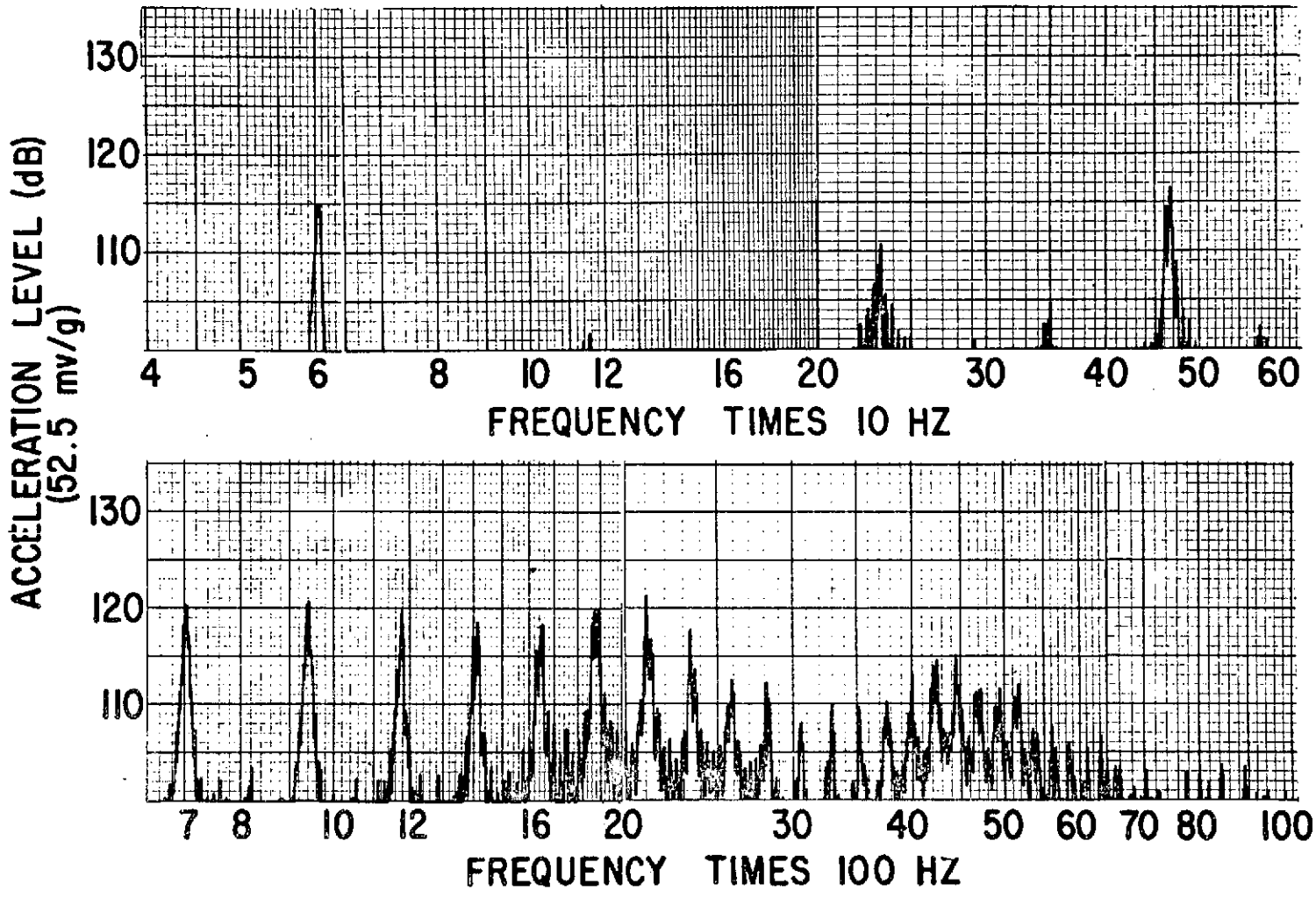

Figure 3.6 Narrow Band Analysis of

Board Vibration

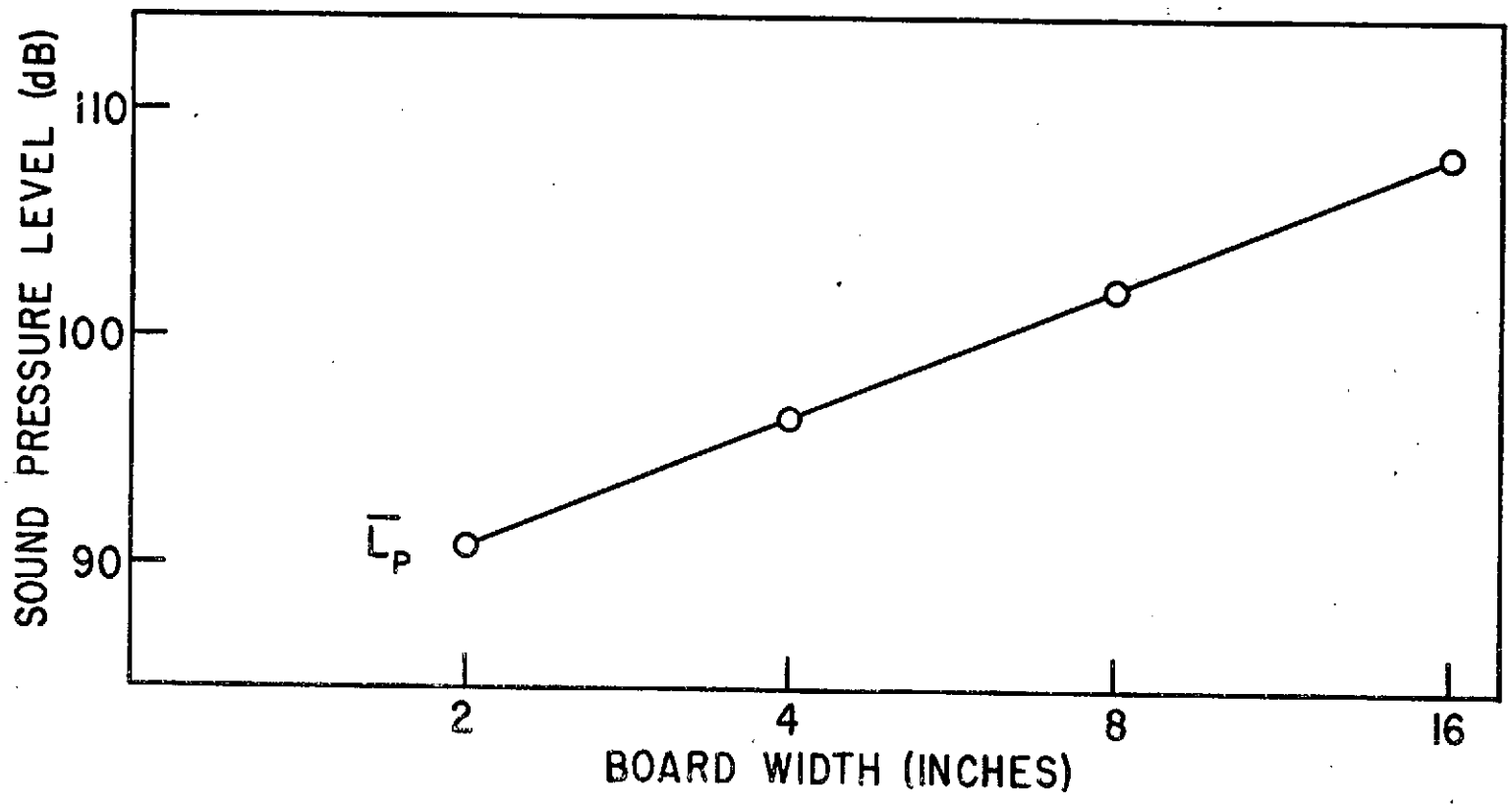

Figure 3.7 Variation in Sound Pressure Level with Board Width

which is discussed in detail in Chapter 5, identifies board radiation as the dominant source of noise for the planer under study. This increase in sound pressure level has been observed for numerous planing operations for roughing and cabinet type planers.

4. THEORETICAL DEVELOPMENT OF A MODEL FOR BOARD VIBRATION

4.1 Introduction

Board radiation has been identified as the major noise source when the machine is in operation. In order to study the radiation of sound from such a vibrating structure, a detailed analysis of the structural vibration field is necessary. Since the response of the board to a given input excitation is governed by the frequency composition of the exciting force and the resonant frequencies of the board itself, such an analysis is justified. The resulting equations of motion for the board give valuable information regarding cutterhead impact characteristics as well as defining the board radiation field. The governing differential equation of motion is solved subject to simply supported boundary conditions using the technique of modal analysis. The solution to the vibration problem is written in terms of Fourier transforms since the Fourier spectrum is of prime interest. A specific solution is obtained for the special case of periodic excitation which is typical of wood planers.

4.2 The Governing Differential Equation of Motion

Board vibration can be modeled by considering a uniform slender beam. The location of the forcing function $F(x,t)$ is arbitrary and it is assumed that the boundary constraints are conservative, i.e., no work is done at the boundaries. The constraints are also assumed to maintain line contact with the beam so that reflected waves from the constraints can be neglected. The assumption of no boundary work is not always true, but facilitates calculations.

For the undamped system, the governing differential equation from simple beam theory can be written as

$$EIg_c \frac{\partial^4 y(x,t)}{\partial x^4} + \rho_b \Omega \frac{\partial^2 y(x,t)}{\partial t^2} = F(x,t) \quad , \tag{4.1}$$

where

E = modulus of elasticity,

I = area moment of inertia of cross section,

$\rho_b \Omega$ = mass per unit length of the beam,

y = lateral displacement,

x = coordinate along the beam length,

t = real time,

g_c = acceleration due to gravity.

In equation (4.1) it is assumed that the system is a uniform, linear, lightly damped, continuous elastic structure excited by a forcing function dependent on space and time. The effects of rotary inertia and shear deformation have been neglected and ρ_b, Ω, E, and I are assumed to be constant.

4.3 Consideration of Boundary Conditions

For natural boundary conditions in which the constraint forces do no work, the natural frequencies of a slender beam are given by

$$\omega_n = (\beta/\ell)^2 \left\{\frac{EIg_c}{\rho_b \Omega}\right\}^{1/2} \tag{4.2}$$

where the coefficient β is characteristic of the particular type of boundary conditions, and

ω_n = natural frequency of the beam for the nth mode,

ℓ = length of the beam,

E = modulus of elasticity,

I = area moment of inertia,

ρ_b = mass density,

Ω = cross sectional area.

For modes of order three or higher ($n \geq 3$), [13] gives the expressions of Table 4.1 for the coefficient β for various boundary conditions.

For the frequencies of interest in the radiation problem, the errors involved in calculating the natural frequencies by assuming the boundary conditions to be simply supported are typically less than ten percent of the lowest frequency of interest. This assumption allows a simple form describing the mode shapes and the natural frequencies to be utilized in place of the more complex functions associated with the true boundary conditions. Thus $\beta = n\pi$ and $f_n(x) = \sin(n\pi x/\ell)$ define the natural frequencies ω_n and mode shapes $f_n(x)$ respectively, for a simply supported beam of length ℓ. Thus, the natural frequencies of the beam under consideration are insensitive to the particular type of boundary conditions for frequencies such that the modes of vibration are above the first few resonances. For realistic beam geometries this is the case and the problem is greatly simplified by assuming the beam to be simply supported. The problem is reduced from the vibration model of Figure 4.1 to the simply supported beam of Figure 4.2.

Table 4.1 Values of the Coefficient β for Various Boundary Conditions

Boundary Conditions	β
Free - Free	$(\frac{2n-1}{2})\pi$
Free - Pinned	$(\frac{4n-3}{4})\pi$
Free - Fixed	$(\frac{2n-1}{2})\pi$
Pinned - Pinned	$(n)\pi$
Pinned - Fixed	$(\frac{4n+1}{4})\pi$
Fixed - Fixed	$(\frac{2n+1}{2})\pi$

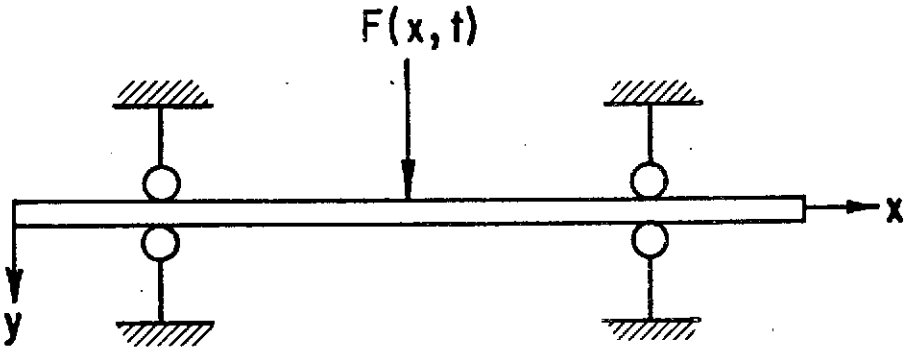

Figure 4.1 Board Vibration Model

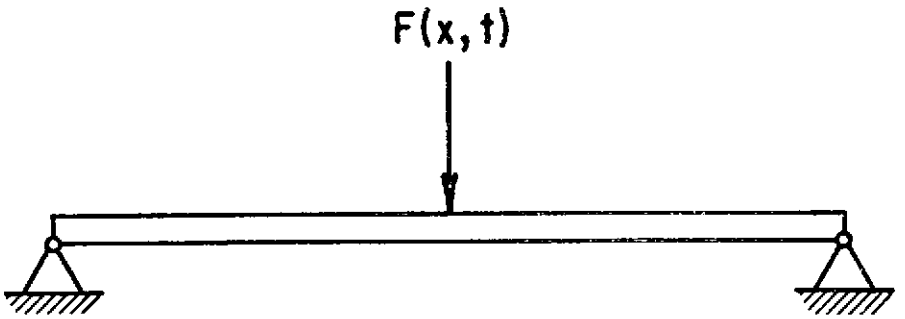

Figure 4.2 Simply Supported Beam

In the following analysis, simple beam theory neglecting rotary inertia and shear deformation is assumed and damping, in general, is ignored. Damping may be introduced into the modal solution by formulation of the differential equation in terms of a generalized coordinate.

4.4 The Modal Solution Technique

Since any deflected shape of the beam can be resolved into spatial harmonic components by the method of Fourier analysis, it follows that

$$y(x,t) = \sum_{n=1}^{\infty} (q_n)(f_n) \quad , \tag{4.3}$$

where the q_n are the Fourier coefficients. For a simply supported beam the terms of the Fourier series are identical with the natural modes of vibration, but for other boundary conditions are more complex functions of x. Thus instead of specifying the function y(x) for all points on the beam, the q_n may be specified. The advantage in this representation is that a good approximation to y(x) may be obtained by using only the first few terms of the series.

If y is a function of space and time, then

$$y(x,t) = \sum_{n=1}^{\infty} q_n(t)\ f_n(x) \quad , \tag{4.4}$$

and the q_n contain the time dependence. The spatial dependence is contained in f_n; the modes of displacement. The q_n are the generalized coordinates corresponding to the modes of displacement f_n.

The functions $f_n(x)$ satisfy the homogeneous form of equation (4.2) subject to the imposed boundary conditions. For the simply supported beam of Figure 4.2 the fundamental mode of vibration is a simple sine wave, and the overtones are sine waves with different integral numbers of half-waves along the beam.

It may be shown from the classical separation of variables approach that the displacement q_n of any one natural mode is governed by the same type of equation as the single degree of freedom system, thus

$$M_n \ddot{q}_n + C_n \dot{q}_n + K_n q_n = L_n \quad . \tag{4.5}$$

The terms M_n, C_n, K_n and L_n are, respectively, the generalized mass, the generalized damping coefficient, the generalized stiffness, and the generalized force corresponding to the nth normal mode. The coupling through the damping terms is ignored in this analysis. The generalized mass is the mass M_n, which has the same kinetic energy when moving with velocity $\dot{q}_n$ as the whole system moving at velocity $\dot{q}_n f_n(x)$, i.e.

$$M_n \dot{q}_n^2/2 = \dot{q}_n^2/2 \int_o^\ell \rho_b \Omega \, (f_n(x))^2 \, dx \quad ,$$

or

$$M_n = \int_o^\ell \rho_b \Omega \, (f_n(x))^2 \, dx \quad . \tag{4.6}$$

The generalized stiffness K_n, is the stiffness of a linear spring which, when displaced by q_n, has the same potential energy as the

actual system when displaced by $q_n f_n(x)$, i.e.

$$K_n q_n^2/2 = q_n^2/2 \int_o^\ell EI (f_n''(x))^2 dx \quad ,$$

where $1/2 \int_o^\ell EI (f_n''(x)^2 dx$ is the flexural strain energy of the simple beam. Thus

$$K_n = \int_o^\ell (f_n''(x))^2 dx \quad , \tag{4.7}$$

The generalized damping coefficient C_n is the rate at which a simple damper moving at $\dot{q}_n$ dissipates energy at the same rate as the whole system of damping forces and pressures on and in the system when moving at $\dot{q}_n f_n(x)$. The generalized viscous damping is given by

$$C_n = \int_o^\ell (f_n(x))^2 c(x) dx \quad , \tag{4.8}$$

where $c(x)$ is a viscous damping coefficient assumed to vary with x.

The generalized force (L_n) is that single force when moved through a small distance q_n, does the same amount of work as all the externally applied forces and pressures acting on the system when the system is

moved through a small displacement $q_n f_n$. Thus

$$L_n = \int_0^{\ell} f_n(x)\ F\ (x,t)\ dx \quad , \tag{4.9}$$

Assuming that

$$c(x) = 2\S_n\ \omega_n\ M \quad , \tag{4.10}$$

equation (4.5) can be written as

$$\ddot{q}_n + 2\S_n\ \omega_n\ \dot{q}_n + \omega_n^2 q_n = L_n/M_n \quad , \tag{4.11}$$

where ω_n is found from the solution to the frequency equation associated with the nth mode of the beam, and $\S_n$ is defined by equation (4.10).

In concluding the modal vibration discussion it is appropriate to review the assumptions made in developing equation (4.11). Equation (4.3) represents the steady state response to equation (4.2) from the contributions of an infinite number of mechanical oscillators (each responding at its modal frequency) weighted by the mode shape of the distributed structure. The mode shapes are dependent upon the physical properties and boundary conditions of the structure. The magnitude of the contribution from the generalized coordinate is given by the solution to equation (4.11) and depends upon the initial conditions of the problem as well as the values of the generalized parameters. The total

response is obtained from the expressions for the mode shapes and generalized coordinates by summing as specified by equation (4.3).

4.4.1 Fourier Transform Representation

For excitation containing many closely spaced harmonic components approaching a continuous spectrum it is convenient to express the steady state solution using Fourier transforms. Define the transform pair as

$$Y(\omega) = \int_{-\infty}^{\infty} y(t)\, e^{-i(\omega t)}\, dt \quad ,$$

$$y(t) = (1/2\pi) \int_{-\infty}^{\infty} Y(\omega) e^{i(\omega t)}\, d\omega \quad , \tag{4.12}$$

where $Y(\omega)$ is the Fourier transform of the displacement response. The functions $Y(\omega)$ and $y(t)$ are equivalent ways of representing the response; the former is a real function in the time domain and the latter a complex function in the frequency domain. Figure 4.3 shows an example of a Fourier transform pair where the time signal $y(t)$ is a square pulse.

Taking the Fourier transform of equation (4.11) under steady state conditions yields

$$[-\omega^2 + i2\S_n\omega_n\omega + \omega_n^2]\, Q_n(\omega) = L(x,\omega)/M_n \quad , \tag{4.13}$$

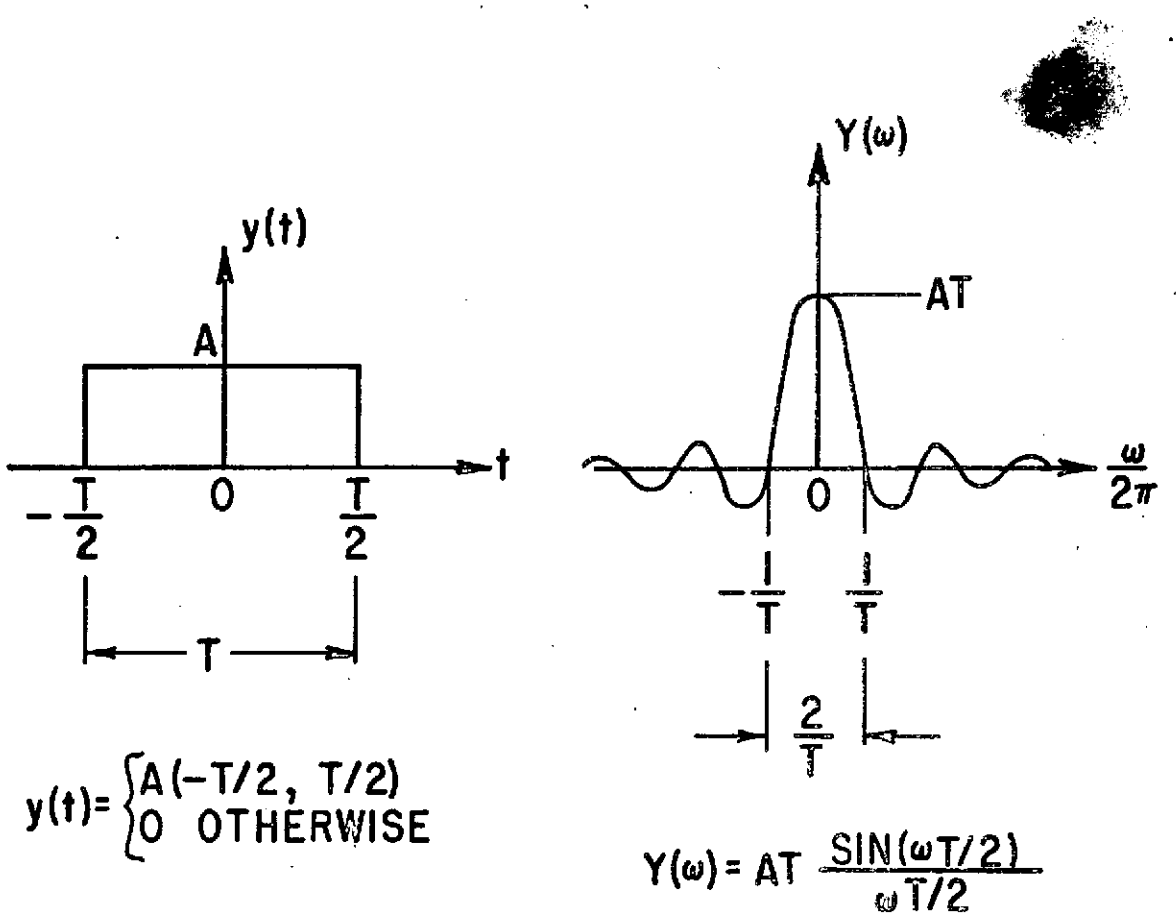

Figure 4.3 Fourier Transform of a Rectangular Pulse

where

$$L_n(x,\omega) = \int_o^{\ell} F(x,\omega)\ f_n(x)\ dx = \int_o^{\ell} L_n(x,t)\ e^{-i(\omega t)} dt. \quad (4.14)$$

Solving for the transform of the generalized coordinate q gives

$$Q_n(\omega) = \frac{1}{M_n \omega_n^2} \left\{ \frac{1}{(1-(\omega/\omega_n)^2 + 2i\S_n(\omega/\omega_n))} \right\} \int_o^{\ell} F(x,\omega) f_n\ dx. \quad (4.15)$$

The term in brackets is known as the transfer impedance function for the system and is denoted by $H_n(\omega)$.

In the previous analysis only viscous damping, in which the component of force due to damping is directly proportional to velocity, was considered. For hysteresis or structural damping the damping term depends on displacement rather than velocity. Thus the term $2\ \S_n\omega/\omega_n$ is replaced by δ_i and the damping is independent of frequency. Since δ_i is generally small the relation valid for structural damping is

$$H_n(\omega) = \frac{1}{(1-(\omega/\omega_n)^2 + i\delta_i)}\ , \quad (4.16)$$

and in general

$$Q_n(\omega) = \left\{ \frac{H_n(\omega)}{M_n \omega_n^2} \right\} \int_o^{\ell} F(x,\omega)\ f_n(x)\ dx \quad (4.17)$$

Since

$$y(x,t) = \sum_{n=1}^{\infty} q_n(t) f_n(x) \quad , \tag{4.18}$$

the complete solution in the frequency domain takes the form

$$\begin{aligned} Y(x,\omega) &= \sum_{n=1}^{\infty} Q_n(\omega) f_n(x) \\ &= \sum_{n=1}^{\infty} f_n(x) \left\{ \frac{H_n(\omega)}{M_n \omega_n^2} \right\} \int_0^{\ell} F(x,\omega)\, f_n(x)\, dx \quad , \end{aligned} \tag{4.19}$$

The displacement in time can be obtained by taking the inverse transform of equation (4.19)

$$y(x,t) = F_e^{-1} \{Y(x,\omega)\} = F_e^{-1} \{\sum_{n=1}^{\infty} Q_n(\omega)\, f_n(x)\} \quad , \tag{4.20}$$

where $F_e^{-1}\{\ \}$ denotes the inverse transform and from equation (4.17), $Q(\omega) = [H_n(\omega)/(M_n\, \omega_n^2)]\, L_n(x,\omega)$.

The convolution in the Fourier sense for two functions $A(\omega)$ and $B(\omega)$ is of the form

$$F_e^{-1} \{A(\omega)\, B(\omega)\} \Longrightarrow \int_0^t A(t-\tau)\, B(\tau)\, d\tau \quad ,$$

Applying the convolution integral to equation (4.19) gives

$$F_e^{-1}\{f_n(x)\ Q(\omega)\} = f_n(x)\ F_e^{-1}\{Q(\omega)\}$$

$$= \int_0^t \left\{\frac{h_n(t-\tau)}{M_n\omega_n^2}\right\} L_n(x,\tau)\ d\tau \quad , \qquad (4.21)$$

and the response can be represented by

$$y(x,t) = \sum_{n=1}^{\infty} f_n(x) \int_0^t \left\{\frac{h_n(t-\tau)}{M_n\omega_n^2}\right\} L_n(x,\tau)\ d\tau \quad , \qquad (4.22)$$

The function $h_n(\tau)$ represents the system response in τ to a unit impulse and L_n denotes the forcing function acting on the system. Equation (4.21) is seen to define a transformation from a product in the frequency domain into a convolution integral in the time domain.

In terms of the Fourier inversion integral the result is

$$y(x,t) = \left(\frac{1}{2\pi}\right) \sum_{n=1}^{\infty} \left\{\frac{f_n(x)}{M_n\omega_n^2}\right\} \int_{-\infty}^{\infty} H_n(\omega)L_n(x,\omega)\ e^{i(\omega t)}d\omega \ . \qquad (4.23)$$

The convolution integral of equation (4.22) represents the response as a linear superposition of free vibration solutions in the time domain, while the Fourier transform solution of equation (4.23) represents the response as a linear superposition in the frequency

domain of steady state responses to simple harmonic excitations. The solutions must be identical and are related by

$$h(t) = (1/2\pi) \int_{-\infty}^{\infty} H(\omega)\ e^{i(\omega t)}\ d\omega \quad , \tag{4.24}$$

and

$$H(\omega) = \int_{-\infty}^{\infty} h(t)\ e^{-i(\omega t)}\ dt \quad , \tag{4.25}$$

which define a Fourier transform pair.

From equation (4.19) the response is

$$Y(x,\omega) = \sum_{n=1}^{\infty} f_n(x) \left\{ \frac{H_n(\omega)}{M_n \omega_n^2} \right\} \int_0^{\ell} F(x,\omega)\ f_n(x)\ dx \quad . \tag{4.26}$$

For a force $F(x,\omega)$ concentrated at $x = x_o$ such that $F(x,\omega)$ $= (F(x)) \cdot (F(\omega))$ then

$$\int_0^{\ell} F(\omega)\ \delta(x-x_o)\ f_n(x)\ dx = F(\omega) \cdot f_n(x_o) \quad , \tag{4.27}$$

Using this fact in equation (4.19) gives

$$Y(x,\omega) = \sum_{n=1}^{\infty} f_n(x) \left\{ \frac{H_n(\omega)}{M_n \omega_n^2} \right\} F(\omega) f_n(x_o)$$

$$= \sum_{n=1}^{\infty} f_n(x) f_n(x_o) \left\{ \frac{H_n(\omega)}{M_n \omega_n^2} \right\} F(\omega) \quad , \tag{4.28}$$

or

$$Y(x,\omega) = (G(\omega)) (F(\omega)) \quad , \tag{4.29}$$

and taking the inverse Fourier transform gives

$$y(x,t) = (1/2\pi) \int_{-\infty}^{\infty} G(\omega) F(\omega) e^{i(\omega t)} d\omega \quad , \tag{4.30}$$

where

$$G(\omega) = \sum_{n=1}^{\infty} \frac{f_n(x) f_n(x_o) H_n(\omega)}{M_n \omega_n^2} \quad .$$

4.4.2 Power Spectral Density

For simple structures the power spectrum $Y(x,\omega)$ can be obtained once the Fourier transform of the excitation signal is found. For an

excitation F(t) that is a stationary process, the two sided power spectral density function is given by [2] as

$$S_f(\omega) = \left|\frac{F(\omega)}{T}\right|^2 , \tag{4.31}$$

where T is the period of the signal. The practical difference between the two sided and one sided power spectral density is that for real signals the magnitude of the former is one-half that of the latter. It can be shown that if a force F(t) is put into a linear system having a transfer function H(ω), the output y(t) is related to the input F(t) through the transforms by

$$\left|Y(\omega)\right|^2 = \left|F(\omega)\right|^2 \left|H(\omega)\right|^2 ,$$

or

$$S_y(\omega) = S_f(\omega) \cdot \left|H(\omega)\right|^2 , \tag{4.32}$$

where $|H(\omega)|^2$ is the square of the transfer function and $S_f(\omega)$ and $S_y(\omega)$ are the input and output power spectral density functions, respectively.

4.4.3 The Special Case of Periodic Signals

For the special case of periodic signals, the signal may be considered as the convolution of one period of the signal with an impulse train of period T.

If F(t) is the periodic signal, let

$$f(t) = F(t);\ t_o < t < t_o + T$$

$$f(t) = 0 \quad ; \quad \text{otherwise}$$

and $F(t_o+jT) = F(t_o)$, where $j = 1,2,3...$.

Making use of the Dirac delta function and the convolution property gives

$$F(t) = f(t) \overset{*}{\sum_{j=-\infty}^{\infty}} \delta(t-jt_o) \quad , \tag{4.33}$$

where the * denotes convolution.

Taking the Fourier transform of both sides of equation (4.33) yields

$$F(\omega) = f(\omega) \sum_{j=-\infty}^{\infty} e^{-i(\omega jT)} \quad , \tag{4.34}$$

or

$$F(\omega) = (f(\omega)/T) \sum_{j=-\infty}^{\infty} \delta(\omega - 2j\pi/T) \quad , \tag{4.35}$$

where the last term in equation (4.35) is periodic in frequency with period 1/T Hz.

As an example consider the periodic pulse train of Figure 4.4. The Fourier transform of the signal is shown in Figure 4.6 and consists

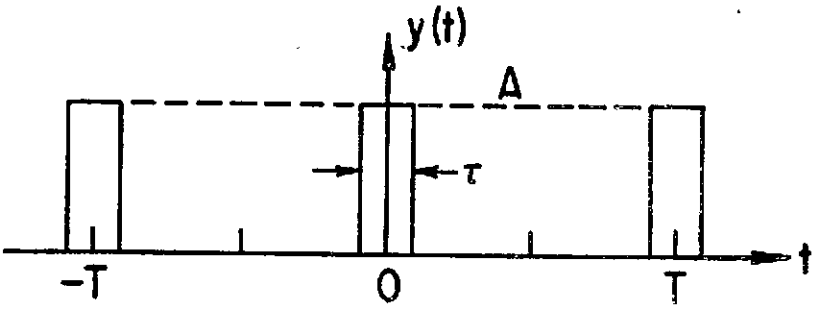

Figure 4.4 Periodic Pulse Train

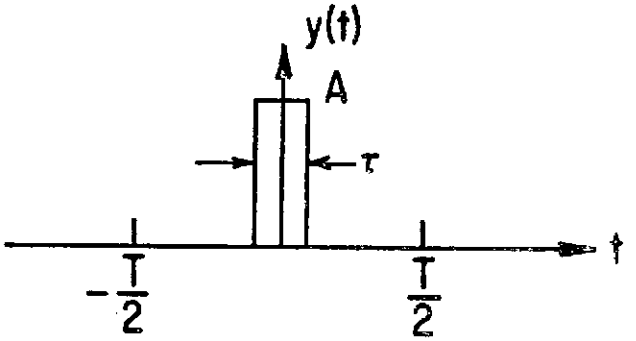

Figure 4.5 One Period of the Pulse Train

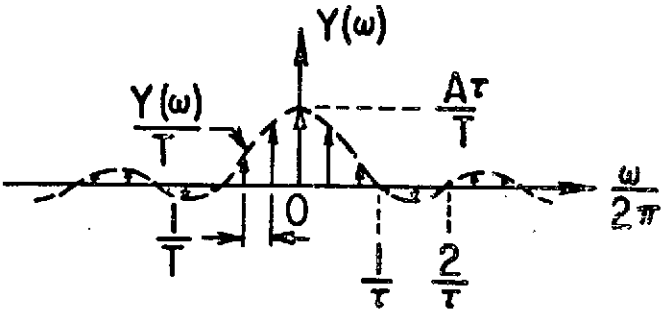

Figure 4.6 Fourier Transform of the Pulse Train

of a series of frequency impulses every 1/T Hz. The magnitude of the impulses is the Fourier transform of the signal over one period divided by the period T, i.e., $F(\omega)/T$.

For the assumed simply supported beam of uniform cross section, the mode shapes and modal frequencies are given by

$$f_n(x) = \sin(n\pi x/\ell) \quad , \tag{4.36}$$

and

$$\omega_n = (n\pi/\ell)^2 \left\{\frac{EIg_c}{\rho_b \Omega}\right\}^{1/2} \quad . \tag{4.37}$$

From equation (4.16), assuming hysteresis damping, the quantity $H_n(\omega)$ is

$$H_n(\omega) = \left\{\frac{1}{(1-(\omega/\omega_n)^2+i\zeta_t)}\right\} \quad , \tag{4.38}$$

so that equation (4.28) is

$$Y(x,\omega) = \sum_{n=1}^{\infty} f_n(x)\, f_n(x_o) \left\{\frac{H_n(\omega)}{M_n \omega_n^2}\right\} F(\omega) \quad . \tag{4.39}$$

For a force $F(x,\omega)$ acting at a position x_o on the beam, $f_n(x_o) = \sin(n\pi x_o/\ell)$ and equation (4.39) for the frequency response

becomes

$$Y(x,\omega) = \sum_{n=1}^{\infty} \frac{\sin(n\pi x/\ell)\ \sin(n\pi x_o/\ell)}{M_n \omega_n^2} \left\{ \frac{1}{(1-(\omega/\omega_n)^2+i\delta_1)} \right\} F(\omega) . \quad (4.40)$$

For a periodic forcing function of the form shown in Figure 4.4 the function $F(\omega)$ can be expressed as

$$F(\omega) = f(\omega) \sum_{j=-\infty}^{\infty} e^{-i(\omega j t)} , \quad (4.41)$$

or

$$F(\omega) = (f(\omega)/T) \sum_{j=-\infty}^{\infty} \delta(\omega - 2j\pi/T) , \quad (4.42)$$

and

$$f(\omega) = (1/T) \int_0^T f(t) e^{-i(2j\pi t/T)}\, dt . \quad (4.43)$$

Thus, equation (4.40) can be written in the form

$$Y(x,\omega) = \sum_{n=1}^{\infty} \frac{\sin(n\pi/\ell)\ \sin(n\pi x_o/\ell)}{M_n \omega_n^2} \left\{ \frac{1}{1-(\omega/\omega_n)^2+i\delta_1} \right\} \cdot \frac{f(\omega)}{T} \sum_{j=-\infty}^{\infty} \delta\left(\omega - \frac{2j\pi}{T}\right) . \quad (4.44)$$

The Fourier series pair for describing periodic signals is

$$F(t) = \sum_{j=-\infty}^{\infty} A_o(j\omega_o)\, e^{i(\omega_o jt)} \quad , \tag{4.45}$$

where ω_o is the fundamental frequency, $\omega_o = 2\pi/T$, and

$$A_o(j\omega_o) = 1/T \int_o^T F(t)\, e^{-i(\omega_o jt)}\, dt \quad . \tag{4.46}$$

The quantity $F(\omega)$ takes the form

$$F(\omega) = \sum_{j=-\infty}^{\infty} A_o(j\omega_o)\, \delta(\omega - j\omega_o) \quad , \tag{4.47}$$

which is convenient for use in conjunction with tabulated series representing various waveforms. Thus

$$Y(x,\omega) = \sum_{n=1}^{\infty} \frac{\sin(n\pi x/\ell)\, \sin(n\pi x_o/\ell)}{M_n \omega_n^{\,2}} \left\{ \frac{1}{1-(\omega/\omega_n)^2 + i\delta_i} \right\}$$

$$\cdot \sum_{j=-\infty}^{\infty} A_o(j\omega_o)\, \delta(\omega - j\omega_o) \quad , \tag{4.48}$$

where $A_o(j\omega_o)$ may be evaluated experimentally or determined from the Fourier series representation. Evaluating the generalized mass for a

uniform beam of length ℓ, density ρ_b, and cross sectional area Ω, gives

$$M_n = \int_o^{\ell} \rho_b \Omega \, f_n(x)^2 \, dx = \rho_b \Omega \ell / 2 \quad , \tag{4.49}$$

so that the frequency response becomes

$$Y(x,\omega) = \left(\frac{2}{\rho_b \Omega \ell}\right) \sum_{n=1}^{\infty} \frac{\sin(n\pi x/\ell) \, \sin(n\pi x_o/\ell)}{\omega_n^2} \left\{ \frac{1}{(1-(\omega/\omega_n)^2)^2+\delta_i^2} \right\}$$

$$\cdot \sum_{j=-\infty}^{\infty} A_o(j\omega_o) \, \delta(\omega - j\omega_o) \quad , \tag{4.50}$$

where the real part of the transfer impedance $H_n(\omega)$ has been taken. The solution is observed to contain only harmonic components at each of the forced frequencies (ω). The free vibration components, in the presence of damping, decrease rapidly with time and for practical purposes disappear. The term $\sin(n\pi x/\ell)$ is the expected sinusoidal spatial variation in the response, and $\sin(n\pi x_o/\ell)$ represents a suppression of frequencies in accord with the location of the force on the beam. The forced vibration is observed to occur at the forced frequency and harmonics with the amplitude being governed by the damping term (δ_i) in the vicinity of resonance ($\omega=\omega_n$).

4.5 Application to Wood Planers

In the planing operation the beam represents the board being surfaced and the harmonic exciting force $F(x,t)$ symbolizes the periodic

impact of the cutting knives on the board. The special case of a square knife cutterhead arrangement can be represented with regard to frequency by a fundamental blade passage frequency and harmonics of this frequency. The contributing frequencies are given by

$$f_h = \text{BPF times n (Hz)} \quad , \tag{4.51}$$

where BPF is the blade passage frequency and n = 1,2,3... .
The blade passage frequency is related to the cutterhead RPM and the number of knives by

$$\text{BPF} = (\text{RPM})(\text{N})/60 \quad , \tag{4.52}$$

where N is the number of knives on the cutterhead.

For any type of periodic impact of the blades on the board the resulting pulse can be subdivided into a series of pure-tone signals which are harmonically related, i.e., all frequencies are integral multiples of the fundamental frequency. Thus for any type of blade impact (cutterhead design) that repeats itself regularly, equation (4.35) is valid. For the case of aperiodic impact, which cannot be subdivided into a set of harmonically related pure-tones, the response can be described in terms of an infinitely large number of pure-tone components of different frequencies spaced an infinitesimal distance apart and with different amplitudes.

5. THEORETICAL DEVELOPMENT OF A MODEL FOR BOARD RADIATION

5.1 Introduction

The vibration analysis has given the response of the board as a function of time (or frequency) and position on the board. This representation is often difficult to use in conjunction with the approximate relations for radiated sound resulting from a vibrating surface. For closely spaced harmonic components the vibration state of the board can be represented by average properties valid strictly for a reverberant vibrational field. Thus, information regarding the vibrational field obtained from energy considerations or experiments takes the place of the exact relations of Chapter 4.

In the formulation of a model for board radiation the phase cell concept of structural vibration is utilized. In effect, the board is considered to be composed of a finite number of radiating piston elements. The critical frequency, which governs the overall radiation of sound from the board, is utilized to divide the radiation problem into three frequency ranges. Expressions for the radiated sound power are derived for each frequency range using formulations for a rectangular baffled piston. The baffled restriction is removed by using a theoretical analogy with a freely suspended disk.

The radiation characteristics of narrow and wide boards are compared theoretically and the radiated power is computed numerically. The computed sound power levels are then converted to average sound pressure levels using the semireverberant substitution technique.

5.2 The Vibrational Field

The board radiation problem can be modeled by considering the beam to be composed of a finite number of piston elements. The vibrational field of the board is defined using energy principles in terms of board geometry and energy delivered to the board. Using a simple piston model to obtain the radiation characteristics and energy considerations to define the velocity field, it is possible to predict the acoustic power output of the vibrating board.

In order to properly dimension and locate the piston elements it is necessary to specify the mode shapes (eigenfunctions) and natural frequencies (eigenfrequencies) of the vibrational field. In this analysis the response of the board is assumed to be reverberant in nature; the individual modes being uncoupled and separated in frequency. This is equivalent to assuming an input force consisting of well spaced pure-tone frequency components with the frequency response of the board concentrated in narrow frequency bands.

5.2.1 The Structural Wavelength

Above the first few natural modes the natural frequencies are relatively independent of the particular type of boundary constraints. The transverse structural wavelength for a uniform, rectangular, slender beam is given by [3] as

$$\lambda_{ns} = \frac{C_B}{f} = \frac{\left[EIg_c/\rho_b\Omega\right]^{1/4}}{\left[(\omega_n)^{1/2}/2\pi\right]} = 6\left\{\frac{t_b}{f}\right\}^{1/2}\left\{\frac{E}{\rho_b}\right\}^{1/4}, \qquad (5.1)$$

where

λ_{ns} = modal structural wavelength of the nth mode,

C_B = transverse bending wave velocity,

$f = \omega_n/2\pi$.

Using equation (4.1) for the natural frequencies of such a beam, i.e.

$$\omega_n = (\beta/\ell)^2 \left\{\frac{EIg_c}{\rho_b \Omega}\right\}^{1/2} , \tag{5.2}$$

in equation (5.1) above, yields

$$\lambda_{ns} = 2\pi\ell/\beta \quad . \tag{5.3}$$

The factor β depends on the particular mode, which in turn, depends on the length of the beam. Equation (5.1) indicates that the modal structural wavelength (λ_{ns}) at a particular resonant frequency is dependent only on the thickness and material constants of the beam. Although the beam length governs the frequency corresponding to a particular mode, the mode shape at a given frequency is independent of beam length. Equation (5.1) is also independent of the boundary conditions. Figure 5.1 shows the theoretical variation in wavelength with frequency as a function of thickness and material. The reference frequency f_o is taken as the fundamental harmonic frequency in the Fourier spectra of the excitation.

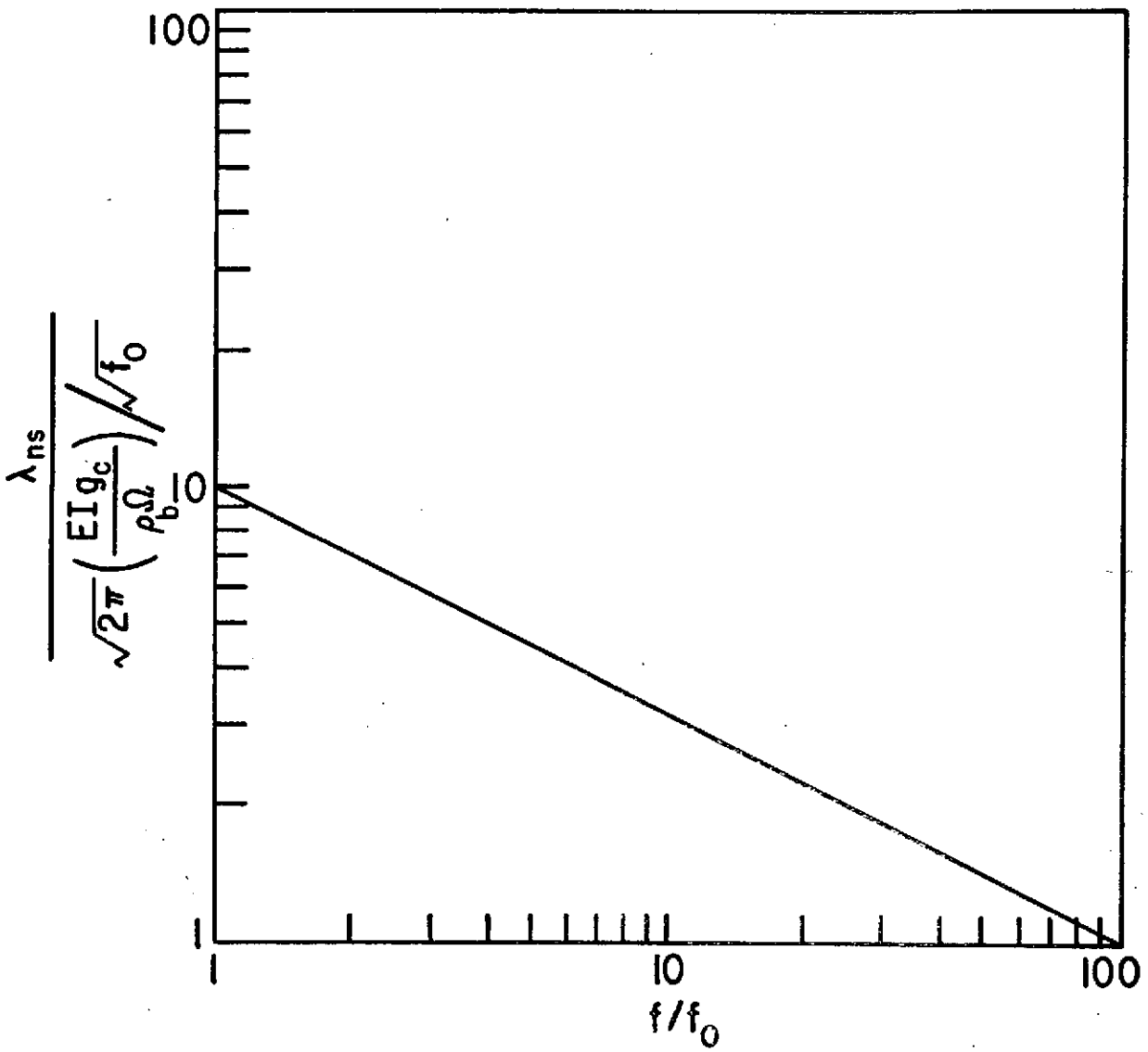

Figure 5.1 Structural Wavelength Parameter Versus Fundamental Frequency Ratio

5.2.2 Power and Energy Considerations

From a statistical energy standpoint, the power supplied to the system must equal the sum of the power lost through damping and the power radiated as sound into the surrounding air. The steps in determining the response are given by [2] as:

(1) The total energy stored in the system equals the sum of the kinetic and potential energies of the structure

$$E_T = M \langle \bar{V}^2 \rangle \quad , \tag{5.4}$$

where M is the total mass of the structure and $\langle \bar{V}^2 \rangle$ is the mean-square transverse vibrational velocity averaged over the structure.

(2) The internal energy dissipation in one cycle of vibration is equal to the total stored energy times the dissipation loss factor η_d. At frequency ω, $P_d = E_T \omega \eta_d$ where P_d is the power dissipated.

(3) The acoustic power radiated into free space is equal to the mean-square velocity times the real part of the radiation impedance function. Thus

$$P_a = \langle \bar{V}^2 \rangle \text{ Re } [Z] = R_{rad} \langle \bar{V}^2 \rangle \quad , \tag{5.5}$$

where P_a is the radiated acoustic power.

Equation (5.5) is strictly valid if the modes are excited by a random noise in a narrow bandwidth $\Delta\omega$ centered on ω, where the space-time average transverse velocities of the modes within the band are equal. This form is chosen since it can be applied when the motion of

the structure is either single mode vibration or a reverberant vibrational field. From equation (5.5) the radiation resistance is defined as

$$R_{rad} = P_a/\langle\bar{V}^2\rangle \quad . \tag{5.6}$$

In this case the radiation resistance is independent of the modal energy of the structure. This is equivalent to assuming that the mechanical resistance and the acoustic resistance achieve values independently of the energy distribution; that is the modes are not coupled. Using equation (5.4) relating energy, velocity, and mass, gives

$$\langle\bar{V}^2\rangle = E_T/M \quad . \tag{5.7}$$

For a beam excited across its entire width (W) by a force (F) per unit width, the energy input varies with width as

$$E_T \sim W \quad \text{or} \quad E_T/W = \text{constant} \; . \tag{5.8}$$

Since the energy input is linearly related to the width, equation (5.7) can be written as

$$\langle\bar{V}^2\rangle = E_T/(\rho_b W t_b \ell) \quad , \tag{5.9}$$

where

$M = \rho_b W t_b \ell$,

ρ_b = density of the beam,

W = width of the beam,

t_b = thickness of the beam,

ℓ = length of the beam.

combining equations (5.8) and (5.9) yields

$$\langle \bar{V}^2 \rangle = (E_T/W)\ (1/(\rho_b t_b \ell)) \sim 1/\ell \qquad (5.10)$$

for a given density and thickness. The velocity term is observed to be independent of beam width since more energy is delivered for the wider beam, thereby rendering the quantity E_T/W constant. Equation (5.10) states that the product of mean-square velocity and board length is constant; a result which will be quite useful in obtaining the total radiated sound power from the beam.

5.3 The Elementary Piston Model for Board Radiation

The present analysis is based on the replacement of the vibrational field of the beam by an array of rectangular piston radiators, having the characteristics of monopole radiators insofar as general behavior is concerned. The phases of the monopoles correspond to the phase of the vibrational field at each position. Each radiator (piston) has the dimensions of d (one-half the structural wavelength, $\lambda_s/2$) and W (the width of the piston) and vibrates out of phase with a neighboring piston.

For classical baffled piston type radiation the radiation resistance is given by [26] in the form

$$R_{rad} \sim \begin{cases} 1 & Ka>>1 \\ (Ka)^2 & Ka<<1 \end{cases} , \qquad (5.11)$$

where

$K = \omega/C_a$,

a = characteristic piston dimension,

ω = circular frequency,

C_a = speed of sound in air.

The expression for the radiation resistance is seen to be dependent on the Ka factor; consequently several frequency ranges must be considered. The size of the piston element to be used in this model is determined by the beam width, (a constant for a given beam) and the structural wavelength, which depends on frequency. In determining the radiation produced by a piston radiator, an important consideration is the ratio of the flexural wavelength in the structure to the wavelength of sound in air at the same frequency, since a compression of air is necessary for acoustic radiation.

5.3.1 The Critical Frequency

When structural and acoustic wavelengths are plotted versus frequency the curves intersect defining a critical frequency for every thickness of the beam (see Figure 5.2). The critical frequency can be

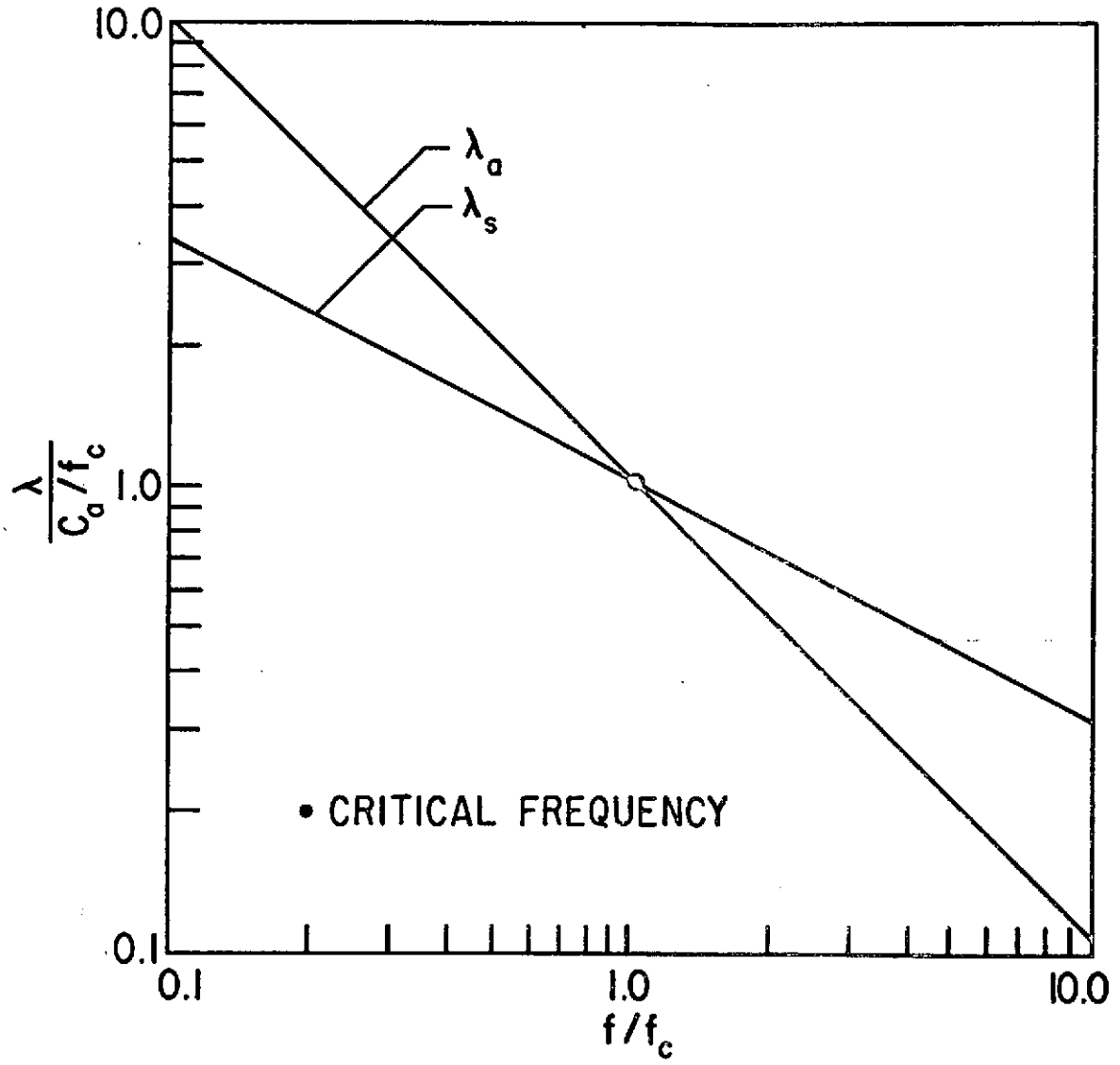

Figure 5.2 Structural and Acoustic Wavelength Versus Critical Frequency Ratio

observed from the points of intersection shown in Figure 5.2 or calculated from [2] as

$$\lambda_s = \lambda_a \quad ; \quad C_B/f = C_a/f \quad ;$$

which gives

$$f_c = (C_a^2/2\pi) \left\{ \frac{\rho_b \Omega}{EIg_c} \right\}^{1/2} , \tag{5.12}$$

where

$$\frac{C_B}{f} = \frac{2\pi (EIg_c/\rho_b \Omega)^{1/4}}{(\omega_n)^{1/2}} ,$$

and

λ_s = the structural wavelength,

λ_a = the acoustic wavelength,

C_a = the acoustic wave velocity,

C_B = structural wave velocity.

Figures 5.3 and 5.4 show the effect of beam thickness and material on the critical frequency, respectively.

The importance of the critical frequency is evident in the radiation of sound by an unbounded flexural wave. If the structural wavelength (λ_s) is larger than the acoustic wavelength (λ_a), then by Huyghens' principle there is a radiated wave on either side of the

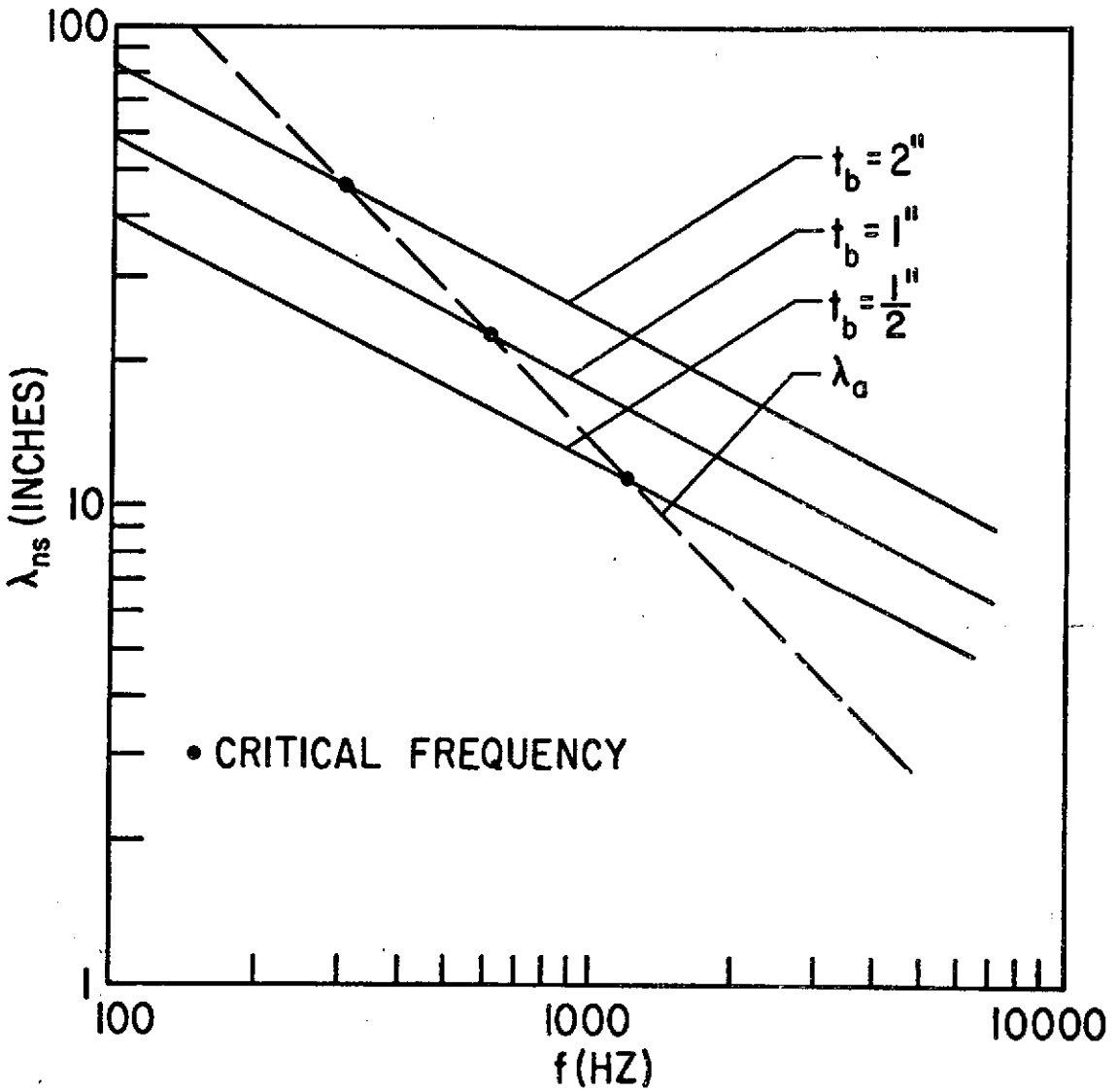

Figure 5.3 Acoustic and Structural Wavelength Versus Frequency

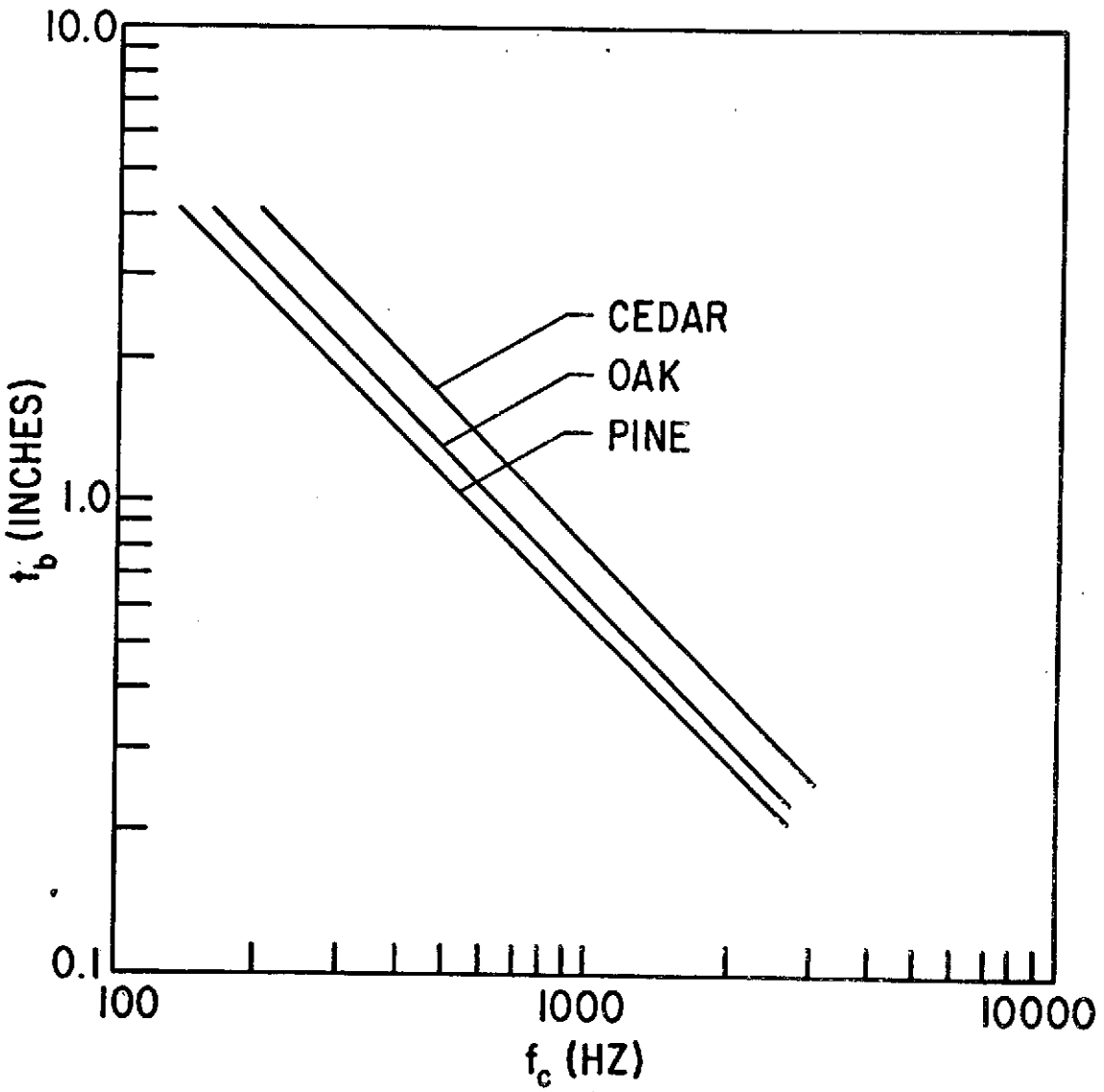

Figure 5.4 Board Thickness Versus Critical Frequency

structure forming the angle $\theta = \sin^{-1}(\lambda_a/\lambda_s)$ between the direction of propagation and the normal to the structure. As λ_s approaches λ_a the angle moves toward its maximum. If λ_a surpasses λ_s then θ becomes imaginary and radiation fails. In effect the contrary motions of adjacent portions of the structure cancel, resulting in zero radiation. For a finite beam, interior sections effectively cancel each other leaving only the end portions as radiators. Three cases of radiation are considered according to the ratio of λ_a to λ_s, which defines the amount of interference between neighboring pistons. This is equivalent to dividing the radiation problem into three frequency ranges, being; above the critical frequency ($\lambda_s > \lambda_a$), at or near the critical frequency ($\lambda_s \approx \lambda_a$), and below the critical frequency ($\lambda_s < \lambda_a$). The three cases can be represented diagramatically, with the shaded areas being the radiating acoustic sources in Figures 5.5, 5.6, and 5.7. Above the critical frequency ($\lambda_s > \lambda_a$) the phase cells of Figure 5.5 are decoupled and cancellation effects are negligible. At or near the critical frequency ($\lambda_s \approx \lambda_a$) the cells are coupled but internal cancellation is incomplete. The radiating area, the shaded portion of Figure 5.6, is a fraction of that for the case above the critical frequency. Below the critical frequency ($\lambda_s < \lambda_a$) the phase cells, acting as point monopoles localized at the cell center, interfere and internal cancellation is complete. Only the edge monopoles of Figure 5.7 of half strength are left as radiators. The three cases considered correspond to $Ka > 1$, $Ka \sim 1$, and $Ka < 1$, respectively, with "a" being a typical piston (phase cell) dimension.

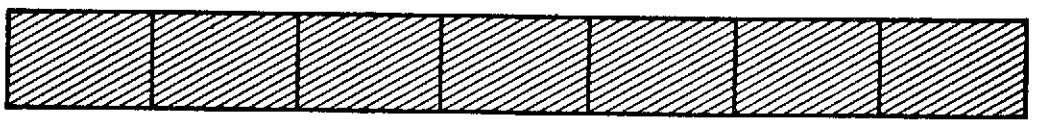

Figure 5.5 Individual Piston Radiation Above the Critical Frequency

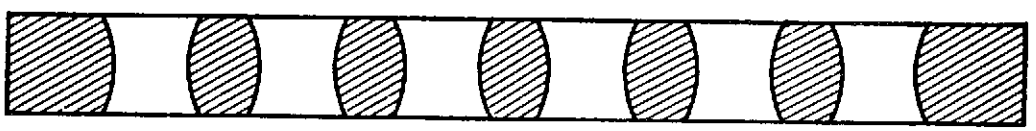

Figure 5.6 Individual Piston Radiation Near the Critical Frequency

Figure 5.7 Individual Piston Radiation Below the Critical Frequency

5.3.2 The Phase Cell Concept

The phase cell concept is used to represent the instantaneous relative phase of neighboring piston elements constituting the beam. The length of each piston is determined by the structural wavelength of the beam at a particular frequency. For example, the pure-tone component shown in Figure 5.8 would be represented by the phase cell arrangement of Figure 5.9. In Figure 5.9 the length of each piston element is $d = \lambda_s/2$; one-half the structural wavelength.

For the case of a beam mounted in an infinite plane baffle the radiation can be characterized by an array of rectangular baffled pistons, with each piston affecting a neighboring piston in accord with the three frequency ranges discussed. The model must be altered, however, to allow for a beam radiating into free space. In analogy with the freely suspended disk of [24], the unbaffled piston elements behave in much the same manner as the baffled piston for cases such that $K\bar{b} > 1$, where $\bar{b}$ is one-half the vector distance between the monopole sources located on each piston face. For values of $K\bar{b}$ such that $K\bar{b} < 1$ the monopole sources on each face of the piston exhibit cancellation effects similar to the case of $\lambda_s < \lambda_a$ for neighboring piston elements. The total radiation of the beam is composed of the contribution of N_p piston elements, where N_p is determined by the beam length, structural wavelength, and Ka factor for the particular frequency of interest.

5.4 Acoustic Power Radiation

Utilizing the phase cell model, the radiation resistance can be approximated in each frequency domain as a function of the various beam

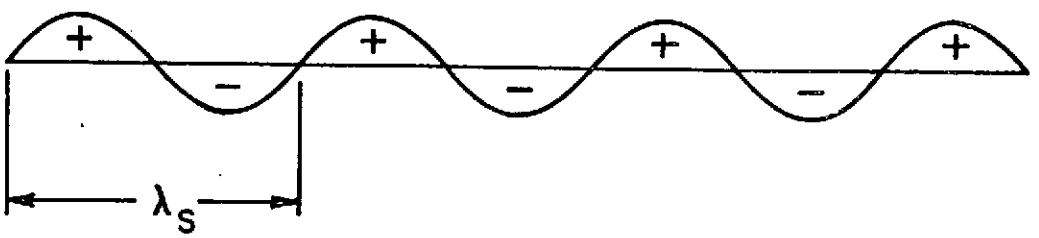

Figure 5.8 Structural Wavelength Illustration

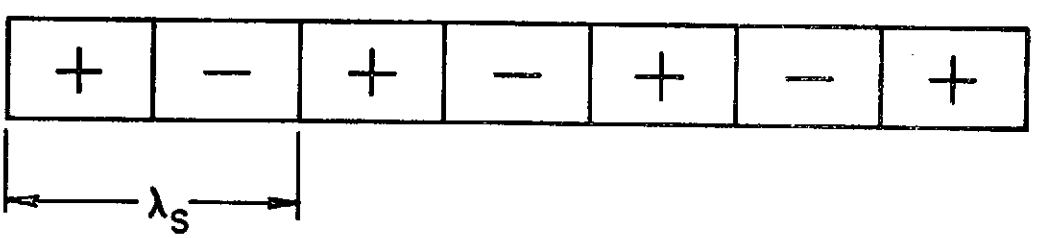

Figure 5.9 Phase Cell Representation of Structural Wavelength

parameters. The total acoustic power (P_a) radiated to the far field is given by [2] as

$$P_a = R_{rad} \langle \bar{V}^2 \rangle \quad . \tag{5.13}$$

The quantity $\langle \bar{V}^2 \rangle$ is the mean-square (space-time averaged) transverse velocity of the beam (or piston element). This velocity may be obtained theoretically using the methods of Chapter 4, or approximated by means of the energy techniques discussed elsewhere in this section. It has been shown, (see equation (5.9)), that the quantity $\langle \bar{V}^2 \rangle$ for a reverberant vibrational field may be expressed in terms of the beam mass and the energy input to the system. The mean-square velocity was observed to decrease with increasing beam length for a constant energy input, as expected from the concept of equipartition of energy for reverberant systems. Repeating equation (5.10)

$$\langle \bar{V}^2 \rangle = E_T/(\rho_b t_b \ell W) \sim 1/\ell \quad . \tag{5.14}$$

The quantity E_T is the energy stored in the beam and is independent of the length of the beam. From equation (5.14) it is observed that for a particular beam the product $\langle \bar{V}^2 \rangle \ell$ is constant and the resulting acoustic power output of the beam can be expressed from equation (5.13) as

$$P_a = (R_{rad}/\ell)(\ell \langle \bar{V}^2 \rangle) = \text{constant} \cdot (R_{rad}/\ell) \quad . \tag{5.15}$$

Thus, the task is reduced to determining the radiation resistance for the different frequency domains and beam geometries.

5.4.1 Individual Piston Behavior

The piston model formulation is general (valid for all values of Ka) for each individual piston, but the number of radiating pistons (N_p) will depend on the particular frequency with respect to the critical frequency. Preliminary to determining the values of the radiation resistance, it is necessary to examine a single unbaffled piston in detail to determine the combined behavior of monopole sources located on each face. This is equivalent to considering a dipole source of strength $Q\bar{b}$ for $K\bar{b}<1$, where Q is the equivalent simple source strength. Thus, the model accounts for short circuiting at low values of $K\bar{b}$ for the unbaffled beam.

Figure 5.10 shows a section through the beam along with an individual piston element. In the equivalent source model of Figure 5.11, the monopole sources are considered to be concentrated at the piston centers, reversed in phase. For the two sources of Figure 5.11 to form an effective dipole, it is required that $\bar{b} < \lambda_a/2$. In analogy with the freely suspended disk of [24], the radiation resistance can be represented by

$$R_{rad} = \begin{cases} (2\rho c)\pi r^2 \text{ for } Kr \gg 1 \\ \\ (3\rho c)(Kr)^4 \pi r^2 \text{ for } Kr \ll 1 \end{cases}, \qquad (5.16)$$

where ρc is the specific acoustic impedance and r is the disk radius.

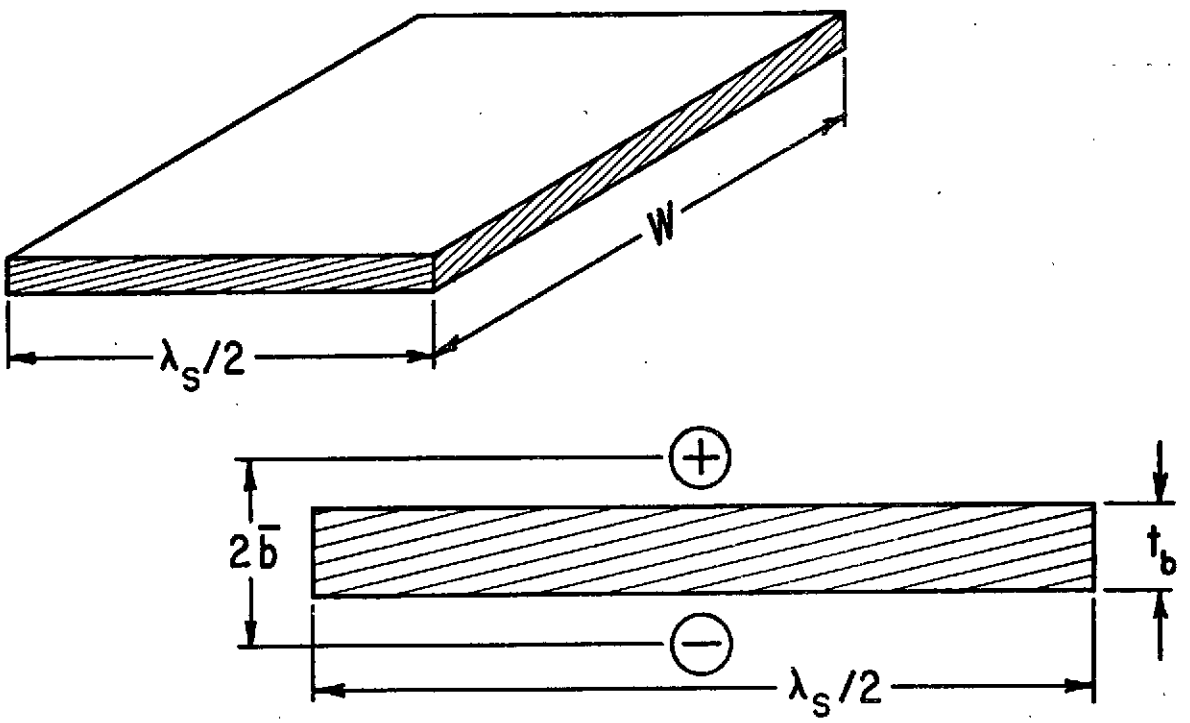

Figure 5.10 Individual Piston Element

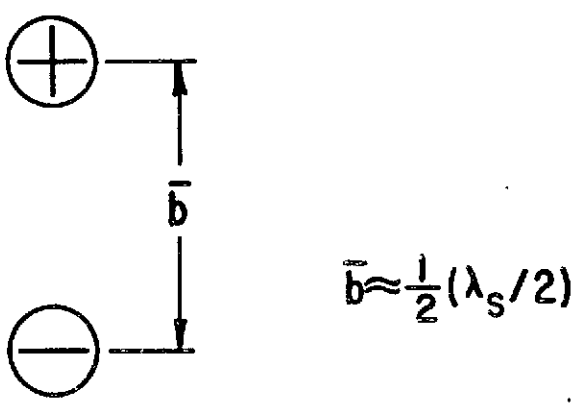

Figure 5.11 Simple Source Model for Piston Radiation

For values of Kr>1 the baffled and unbaffled piston radiation differs by a factor of two, accounting for radiation from both sides for the latter case. The radiation is altered only in the range of Kr<1. In this region (Kr<1) the following expressions for the radiation resistance are appropriate

$$R_{rad} = \begin{cases} \rho cA(Kr)^2/2 & \text{(baffled)} \\ 3\rho cA(Kr)^4 & \text{(unbaffled)} \end{cases} , \qquad (5.17)$$

for Kr<1.

The radiation efficiency, defined as radiation resistance divided by ρcA, takes the form

$$\sigma = \frac{R_{rad}}{\rho cA} = \begin{cases} (Kr)^2/2 & \text{(baffled)} \\ 3(Kr)^4 & \text{(unbaffled)} \end{cases} , \qquad (5.18)$$

for Kr<1.

Thus the radiation efficiency for the baffled piston is greater than that for the unbaffled piston for small Kr, (Kr<1). The value of Kr where the curves of σ versus Kr intersect for the two cases is found from equation (5.17) as

$$(Kr)^2/2 = 3(Kr)^4 \quad \text{or} \quad Kr = 1/\sqrt{6} \ . \qquad (5.19)$$

Short circuiting is possible for values of $Kr<1\sqrt{6}$; for values of $Kr>1\sqrt{6}$ the radiation for the baffled and unbaffled pistons differ only by a factor of two. Figure 5.12 indicates the difference in the radiation characteristics for the two cases for $Kr<1\sqrt{6}$. For a typical piston dimension "a" (a = 2r) it is assumed for Ka<1 short circuiting effects are possible and for Ka>1 they are not possible.

The radiation field for a flat, rectangular piston set in a plane rigid wall is considered; the far field relations for the radiation impedance being deduced from the well known case of the baffled circular piston. As indicated, the deviation of the unbaffled beam from the baffled case due to cancellation is apparent only for values of Ka such that Ka<1, where "a" represents an effective diameter.

In accord with [24] for a baffled circular piston

$$R_{rad} = \rho c A \, \theta_o(Ka) \quad , \tag{5.20}$$

where

$$\theta_o(Ka) = [1-(2/Ka)J_1(Ka)] \quad ,$$

and J_1 is the Bessel function of order one. The function $\theta_o(Ka)$ is plotted versus Ka in Figure 5.13.

In converting from the baffled circular piston to the baffled rectangular piston the approximate result given in [24] is

$$R_{rad} \simeq \rho c A \left\{ \frac{[a^2 \, \theta_{\square}(Ka) - b^2 \theta_{\square}(Kb)]}{[a^2 - b^2]} \right\} \quad , \tag{5.21}$$

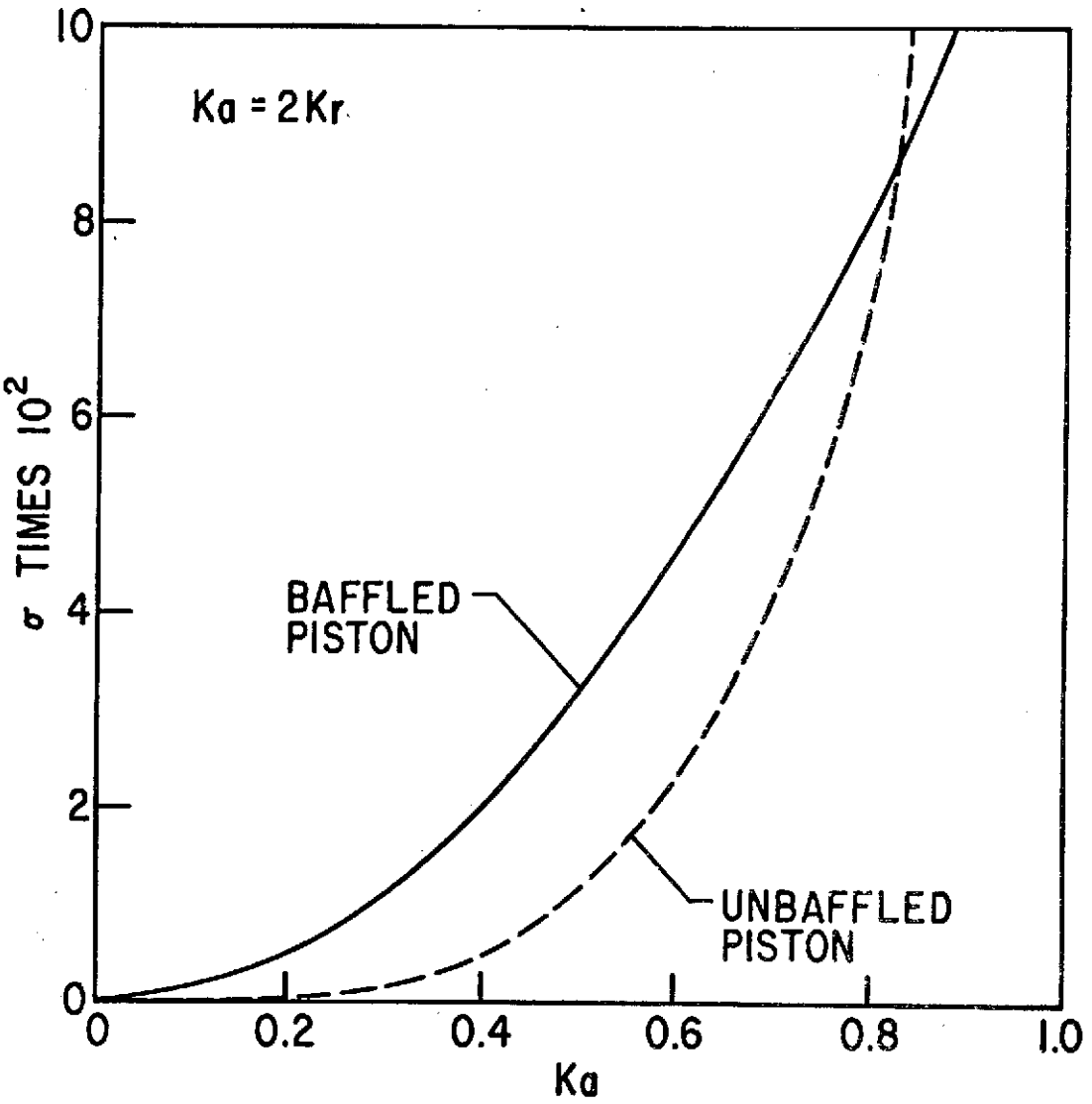

Figure 5.12 Radiation Efficiency for Baffled and Unbaffled Pistons at Low Ka

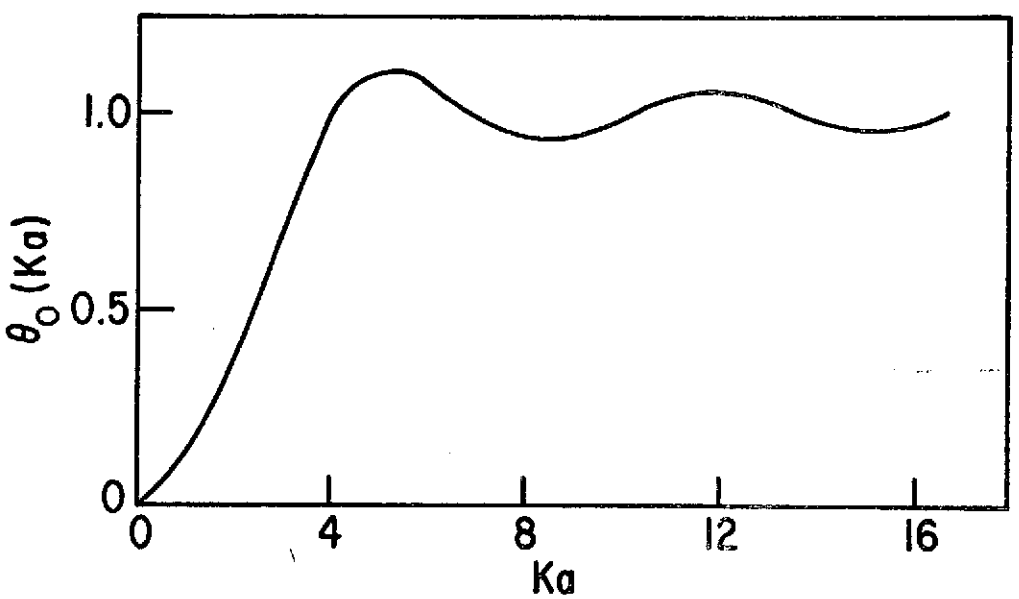

Figure 5.13 Radiation Efficiency Versus Ka for a Baffled Circular Piston (after [15])

where

$$\theta_{\square}(Ka) = 1-4\left\{\frac{1-J_o(Ka)}{(Ka)^2}\right\} \tag{5.22}$$

and the piston area (A) = ab, with J_o the Bessel function of zero order. Figure 5.14 indicates the variation of $\theta_{\square}$ with Ka for a rectangular piston.

For the special case of a square baffled piston the radiation resistance formula reduces to

$$R_{rad} = \rho cA\ \theta_o(Ka)\ , \tag{5.23}$$

where θ_o is defined by equation (5.20). The function $\theta_o(Ka)$ exhibits the following properties;

$$\begin{aligned} &\theta_o(Ka) \sim 1 \quad ; \quad Ka>4 \\ &\theta_o(Ka) \sim Ka \quad ; \quad 2<Ka<4 \\ &\theta_o(Ka) \sim (Ka)^2 \quad ; \quad Ka<2 \end{aligned} \tag{5.24}$$

Combining equations (5.24) and 5.23) gives

$$R_{rad} \sim \begin{cases} \rho cA & ; \quad Ka>4 \\ \rho cA(Ka) & ; \quad 2<Ka<4 \\ \rho cK^2A^2 & ; \quad Ka<2 \end{cases} . \tag{5.25}$$

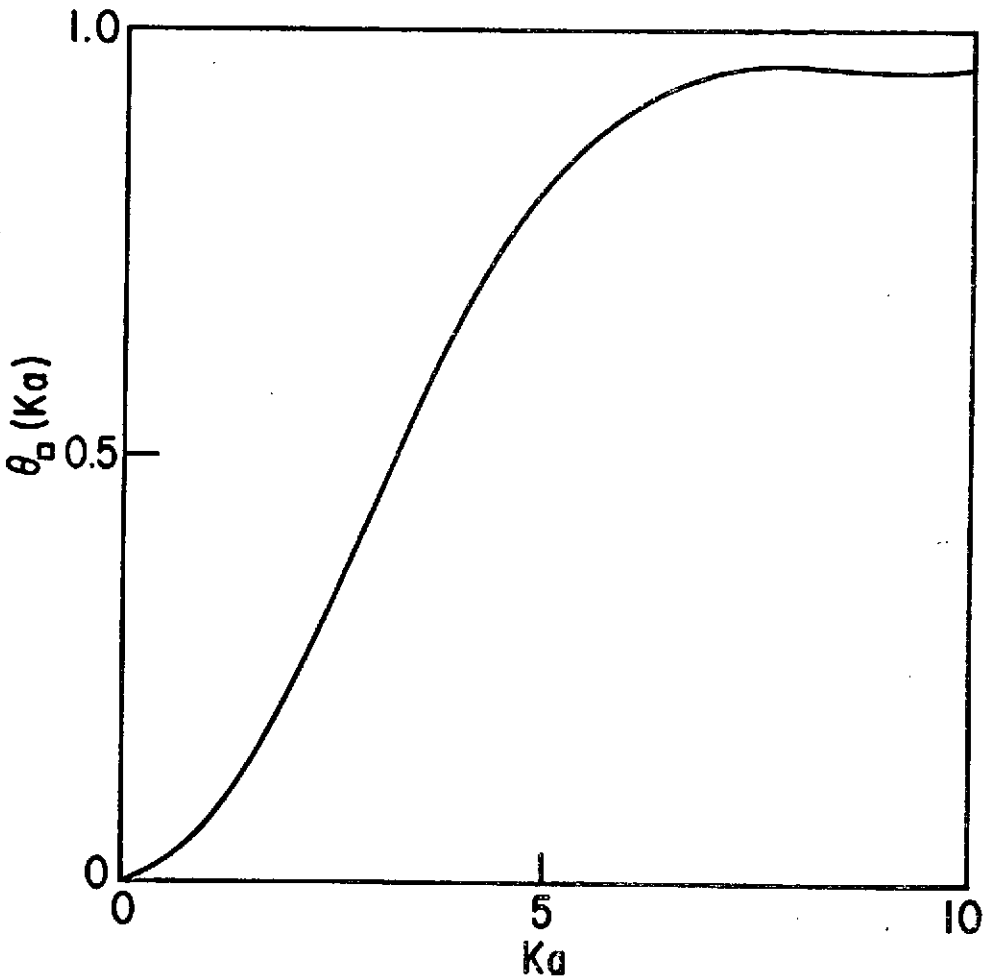

Figure 5.14 Radiation Efficiency Versus Ka for a Baffled Rectangular Piston (after [24])

The function $\theta_o(Ka)$ is plotted versus Ka in Figure 5.15. Interference effects occurring between faces of the individual unbaffled pistons are indicated by the dashed portion of the curve for Ka<1.

For an unbaffled beam the value of θ_o to be used in equation (5.23) is twice that read from Figure 5.15 since Figure 5.15 is based on a radiating area of only one piston face. The dashed portion of the curve for Ka<1 should be used, since short circuiting may occur for the unbaffled case. The curve applies to each individual piston, thus the total radiation resistance for the entire beam involves a summation over the number of radiating pistons. The number of contributing pistons, as pointed out, depends on the ratio of the structural and acoustic wavelength for each frequency.

5.4.2 Application of the Piston Model to a Finite Beam

The piston model cannot be applied to the beam radiation problem over the entire frequency range of interest since the number of contributing piston elements differ in each frequency domain. For this reason, the radiation problem is divided into three frequency domains depending on the critical frequency:

(1) Frequencies above the critical frequency where all the piston elements contribute to the radiation.

(2) Frequencies at or near the critical frequency where a fraction of the piston elements contribute.

(3) Frequencies below the critical frequency where only the end portions of the beam are assumed to radiate.

The phase cell representation concept discussed earlier is shown in Figure 5.15.

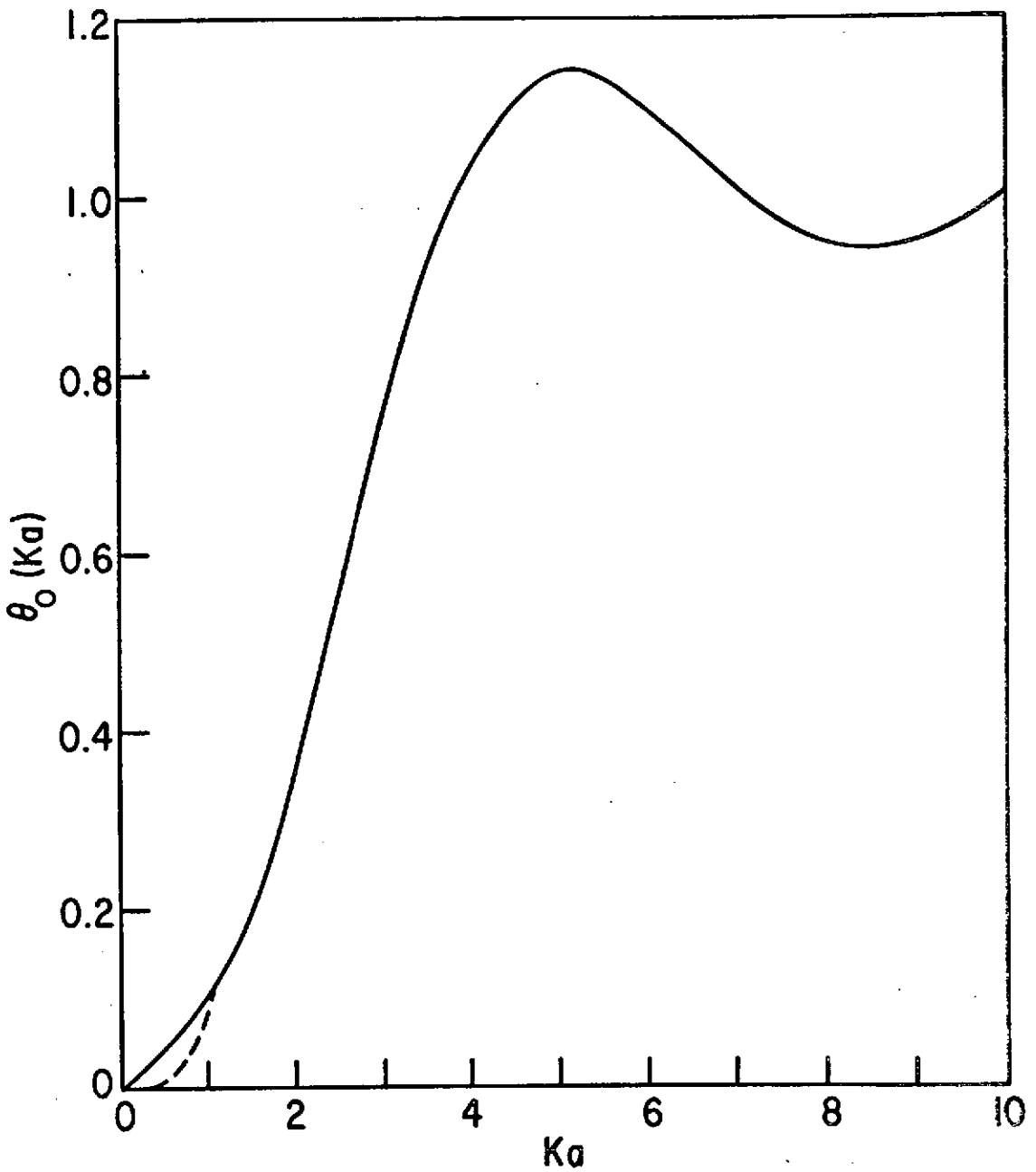

Figure 5.15 Radiation Efficiency Parameter Versus Ka for Baffled and Unbaffled Pistons

Case 1. - Above the Critical Frequency

The assumptions for this case are:

(1) Above the critical frequency the individual piston elements of Figure 5.16 radiate independently, i.e., cancellation effects are not present.

(2) The length of the beam is great compared to the acoustic wavelength in air for frequencies above the critical frequency.

(3) The piston element dimensions are approximately equal and the simplified square piston model is sufficiently accurate.

(4) The Ka factor is such that Ka>1 so that the radiation for the baffled and unbaffled cases differ only by a factor of two.

Assumption (3) is justified since for typical beam (board) thicknesses of one-half to two inches the range of frequencies involved is 1000 to 5000 Hz. From Figure 5.3 it is noted that $4'' < \lambda_s/2 < 10''$ and beam widths (W) typically vary from four to twelve inches ($4'' < W < 12''$).

In light of these assumptions, equation (5.21) for the radiation resistance takes the simplified form of equation (5.23), and for $a = \lambda_s/2$ and $b = W$ becomes

$$R_{rad} = \rho c(\lambda_s/2)W\ [\theta_o(K\lambda_s/2)] \quad , \tag{5.26}$$

for the baffled piston, and

$$R_{rad} = 2\rho c(\lambda_s/2)W\ [\theta_o(K\lambda_s/2)] \quad , \tag{5.27}$$

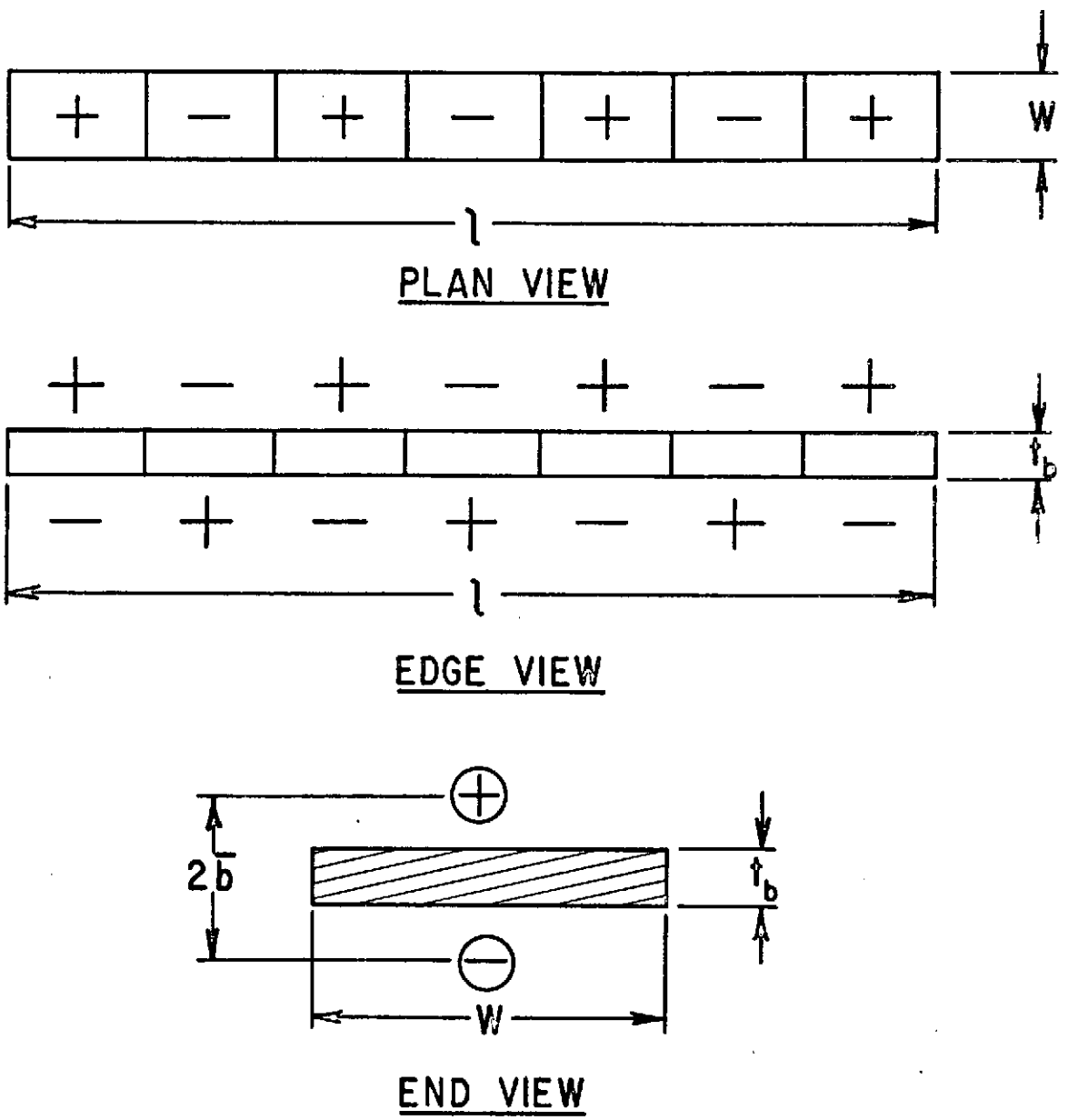

Figure 5.16 Different Views of the Phase Cell Representation of the Beam

for the unbaffled piston. The previous two equations can be written in the form

$$R_{rad} = \rho c(\lambda_s/2)W\ [\theta_o(K\lambda_s/2)] \begin{Bmatrix}1\\2\end{Bmatrix} , \tag{5.28}$$

where the symbol $\begin{Bmatrix}1\\2\end{Bmatrix}$ is understood to mean that the first term is to be multiplied by a factor of one for the baffled beam and by a factor of two for the unbaffled case. This convention will be adopted for subsequent equations.

Accounting for the number of piston elements constituting the beam (N_p), equation (5.23) becomes

$$R_{\substack{rad\\total}} = N_p \cdot R_{rad} = \rho cW\ell\ [\theta_o(K\lambda_s/2)] \begin{Bmatrix}1\\2\end{Bmatrix} , \tag{5.29}$$

where the beam length (ℓ) and the number of radiating pistons (N_p) are related through the structural wavelength (λ_s) by

$$\ell = N_p(\lambda_s/2) \quad \text{or} \quad N_p = \ell/(\lambda_s/2) . \tag{5.30}$$

For the special case when the Ka factor is much greater than unity (Ka>>1, Ka>4 is sufficient) the function $\theta_o(Ka)$ of equation (5.29) approaches unity (see Figure 5.15) and the radiation resistance is essentially independent of Ka. For this case equations (5.28) and (5.29) can be written as

$$R_{rad} = \rho c(\lambda_s/2)W \begin{Bmatrix}1\\2\end{Bmatrix} , \tag{5.31}$$

and for N_p radiating piston elements

$$R_{\substack{rad \\ total}} = N_p \cdot R_{rad} = \rho c W \ell \begin{Bmatrix} 1 \\ 2 \end{Bmatrix} . \tag{5.32}$$

Thus, at high values of Ka the radiated wavelength is small compared to "a" and each portion of the surface radiates independently and is separately loaded. At high frequency the impendance is resistive; equal to the piston area times the characteristic impedance (ρcA).

For values of Ka such that $1<Ka<4$ the curve of $\theta_o(Ka)$ versus Ka of Figure 5.15 can be roughly approximated by obtaining the slope of the curve in the region $2<Ka<3$; or

$$\theta_o \simeq Ka/2 . \tag{5.33}$$

Using equation (5.33) in equation (5.28) gives for the radiation resistance

$$R_{rad} = \rho c K W^2 (\lambda_s/2) \begin{Bmatrix} 1/2 \\ 1 \end{Bmatrix} . \tag{5.34}$$

Note that the quantity $(K\lambda_s/2)$ can be replaced by KW, since a square piston has been assumed ($W=\lambda_s/2$). The radiation resistance for the entire beam is found by multiplying equation (5.34) by N_p; the number of radiating piston elements, thus

$$R_{\substack{rad \\ total}} = \rho c K W^2 \ell \begin{Bmatrix} 1/2 \\ 1 \end{Bmatrix} . \tag{5.35}$$

The results obtained for the baffled beam can be compared with the results obtained in [21] and [22]. Defining the surface area S ($S = W\ell$) the radiation resistance for the baffled case, as given by equations (5.32) and (5.35), is

$$R_{\substack{rad \\ total}} = \begin{cases} \rho cS & ; \quad KW \geq 4 \\ \frac{1}{2}\rho cKWS & ; \quad 1 < KW < 4 \end{cases} \tag{5.36}$$

For frequencies above the critical frequency such that $\lambda_s > \lambda_a$ and $\pi\ell > \lambda_a$, [21] gives the radiation resistance as

$$R_{rad} \approx \rho cS(1-(\lambda_a/\lambda_s)^2)^{1/2} \approx \rho cS \ , \tag{5.37}$$

where $\gamma < 1$ (high Ka) and γ is taken as $\frac{1}{2} KW(1-(\lambda_a/\lambda_s)^2)^{1/2}$. For $\gamma < 1$, the radiation resistance is given as

$$R_{rad} = \frac{1}{2} S\rho cKW \ , \tag{5.38}$$

which is also the result obtained in [22] for a narrow beam.

Case 2. - Near the Critical Frequency

The assumptions for this case are:

(1) At or near the critical frequency the piston elements of Figure 5.16 do not radiate independently. The radiation from one phase cell partially cancels that from adjacent cells since they are 180 degrees out of phase. The degree of cancellation ranges from

zero, slightly above the critical frequency, to unity below the critical frequency.

(2) The beam is long compared to the acoustic wavelength ($\ell > \lambda_a/2$).

(3) The $K\bar{b}$ factor is such that $K\bar{b} > 1$ so that the faces of an individual piston element radiate independently.

(4) The assumption made on the fraction of cancellation overpowers the magnitude of the errors involved in assuming that $\lambda_s/2 \approx W$ in this frequency range, so that the square piston model is again assumed.

In regard to assumption (1), the exact degree of cancellation between neighboring phase cells in the vicinity of the critical frequency is unknown. In this narrow frequency range the cancellation, theoretically, jumps from zero to unity. To account for this effect an average amount of cancellation of one-half can be assumed without great inaccuracies, which is essentially what is done in [21]. Assumption (3) is justified since for midrange values of $Ka(1/2 < Ka < 4)$ the two faces of an individual phase cell radiate as independent monopoles.

Assuming that neighboring pistons, spaced one-half of a structural wavelength apart, partially cancel resulting in an effective decrease in the number of radiating piston elements by a factor of one-half, the expression for the radiation resistance for the square piston model is

$$R_{rad_{total}} = N_p \cdot R_{rad} = \frac{1}{2} \rho c W \ell \theta_o (K\lambda_s/2) \begin{Bmatrix} 1 \\ 2 \end{Bmatrix}, \qquad (5.39)$$

where

$$R_{rad} = \rho c(\lambda_s/2)W\ \theta_o(K\lambda_s/2) \begin{Bmatrix} 1 \\ 2 \end{Bmatrix} , \tag{5.40}$$

and $N_p = 1/2\ [\ell/\lambda_s/2]$ since effectively only half of the pistons contribute.

The more accurate expression for the rectangular piston model given by equation (5.21) is

$$R_{\substack{rad \\ total}} = N_p \cdot R_{rad} = \frac{1}{2} \rho c W \ell \left[\frac{(\lambda_s/2)^2 \theta_{\square}(K\lambda_s/2) - W^2 \theta_{\square}(KW)}{((\lambda_s/2)^2 - W^2)}\right] \begin{Bmatrix} 1 \\ 2 \end{Bmatrix} . \tag{5.41}$$

Several special approximations depending on the Ka factor are presented.

Ka factor less than unity (Ka<1). The function θ_o for the baffled and unbaffled piston elements is approximated by

$$\theta_o \sim \begin{cases} (Ka)^2/2 & \text{(baffled)} \\ 3(Ka)^4 & \text{(unbaffled)} \end{cases} , \tag{5.42}$$

so that

$$R_{rad} = \rho c(\lambda_s/2)W \begin{cases} (K\lambda_s/2)^2/2 \\ 6(K\lambda_s/2)^4 \end{cases} , \tag{5.43}$$

and

$$R_{\substack{rad \\ total}} = N_p \cdot R_{rad} = \frac{1}{2} \rho c W \ell \begin{Bmatrix} (K\lambda_s/2)^2/2 \\ \\ 6(K\lambda_s/2)^4 \end{Bmatrix} , \tag{5.44}$$

Ka factor ranging from one to four ($1<Ka<4$). In this region the curve of Figure 5.15 is approximated by

$$\theta_o \simeq Ka/2 = (K\lambda_s/2)/2 = KW/2 , \tag{5.45}$$

so that

$$R_{rad} = \rho c K W^2 (\lambda_s/2) \begin{Bmatrix} 1/2 \\ \\ 1 \end{Bmatrix} \tag{5.46}$$

and

$$R_{\substack{rad \\ total}} = N_p \cdot R_{rad} = \frac{1}{2} \rho c K W^2 \ell \begin{Bmatrix} 1/2 \\ 1 \end{Bmatrix} \tag{5.47}$$

Ka factor greater than four ($Ka>4$). In this Ka region the function $\theta_o(Ka)$ becomes independent of Ka and approaches unity

$$\theta_o \simeq 1 , \tag{5.48}$$

so that

$$R_{rad} = \rho c(\lambda_s/2)W \begin{Bmatrix} 1 \\ 2 \end{Bmatrix} , \tag{5.49}$$

and

$$R_{\substack{rad \\ total}} = N_p \cdot R_{rad} = \frac{1}{2} \rho c W \ell \begin{Bmatrix} 1 \\ 2 \end{Bmatrix} , \tag{5.50}$$

Since the square piston model has been assumed, the terms $(\lambda_s/2)$ and W have been used interchangeably.

In summary, the following approximate results are obtained for the radiation resistance for several ranges of Ka for frequencies near the critical beam frequency.

$$R_{\substack{rad \\ total}} = \begin{cases} \rho c W \ell (KW)^2 \begin{Bmatrix} 1/4 \\ 3(KW)^2 \end{Bmatrix} & ; \quad KW<1 \\ \rho c W^2 \ell K \begin{Bmatrix} 1/4 \\ 1/2 \end{Bmatrix} & ; \quad 1<KW<4 \\ \rho c W \ell \begin{Bmatrix} 1/2 \\ 1 \end{Bmatrix} & ; \quad KW>4 \end{cases} \tag{5.51}$$

The result obtained in equation (5.51) for $1<Ka<4$ may be compared with that of [21] for the baffled beam which also gives

$$R_{rad} = \frac{1}{4} \rho c K W^2 \ell . \tag{5.52}$$

Case 3. - Below the Critical Frequency

Below the critical frequency the mode shape of the beam $f_n(x)$ is such that the structural wavelength is very short compared to the acoustic wavelength. Thus the radiation from a crest to a node segment, shown in Figure 5.17, is effectively cancelled by the radiation from the adjacent segment, which is 180 degrees out of phase. By extending this argument, it is concluded that all the radiation from the central portion is effectively cancelled, so that the radiation must be accounted for by the end segments of length $(\lambda_s/4)$. The radiation is equivalent to the coupling of a pair of rigid pistons, each having a mean-square velocity equal to the mean-square velocity of the whole beam and vibrating with the same relative phase as the end regions of the beam.

Below the critical frequency the faces of individual piston elements may act as monopoles radiating independently or, for the unbaffled case, a higher order source (dipole) depending on the frequency and piston geometry. As discussed earlier, the baffled and unbaffled pistons differ by a factor of two for Ka>1, since the effective radiating area is doubled. For Ka<1 short circuiting may occur between the two radiating faces of the piston for the unbaffled case. This leads to lower values of the radiation resistance than the values for a completely baffled piston. The short circuiting ($(Ka)^4$ term) effect is shown in Figure 5.12 along with the baffled piston curve ($(Ka)^2$ term) for low values of Ka. The simplified model for the square piston element is assumed since in this frequency range the piston (beam) width is approximately equal to the quantity $(\lambda_s/4)$. If the width (W)

is such that $4'' < W < 12''$ and the frequency range under consideration satisfies the relationship $100 < f < 1000$ (Hz), then from Figure 5.2 $5'' < \lambda_s/4 < 12''$ so that the square piston model assumption is again justified.

In Figure 5.12 $(Ka)^4$ and $(Ka)^2$ like terms were plotted versus Ka up to the point of intersection of the two curves. The dipole effect of the piston faces is present only for such Ka that the term $3(Ka)^4$ is less than $(Ka)^2/2$ since the dipole cannot surpass the monopole in efficiency. The radiation resistance relations are again based on the square piston model, but in the frequency range below the critical frequency the model cannot be applied without certain restrictions concerning Ka and the beam length. The size of the end piston elements which radiate is now $(\lambda_s/4) \times (W)$, as shown in Figure 5.18.

Several special cases of beam radiation below the critical frequency will be considered.

Radiation from a long beam with $(\ell > \lambda_a/2 > \lambda_s/2 \quad ; \quad KW > 1)$. This is equivalent to assuming that the end pistons are sufficiently far apart to radiate as independent monopoles and the individual pistons faces radiate independently as if in a baffle. The expression for the radiation resistance from equation (5.23) is

$$R_{rad} = \rho c a b \theta_o (Ka) \begin{Bmatrix} 1 \\ 2 \end{Bmatrix}$$

$$= \rho c (\lambda_s/4) W \theta_o (K\lambda_s/4) \begin{Bmatrix} 1 \\ 2 \end{Bmatrix} . \qquad (5.53)$$

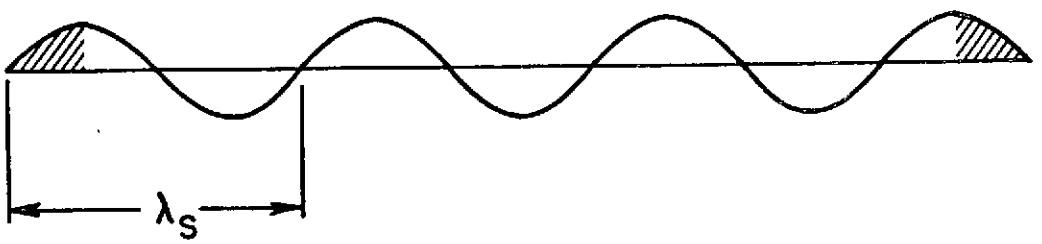

Figure 5.17 Diagram of Beam Radiation Below the Critical Frequency

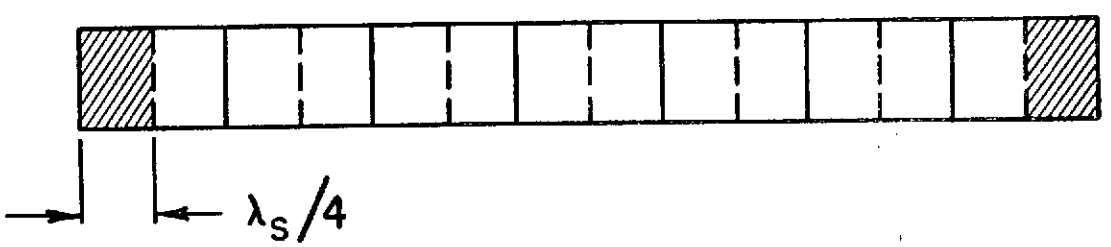

Figure 5.18 Phase Cell Representation of Beam Radiation Below the Critical Frequency

and since only two piston elements radiate ($N_p = 2$)

$$R_{\substack{rad \\ total}} = N_p \cdot R_{rad} = 2\rho c(\lambda_s/4)W\,[\theta_o(K\lambda_s/4)] \begin{Bmatrix} 1 \\ 2 \end{Bmatrix} . \tag{5.54}$$

The function $\theta_o(Ka)$ is again approximated for $1<Ka<4$ by

$$\theta_o \simeq Ka/2 \simeq K(\lambda_s/4)/2 \quad , \tag{5.55}$$

and since the square piston model is assumed to be valid

$$\theta_o \simeq KW/2 \quad . \tag{5.56}$$

Combining equations (5.54), (5.55), and (5.56) and again noting that only two piston elements radiate ($N_p=2$) the radiation resistance for the beam becomes

$$R_{\substack{rad \\ total}} = 2\rho cKW(\lambda_s/4)^2 \begin{Bmatrix} 1 \\ 2 \end{Bmatrix} \quad , \tag{5.57}$$

for $1<Ka<4$, where $\lambda_s/4$ has been replaced by W, the piston width.

The results obtained can be compared with those of [21] which gives

$$R_{rad} \simeq \rho c \frac{W}{K} \left(\frac{\lambda_s}{\lambda_a}\right)^2 \frac{[2-(\lambda_s/\lambda_a)^2]}{[(1-(\lambda_s/\lambda_a)^2)^{3/2}]} \quad , \tag{5.58}$$

or

$$R_{rad} \sim \rho c W K (\lambda_s/4)^2 \quad , \tag{5.59}$$

for the baffled piston since the acoustic wavelength is related to K by $\lambda_a = 2\pi/K$.

Radiation from a long beam with ($\ell > \lambda_a/2 > \lambda_s/2$; $KW < 1$). This is the case of a beam, long compared to the acoustic wavelength (λ_a), but exhibiting dipole effects due to the interference between the faces of each piston. Thus the baffled and unbaffled beam must be analyzed separately. The function θ_o in this frequency range is noted from Figure 5.15 to be

$$\begin{aligned} \theta_o &\sim (Ka)^2/2 \quad \text{(baffled)} \\ \theta_o &\sim 3(Ka)^4 \quad \text{(unbaffled)} \end{aligned} \tag{5.60}$$

Using equation (5.23) for the square piston model, the radiation resistance per piston becomes

$$R_{rad} = \rho c (\lambda_s/4) W \, \theta_o (K\lambda_s/4) \begin{Bmatrix} 1 \\ 2 \end{Bmatrix} \tag{5.61}$$

Using equation (5.60) in (5.61) and accounting for two radiating pistons gives

$$R_{\substack{rad \\ total}} = N_p \cdot R_{rad} = 2\rho c(\lambda_s/4)W \begin{cases} (KW)^2/2 \\ \\ 3(KW)^4 \end{cases} , \qquad (5.62)$$

for Ka<1.

For the case of a baffled beam, [21] gives the radiation resistance for $\lambda_a > \lambda_s$, $\pi\ell > \lambda_a$ and $\pi W < \lambda_a$ as

$$R_{rad} \sim \rho c W^2 (K\lambda_s/4)^2 , \qquad (5.63)$$

which is in agreement with equation (5.62).

The remaining cases to be considered are beams which are not long compared to the acoustic wavelength. This is not the usual case, since in most practical situations the beam length (ℓ) is greater than three feet (a machine operation requirement) and such low frequencies that ($3' << \lambda_a/2$) are of little interest. For this case the edge monopoles are coupled, and (a) the individual piston faces are uncoupled (Ka>1), or (b) the value of Ka is less than unity and the faces are also coupled (this is applicable to the unbaffled beam only).

There are two further cases to consider:

(1) The edge monopoles are in phase, and the interference is constructive producing a total radiated power twice that if separated.

(2) The edge monopoles are opposite in phase giving rise to a dipole, radiating power that is second order to that of a monopole.

The resulting radiation may thus be characterized as monopole, dipole, or quadrupole in nature depending on the relative phase of the end portions and whether the beam is baffled or unbaffled.

The equations governing the radiation resistance in the three frequency domains associated with the critical frequency are given in Table 5.1 for baffled and unbaffled beams. The critical frequency to be used in Table 5.1 for a particular beam geometry and material is found from Figure 5.2.

5.4.3 An Exact Solution for Beam Radiation

The exact solution for the radiation from an infinitely long cylindrical beam given by [24] has been generalized in [14] to apply to beams of elliptic cross section and extended to include beams of rectangular cross section. An outline of this analysis is presented, subject to the following assumptions:

(1) The beam is infinite in extent, thus the radiation is limited to frequencies above the critical frequency ($\lambda_s > \lambda_a$).

(2) Coupling between normal modes of vibration due to damping is neglected since the modes are well separated and in theory a uniform damping force will not couple transverse vibratory modes.

(3) Internal damping is independent of frequency but does depend on such factors as material, size, and moisture content and is specified experimentally.

(4) Air viscosity is neglected, reducing the problem to that of acoustic radiation.

(5) The amplitude variation is sinusoidal and end effects are neglected.

Table 5.1 Radiation Resistance for Different Values of the Ka Factor for Each Frequency Range

Ka Factor	Beam Length Assumption	Piston Dimensions	Frequency Range	Radiation Resistance
ALL*	$\ell > \lambda a/2$	$\lambda s/2 \simeq W$	$f > f_c$	$\rho c W \ell \theta_o(KW) \begin{Bmatrix} 1 \\ 2 \end{Bmatrix}$
KW>4	$\ell > \lambda a/2$	$\lambda s/2 \simeq W$	$f > f_c$	$\rho c W \ell \begin{Bmatrix} 1 \\ 2 \end{Bmatrix}$
K<W<4	$\ell > \lambda a/2$	$\lambda s/2 \simeq W$	$f > f_c$	$1/2 \rho c W^2 \ell K \begin{Bmatrix} 1 \\ 2 \end{Bmatrix}$
ALL*	$\ell > \lambda a/2$	$\lambda s/2 \simeq W$	$f \simeq f_c$	$1/2 \rho c W \ell \theta_o(KW) \begin{Bmatrix} 1 \\ 2 \end{Bmatrix}$
K<W<4	$\ell > \lambda a/2$	$\lambda s/2 \simeq W$	$f \simeq f_c$	$1/4 \rho c K W^2 \ell \begin{Bmatrix} 1 \\ 2 \end{Bmatrix}$
KW<1	$\ell > \lambda a/2$	$\lambda s/2 \simeq W$	$f \simeq f_c$	$\rho c W \ell \begin{Bmatrix} (KW)2/4 \\ 3(KW)^4 \end{Bmatrix}$
ALL*	$\ell > \lambda a/2$	$\lambda s/2 \simeq W$	$f < f_c$	$\rho c W^2 \theta_o(KW) \begin{Bmatrix} 1 \\ 2 \end{Bmatrix}$
K<W<4	$\ell > \lambda a/2$	$\lambda s/2 \simeq W$	$f < f_c$	$\rho c W^2 (KW) \begin{Bmatrix} 1 \\ 2 \end{Bmatrix}$
KW<1	$\ell > \lambda a/2$	$\lambda s/2 \simeq W$	$f < f_c$	$\rho c W^2 \begin{Bmatrix} (KW)^2 \\ 6(KW)^4 \end{Bmatrix}$

* For values of KW<1 the expression given for the radiation resistance is valid provided the curve corresponding to the baffled or unbaffled case in Figure (5.16) is used.

Finite beams vibrating in modes above the first few resonances usually meet the above assumptions. Subject to these assumptions, [14] gives the acoustic loss factor (η_a) as

$$\eta_a = -\mathrm{Re}\{F_R/v_o \cos(Kx) e^{-i\omega t})\}\ (1/(\omega \rho_b W t_b)) \quad , \tag{5.64}$$

where

F_R = beam radiation loading,

η_a = acoustic loss factor,

Re = real part of quantity,

ρ_b = mass density of the beam,

ω = circular frequency,

W = beam width,

i = $\sqrt{-1}$,

t_b = beam thickness,

t = real time,

v_o = surface velocity.

The loading term F_R is a quite complicated combination of Mathieu functions and their derivatives for which expansions in terms of Bessel and Hankel functions are required. The values of the loss factor (η_a) versus a dimensionless frequency parameter (q) are shown in Figure 5.19 for various beam width to thickness ratios. A plot of K_d given by $[(2\pi/\lambda_a)^2-(2\pi/\lambda_s)^2]^{1/2}$ versus frequency reveals that for the thickness range of interest K_d is essentially ir iependent of thickenss, making

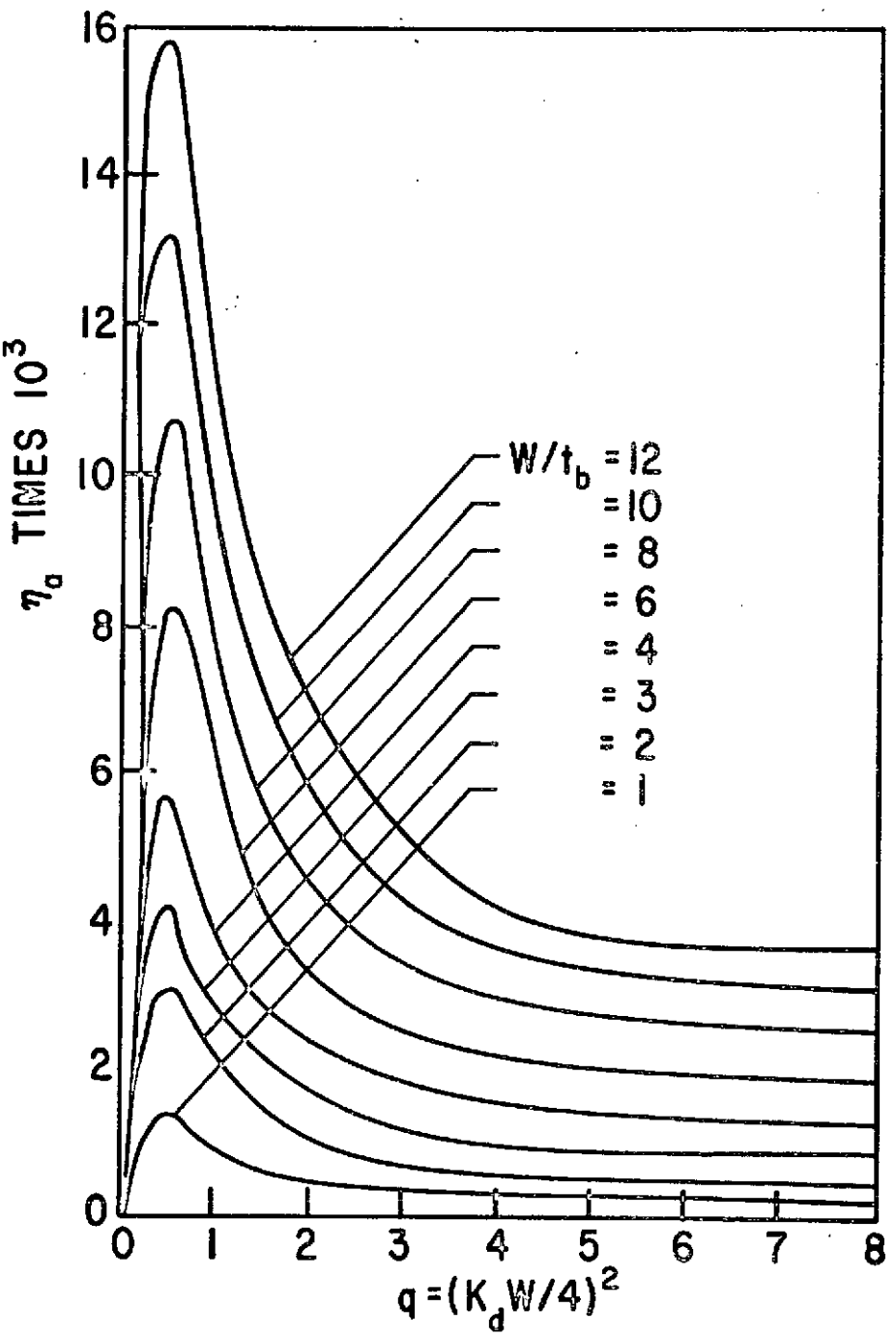

Figure 5.19 Radiation Loss Factor Versus Ka Parameter (after [14])

it possible to plot η_a versus frequency for various beam widths. The results, shown in Figure 5.20, are valid only above the critical frequency for each particular thickness of the beam.

The relation between the radiation resistance (R_{rad}) and the loss factor (η_a) for finite beams is given by

$$R_{rad} = \omega M \eta_a \quad , \tag{5.65}$$

where ω is the circular frequency and M is the total mass of the structure.

At first glance the radiation resistance appears to depend on the mass of the beam, which was not the case in the piston model. This is explained by observing the following proportionalities:

$$\eta_a \sim - (1/(\omega \rho_b W t_b))\ \mathrm{Re}\{F_R/v_o\} \sim (\rho_a/\rho_b)(W/t_b) \quad . \tag{5.66}$$

Letting $M = \rho_b\ W t_b \ell$, equation (5.65) becomes

$$R_{rad} \sim \omega\ (\rho_b W t_b \ell)(\rho_a/\rho_b)(W/t_b) = \rho_a c_a\ K W^2 \ell \quad . \tag{5.67}$$

The result given in equation (5.67) is similar in form to the results of the piston model near the critical frequency. In this case, however, the dependence of η_a on frequency is quite complex.

A comparison of the radiation efficiency (σ) above the critical frequency is shown in Figure 5.21 for the exact method of [14] and the

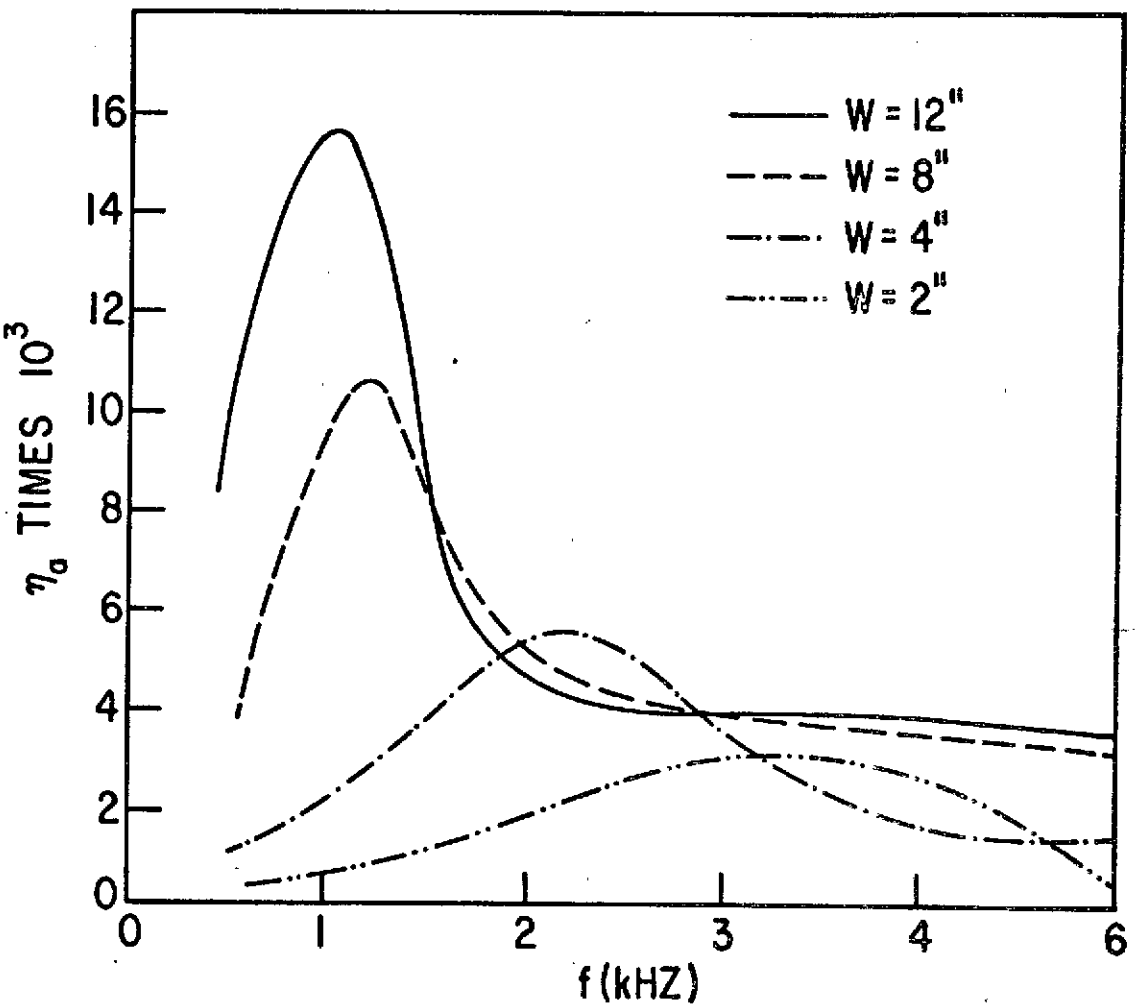

Figure 5.20 Radiation Loss Factor Versus Frequency for Different Board Widths

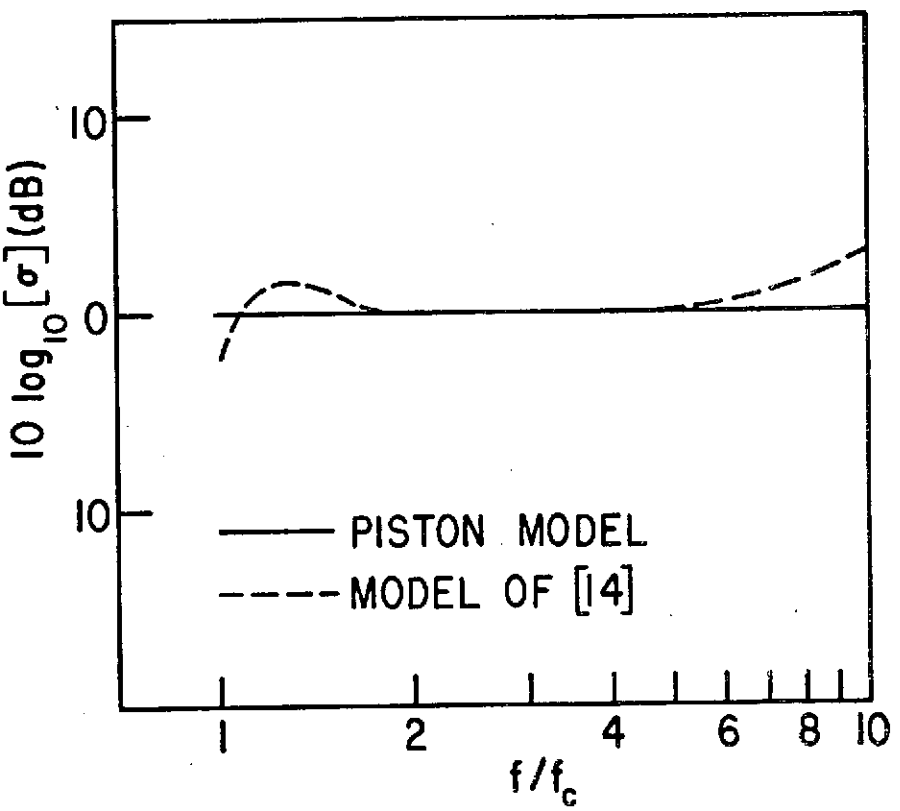

Figure 5.21 Radiation Efficiency Versus Critical Frequency Ratio for the Piston Model and the Model of [14]

elementary piston model. The curves are plotted for an eight inch wide, one inch thick, oak board having a critical frequency of about 700 Hz. The two curves are in excellent agreement above the critical frequency. The radiation efficiency (σ) used in Figure 5.21 was defined previously as

$$\sigma = R_{rad}/(\rho c A) \quad , \tag{5.68}$$

where A is the total radiating area.

5.5 Theoretical Trends and Comparisons

It is of interest to examine the radiation characteristics of beams of different widths. For comparison purposes, beams of two and eight inch widths will be considered. Only the frequencies above and near the critical frequency will be considered, since the lower frequencies do not contribute appreciably to the total radiated power. To define a specific critical frequency, a one inch thick, red oak beam is considered which corresponds to a critical frequency of about 700 Hz. At the critical frequency the values of KW for the two beams are

$$\begin{aligned} KW(W=8'') &= 2\pi f_c\, W/C_a \approx 2.60 \\ KW(W=2'') &= 2\pi f_c\, W/C_a \approx 0.65 \quad . \end{aligned} \tag{5.69}$$

The case of an unbaffled beam will be considered. From Table 5.1, the radiation resistances above the critical frequency are

$$R_{rad}(W=8'') = 2\rho cW\ell\theta_o(KW)$$
$$R_{rad}(W=2'') = 2\rho cW\ell\theta_o(KW) \quad , \tag{5.70}$$

and

$$R_{rad}(W=8'') \simeq 2\rho cW\ell \text{ for } KW>4$$
$$R_{rad}(W=2'') \simeq \rho cW^2K\ell \text{ for } 1<KW<4 \quad . \tag{5.71}$$

Near the critical frequency the radiation resistances are

$$R_{rad}(W=8'') = \rho cW\ell\theta_o(KW)$$
$$R_{rad}(W=2'') = \rho cW\ell\theta_o(KW) \quad , \tag{5.72}$$

and

$$R_{rad}(W=8'') \simeq \frac{1}{2}\rho cKW^2\ell$$
$$R_{rad}(W=2'') \simeq 3\rho cW\ell(KW)^4 \quad . \tag{5.73}$$

The values of $\theta_o(KW)$, based on Figure 5.15, are given in Table 5.2.

Forming the parameter R_{rad}/ϕ, where $\phi = 2\rho c\ell KW_o t_{bo}$, the radiation resistance expressions become

$$R_{rad}/\phi = \begin{cases} W\theta_o(KW)/(KW_o t_{bo}) & \text{for } f>f_c \\ W\theta_o(KW)/(2KW_o t_{bo}) & \text{for } f\approx f_c \end{cases} , \tag{5.74}$$

and the approximate forms are

$$R_{rad}/\phi(W=8") \approx \begin{cases} W/(W_o K t_{bo}) & \text{for } f>f_c \\ \frac{1}{4}(W^2/(W_o t_{bo})) & \text{for } f\approx f_c \end{cases} , \tag{5.75}$$

and

$$R_{rad}/\phi(W=2") \approx \begin{cases} \frac{1}{2}(W^2/(W_o t_{bo})) & \text{for } f>f_c \\ 0 & \text{for } f\approx f_c \end{cases} \tag{5.76}$$

These expressions may be conveniently compared with the results obtained in [14]. Recalling equation (5.65)

$$R_{rad} = \omega M n_a = \omega \rho_b W t_b \ell n_a , \tag{5.77}$$

thus

$$\begin{aligned} R_{rad}/\phi &= \omega\rho_b(W/W_o)(t_b/t_{bo}) \\ &= \tfrac{1}{2}(\rho_b/\rho_a)(W/W_o)(t_b/t_{bo})n_a , \end{aligned} \tag{5.78}$$

where the value of η_a is found from Figure 5.20. Since Figure 5.20 is based on $\rho_a/\rho_b = 1.55 \times 10^{-3}$, which corresponds approximately to red oak, the radiation parameter becomes

$$R_{rad}/\phi \approx 324\eta_a(W/W_o)(t_b/t_{bo}) \quad . \tag{5.79}$$

The values obtained for η_a from Figure 5.20 are given in Table 5.3 and the values of the quantity R_{rad}/ϕ for $W_o = t_o = 1$ inch are given in Table 5.4, and plotted in Figure 5.22. From Figure 5.22 it is observed that the theoretical trend of [14] which predicts that the major contribution to the radiation parameter for the wider board is concentrated in the vicinity of the critical frequency, while that for the narrower board is spread out, is also apparent from the simple piston model. The piston model is noted to exhibit the theoretical trends while allowing quite simple computations of the radiated sound power.

5.5.1 A Comparison of the Radiation Characteristics of Wide and Narrow Beams

The radiated sound power for two beams of four and eight inch widths is of interest. The beams are excited across their width at a blade passage frequency of 240 Hz. The beams are assumed to be of the same material and the same length (five feet). The mean-square velocity - length product ($\langle\bar{V}^2\rangle\ell$) is assumed to be constant and the velocity magnitude and frequency spectra are assumed to be the same for each beam. The beams are assumed to radiate from an infinite baffle.

Table 5.2 Radiation Efficiency Parameter for Different Values of KW for Each Beam

f (Hz)	(KW) (W=8")	θ_o(KW) (W=8")	(KW) (W=2")	θ_o(KW) (W=2")
500	1.80	0.40	0.46	0
700	2.62	0.60	0.66	0.02
1000	3.75	1.00	0.93	0.08
2000	7.50	0.95	1.88	0.40
3000	11.00	1.00	2.80	0.75
4000	14.00	1.00	3.70	1.00

Table 5.3 Acoustic Loss Factor for Different Frequencies.

f (Hz)	η_a (W=2")	η_a (W=8")
1000	1.00×10^{-3}	9.00×10^{-3}
2000	2.00×10^{-3}	4.50×10^{-3}
3000	3.00×10^{-3}	3.50×10^{-3}
4000	2.70×10^{-3}	2.70×10^{-3}

Table 5.4 Comparison of Radiation Parameters for Different Mathematical Models

Frequency (Hz)	Exact Method [14] $R_{rad}/(2\rho cK\ell W_o t_o)$		Piston Model (Exact) $R_{rad}/(2\rho cK\ell W_o t_o)$		Piston Model (Approximate) $R_{rad}/(2\rho cK\ell W_o t_o)$	
	W=2"	W=8"	W=2"	W=8"	W=2"	W=8"
500	0	0	0	0	0	0
700	0	0	0.13	7.30	2.00	7.00
1000	0.65	23.40	0.34	17.00	2.00	15.20
2000	1.30	11.60	0.85	8.10	2.00	9.00
3000	1.93	9.00	1.07	5.70	2.00	6.00
4000	1.74	7.00	1.10	4.30	2.00	4.00

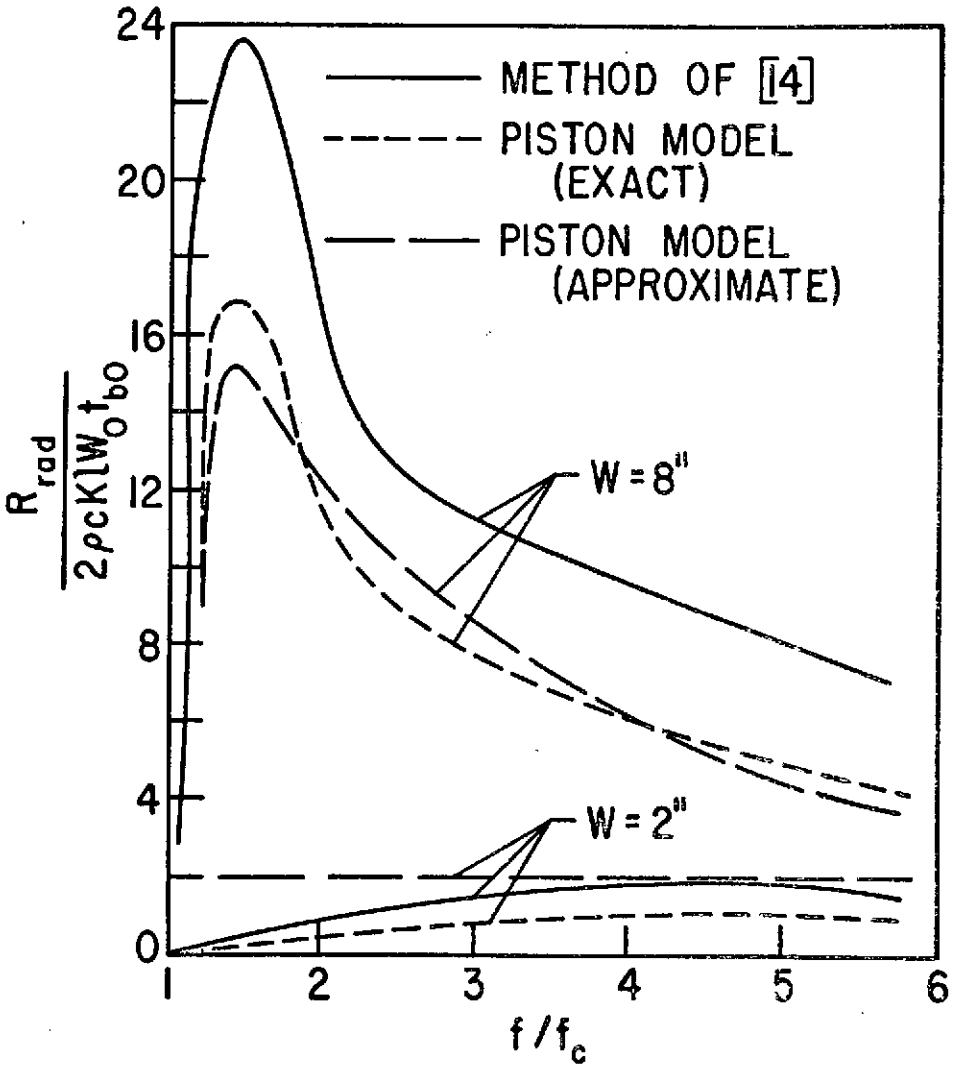

Figure 5.22 Radiation Parameter Versus Critical Frequency Ratio for the Piston Models and the Model of [14]

Equation (5.13) gave the radiated sound power for this case as

$$Pa = R_{rad} \langle \bar{V}^2 \rangle = (R_{rad}/\ell)(\ell \langle \bar{V}^2 \rangle) \quad , \tag{5.80}$$

The values of the radiation resistance for the three frequency ranges are given in Table 5.1 for the baffled beam as

$$R_{rad} = \begin{cases} \rho c W \ell \theta_o(KW) & \text{for } f > f_c \\ \frac{1}{2} \rho c W \ell \theta_o(KW) & \text{for } f \approx f_c \\ \rho c W^2 \theta_o(KW) & \text{for } f < f_c \end{cases} \tag{5.81}$$

for the square piston model based on beam width.

Defining the radiation efficiency as

$$\sigma = R_{rad}/(\rho c \ell W) \quad , \tag{5.82}$$

the sound power may be written as

$$Pa = \sigma(\rho c W) \langle \ell \bar{V}^2 \rangle \quad . \tag{5.83}$$

Table 5.5 is obtained from Figure 5.15 for a blade passage frequency of 240 Hz and harmonic frequencies for the two beams under consideration. A plot of the radiation efficiency (σ) versus frequency for the eight and four inch wide beams is shown in Figure 5.23.

Table 5.5 Radiation Efficiency for Different KW Values of Each Beam

f	K	KW (W=8")	KW (W=4")	θ_o (W=8")	θ_o (W=4")	σ (W=8")	σ (W=4")
240	0.11	0.88	0.44	0	0	0.02	0
480	0.22	1.76	0.88	0.30	0.09	0.08	0
720	0.33	2.64	1.32	0.67	0.15	0.34	0.08
960	0.44	3.52	1.76	0.92	0.35	0.92	0.35
1200	0.55	4.40	2.20	1.10	0.50	1.10	0.50
1440	0.66	5.30	2.64	1.12	0.65	1.12	0.65
1680	0.77	6.20	3.10	1.05	0.80	1.05	0.80
1920	0.88	7.00	3.50	1.00	0.92	1.00	0.92
2160	0.99	>7.00	3.96	1.00	1.05	1.00	1.05
2400	1.10	-	4.40	1.00	1.10	1.00	1.10
2640	1.21	-	4.85	1.00	1.12	1.00	1.12
2880	1.32	-	5.30	1.00	1.12	1.00	1.12
3120	1.43	-	5.65	1.00	1.10	1.00	1.10
3360	1.54	-	6.20	1.00	1.05	1.00	1.05
3600	1.65	-	6.60	1.00	1.00	1.00	1.00
3840	1.76	-	7.00	1.00	1.00	1.00	1.00

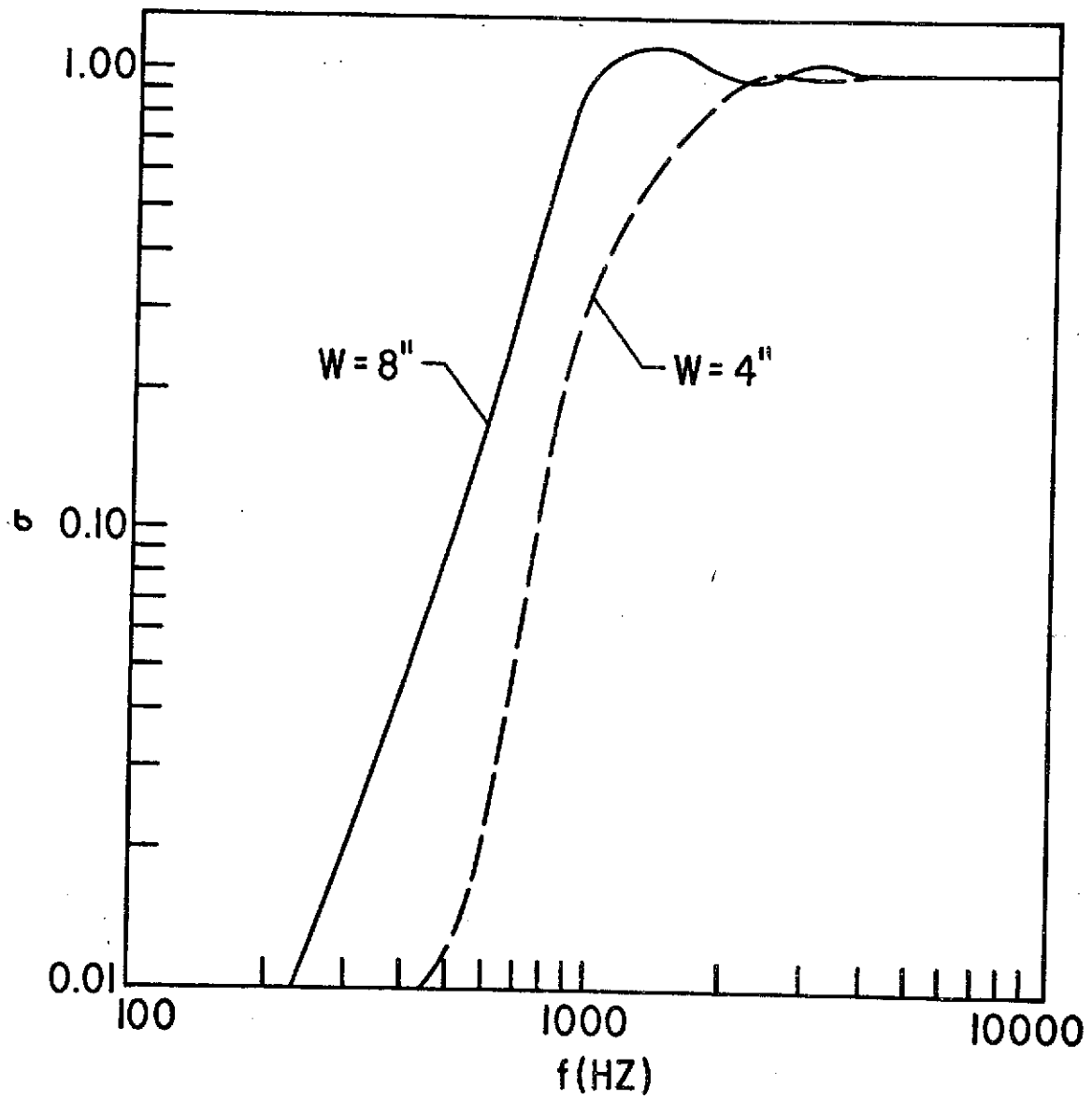

Figure 5.23 Radiation Efficiency Versus Frequency for the Eight and Four Inch Beam Widths

It has been observed experimentally that the force-frequency characteristics of the input force (F) and the frequency response characteristics of typical boards (H_n) are such that the acceleration response of the board ($\langle \bar{a}^2 \rangle$) is essentially constant over a wide frequency range. These quantities are in general related by

$$S_y(\omega) = S_f(\omega) \; |H(\omega)|^2 \quad , \tag{5.84}$$

where

$S_f(\omega)$ = input power spectral density = $F(\omega)/T$,

$S_y(\omega)$ = output power spectral density = $Y(\omega)/T$.

The quantities $F(\omega)$ and $Y(\omega)$ are the Fourier transforms of the input function F(t) and the response function y(t), respectively. In terms of the radiation resistance, the power expression for a constant acceleration - frequency spectrum is

$$Pa = R_{rad} \langle \bar{v}^2 \rangle = R_{rad} \langle \bar{a}^2 \rangle / \omega^2 \quad , \tag{5.85}$$

since for single frequency components

$$\langle \bar{v}^2 \rangle = \langle \bar{a}^2 \rangle / \omega^2 \quad . \tag{5.86}$$

Thus, for constant acceleration response, the mean-square velocity decreases with frequency as $1/\omega^2$. Figure 5.24 shows the mean-square

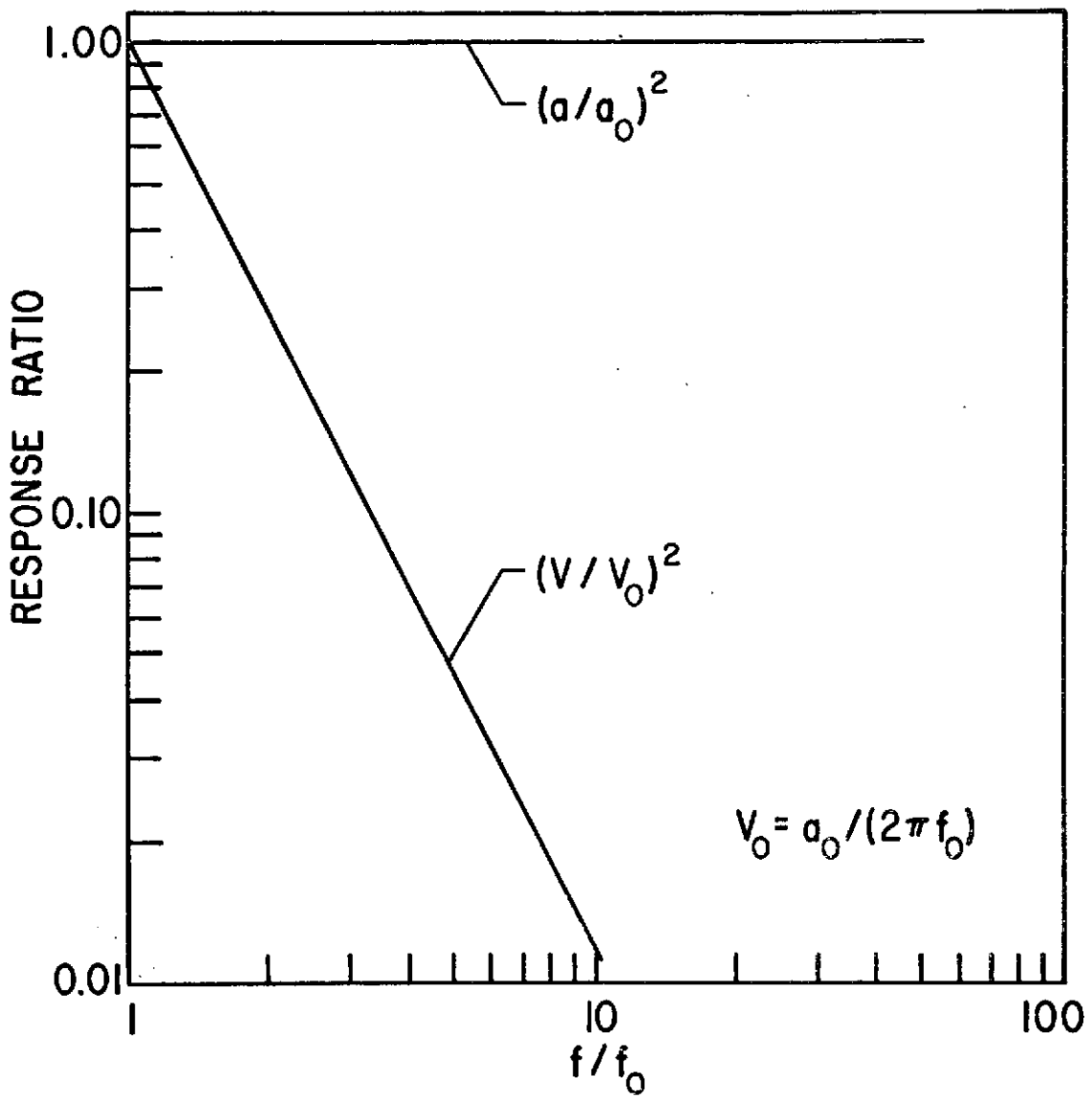

Figure 5.24 Response Ratios Versus Fundamental Frequency Ratio for Constant Acceleration

velocity frequency response under this assumption, plotted against a dimensionless frequency parameter f/f_o. It is convenient to take f_o as the fundamental blade passage frequency. Noting that $V_o = a_o/\omega$, the velocity ratio can be written as

$$(V/V_o)^2 = 1/(\omega/\omega_o)^2 = 1/(f/f_o)^2 \quad , \tag{5.87}$$

where $V_o = a_o/\omega_o = 2\pi f_o$.

Recalling the expression for radiated power

$$Pa = R_{rad} \langle\bar{V}^2\rangle = (R_{rad}/\ell) \langle\bar{V}^2/\bar{V}_o^2\rangle (\langle\bar{V}_o^2\rangle\ell) \quad ,$$

and using equation (5.83), gives

$$Pa = \rho c W \sigma \langle\bar{V}^2/\bar{V}_o^2\rangle (\langle\bar{V}_o^2\rangle\ell) \quad . \tag{5.88}$$

The variables in equation (5.88) are the product $\sigma\langle\bar{V}^2/\bar{V}_o^2\rangle$ and the beam width (W) since the quantity $\langle\bar{V}_o^2\rangle\ell$ is assumed to be constant. Combining the radiation resistance curves of Figure 5.23 and using Figure 5.24 for the velocity variation, results in Figure 5.26, which is a plot of $\sigma\langle\bar{V}^2/\bar{V}_o^2\rangle(W/W_o)$ versus the frequency ratio f/f_o. The frequency variation in the velocity term of equation (5.88) is accounted for by the factor $(\langle\bar{V}^2/\bar{V}_o^2\rangle)$ and the velocity amplitude, which depends on beam length, is taken into account by the term $\langle\bar{V}_o^2\rangle\ell$ shown in Figure 5.25.

The frequencies that contribute to the overall power output are noted from Figure 5.26 to be; (a) the fourth harmonic (f/f_o=4) for the

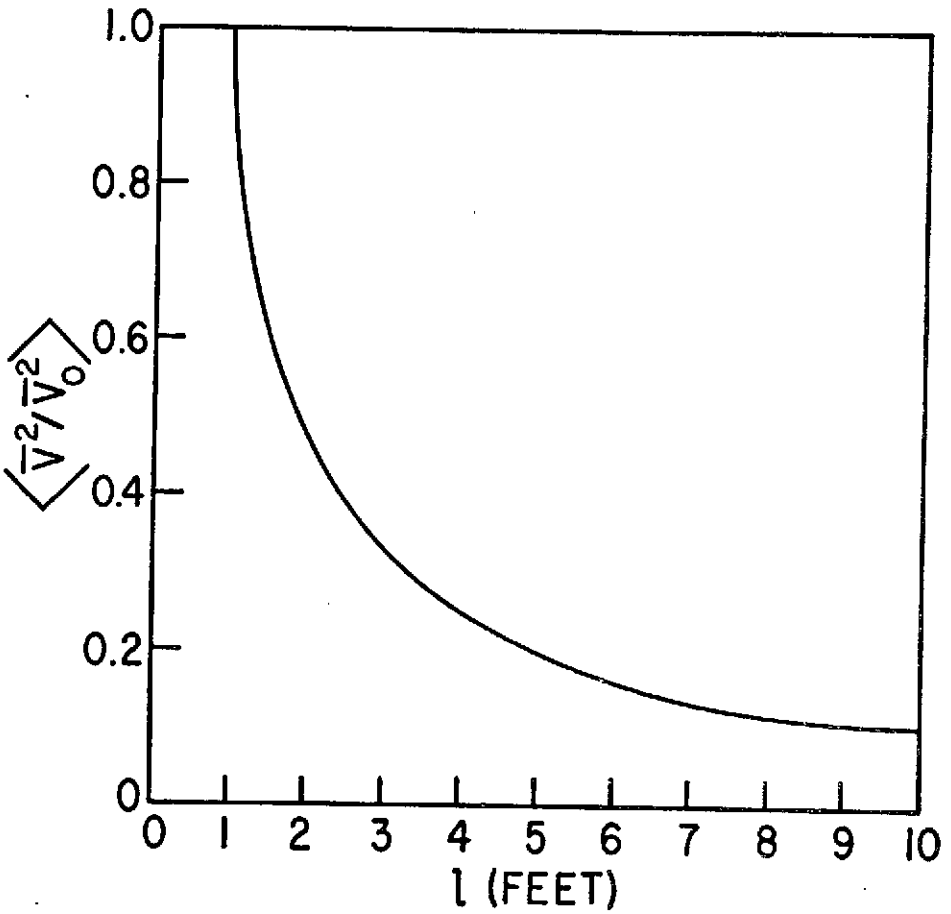

Figure 5.25 Mean-square Velocity Ratio Versus Beam Length for Constant $\langle \bar{v}^2/\bar{v}_o^2 \rangle_\ell$

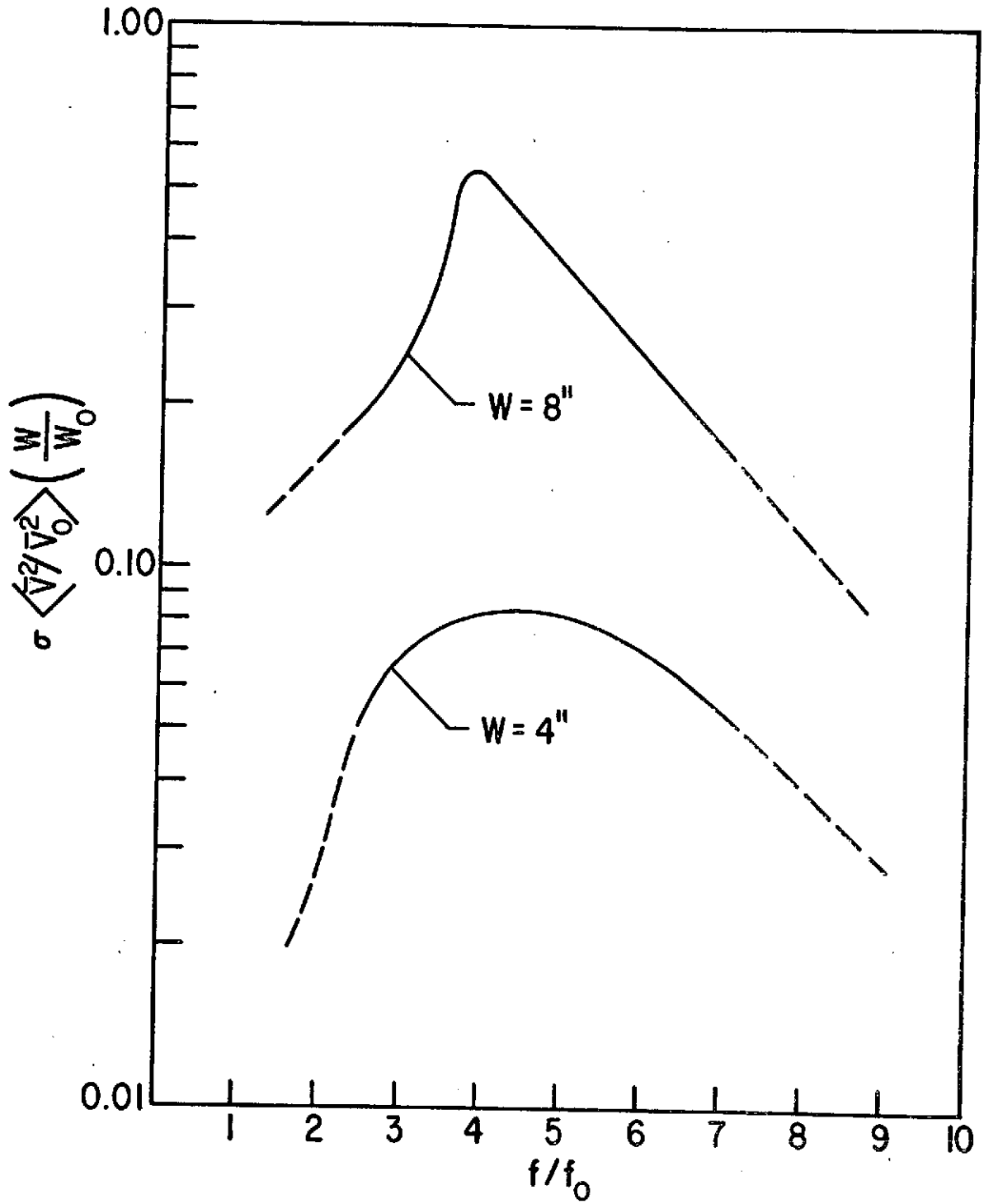

Figure 5.26 Acoustic Power Parameter Versus Fundamental Frequency Ratio for the Eight and Four Inch Beam Widths

eight inch beam, and (b) the fourth, fifth, and sixth harmonics (f/f_o = 4, 5, 6) for the four inch wide beam.

The discrete frequency sound power levels (L_W) can be obtained by defining a suitable reference power (P_o) and performing the operation $10 \log_{10}(P_a/P_o)$, thus

$$L_W(f/f_o) = 10 \log (P_a/P_o)$$

$$= 10 \log_{10}[(\sigma\langle\bar{V}^2/\bar{V}_o^2\rangle W)\ (\rho c)\ (\ell\langle\bar{V}_o^2\rangle)/P_o] \quad ,$$

or

$$L_W(f/f_o) = 10 \log_{10}[\sigma\langle\bar{V}^2/\bar{V}_o^2\rangle W] + 10 \log_{10}[\ell\langle\bar{V}_o^2\rangle] + 10 \log_{10}[\rho c/P_o] \quad , \tag{5.89}$$

where the first term is obtained from Figure 5.26 and the second term is specified experimentally or calculated from energy considerations.

When the value of $\langle\bar{V}^2\rangle$, the mean-square velocity, is known as a function of frequency for the board under consideration, equation (5.89) can be written in the more useful form

$$L_W(f/f_o) = 10 \log_{10}[\sigma] + 10 \log_{10}[W] + 10 \log_{10}[\ell] + 10 \log_{10}[\langle\bar{V}^2\rangle] + 10 \log_{10}[\rho c/P_o] \quad . \tag{5.90}$$

The radiation efficiency (σ) is plotted versus frequency in Figure 5.23 for the beam widths of interest.

Equation (5.89) can be simplified by making an approximation based on the frequencies at which the beams radiate significant power. The fourth and fifth harmonics ($f/f_o = 4, 5$) correspond to frequencies of 960 and 1200 Hz which are near the critical frequency for typical beam thicknesses (see Figure 5.3). The approximation from Table 5.1 for the radiation resistance of a baffled beam for $1<KW<4$ is

$$R_{rad} = \rho c W \ell \sigma = \frac{1}{4} \rho c K W^2 \ell \quad , \tag{5.91}$$

so that

$$\sigma = \frac{1}{4} KW \quad . \tag{5.92}$$

Substituting equation (5.92) into equation (5.89) gives

$$\begin{aligned} L_W(\omega) = {} & 10 \log_{10}[\tfrac{1}{4} KW^2 \langle \bar{V}^2/\bar{V}_o^2 \rangle] \\ & + 10 \log_{10}[\ell \langle \bar{V}_o^2 \rangle] \\ & + 10 \log_{10}[\rho c/P_o] \quad . \end{aligned} \tag{5.93}$$

Using the relationship $K = \omega/C_a = 2\pi f/C_a$ gives

$$\begin{aligned} L_W(f) = {} & 10 \log_{10}[W^2] + 10 \log_{10}[\langle \bar{V}^2/\bar{V}_o^2 \rangle f] \\ & + 10 \log_{10}[\pi \rho_a/(2P_o)] + 10 \log_{10}[\ell \langle \bar{V}_o^2 \rangle] \quad . \end{aligned} \tag{5.94}$$

From equation (5.87), $(V/V_o)^2 = 1/(f/f_o)^2$,

so that

$$f \langle \bar{V}^2/\bar{V}_o^2 \rangle = f_o^2/f \quad , \tag{5.95}$$

and

$$L_W(f) = 10 \log_{10}[W^2] + 20 \log_{10}[f_o] + 10 \log_{10}[\pi\rho_a/(2P_o)]$$
$$+ 10 \log_{10}[\ell\langle\bar{V}_o^2\rangle] - 10 \log_{10}[f] \quad . \tag{5.96}$$

The unbaffled beam at frequencies near the critical frequency differs from the baffled case (equation (5.88)) by a factor of two. The sound power level, under identical conditions, would be three decibels greater for the unbaffled beam.

In the immediate vicinity of the critical frequency, where the sound radiation is concentrated, the last four terms of equation (5.96) are the same for either beam and represent an additive constant. In this case the sound power output proportionality is

$$L_W(f=f_c) \sim 10 \log_{10}[W^2] = 20 \log_{10}[W] \quad . \tag{5.97}$$

The power produced is observed to depend primarily on beam width and increases six decibels for each doubling of beam width. The assumptions made in reaching this conclusion are met for most planing operations and

the six decibel increase in radiated power has been observed experimentally for a wide variety of operations.

5.5.2 A Numerical Calculation of Radiated Sound Power

To compute the actual value of the radiated sound power for each beam, equation (5.89) is utilized, i.e.;

$$L_W(f/f_o) = 10 \log_{10}[\sigma \langle \bar{V}^2/\bar{V}_o^2 \rangle W] + 10 \log_{10}[\ell \langle \bar{V}_o^2 \rangle] + 10 \log_{10}[\rho c/P_o] \ . \qquad (5.98)$$

Using Figure 5.26 for the values of the first term in equation (5.98) gives the data shown in Table 5.6. Using a reference power of 10^{-13} watts, the quantity $10 \log_{10}[\rho c/P_o]$ is approximately 128 decibels under standard atmospheric conditions.

The product of board length and mean-square velocity in equation (5.98) is, in general, unknown. The velocity response of the board can be calculated, theoretically, by the methods of Chapter 4 or approximated using the energy considerations of Chapter 5. In either case the magnitude of the excitation force must be specified. This magnitude is difficult to ascertain either analytically or experimentally, since it is governed by the particular energy transfer mechanism between the cutterhead and the board. To facilitate the comparison of the theoretical and experimental results, a rough approximation of the quantity $\langle \bar{V}_o^2 \rangle \ell$ based on experimental data is utilized. For frequencies near the critical frequency, experiments indicate that typical values

are of the order of unity. Using $\ell\langle\bar{V}_o^2\rangle = 1$, equation (5.98) becomes

$$L_W(f/f_o) = 10 \log_{10}[\sigma\langle\bar{V}^2/\bar{V}_o^2\rangle W] + 128 \text{ dB} . \qquad (5.99)$$

The sound power output under this assumption for the eight and four inch board widths is presented in Table 5.7.

For a semireverberant environment, typical of most industrial plants, [11] relates the average sound pressure level at a specific radius (r) to the sound power level by

$$L_W = \bar{L}_p - 10 \log_{10}(1/S_H+4/R) - .5 \text{ dB} , \qquad (5.100)$$

where

L_W = sound power level in decibels (re 10^{-13} watts),

$\bar{L}_p$ = sound pressure level averaged on the surface of a hemisphere surrounding the source,

S_H = surface area of the test hemisphere ($2\pi r^2$), where r is the radius of the hemisphere in feet,

R = the room constant.

The expression for R is given by [11] as

$$R = \bar{\alpha}A_r/(1-\bar{\alpha}) ,$$

where $\bar{\alpha}$ is defined as the ratio of energy absorbed by the walls to the

Table 5.6 Radiation Efficiency Parameter for Several Values of the Fundamental Frequency Ratio

f/f_o	$\sigma\langle\bar{v}^2/\bar{v}_o^2\rangle_W$ (W=8")	$\sigma\langle\bar{v}^2/\bar{v}_o^2\rangle_W$ (W=8")	$10\log_{10}[\sigma\langle\bar{v}^2/\bar{v}_o^2\rangle_W]$ (dB) (W=8")	$10\log_{10}[\sigma\langle\bar{v}^2/\bar{v}_o^2\rangle_W]$ (dB) (W=4")
3	0.24	0.07	-6.25	-11.60
4	0.50	0.08	-3.00	-11.00
5	0.32	0.08	-5.00	-11.00
6	0.23	0.07	-6.40	-11.60

Table 5.7 Sound Power Level for Each Beam

f/f_o	L_W (dB) (W=8")	L_W (dB) (W=4")
3	121.75	116.40
4	125.00	117.00
5	123.00	117.00
6	121.60	116.40

energy incident on the walls and A_r is the total area of the reflecting surfaces. For typical rooms ($\bar{\alpha} \approx 0.2$) R ranges from 700 to 1000 ft^2, so that $4/R \approx 0.001$ and $1/S_H \approx 0.006$ at a radius of five feet from the machine. Thus $4/R + 1/S_H \approx 0.007$ so that $10 \log_{10}(0.007) \approx -22$ decibels. Equation (5.100) relating the sound power level and the sound pressure level for a radius of five feet, becomes

$$L_W = \bar{L}_p(r=5') + 22 \text{ dB} \quad ,$$

or

$$\bar{L}_p(r=5') = L_W - 22 \text{ dB} \quad .$$

The sound power levels and sound pressure levels at a radius of five feet from the machine for the two board widths are given in Table 5.8 along with the overall levels.

Table 5.8 Sound Power and Sound Pressure Levels for Each Beam

f/f_o	L_W (W=8")	$\bar{L}_p$ (W=8")	L_W (W=4")	$\bar{L}_p$ (W=4")
3	122.0	100.0	116.5	94.5
4	125.0	103.0	117.0	95.0
5	123.0	101.0	117.0	95.0
6	121.5	99.5	116.5	94.5
Overall (dB) Levels	L_W = 129	$\bar{L}_p$ = 107	L_W = 123	$\bar{L}_p$ = 101

6. EXPERIMENTAL INVESTIGATION OF WOOD PLANER NOISE

6.1 Introduction

The experimental program was directed primarily toward the noise produced by a single head surfacer, although many of the conclusions reached carry directly over to the more complex cases of double surfacers, moulders, and heavy duty planers. The experimental study is divided into the following areas:

(1) Identification of sources of planer noise.

(2) Identification of the factors influencing noise.

(3) Techniques of noise reduction.

(4) Practical noise control study areas.

The practical noise control study was concentrated in three major areas:

(1) Mechanical redesign of cutterheads to reduce the energy input into the board and thus the energy radiated as sound.

(2) Treatment of vibrating surfaces including techniques of damping, absorbing, and reflecting vibratory energy.

(3) Sound absorption techniques including the design of acoustic enclosures.

6.2 Reiteration of the Sources of Planer Noise

The noise sources which are considered to contribute to the overall planer noise problem were listed in Chapter 3 and are repeated here for convenience.

(1) Board radiation due to the vibration of the board itself.

(2) Anvil radiation caused by structural vibration.

(3) Aerodynamic noise produced by the rotation of the cutterhead near stationary surfaces.

(4) Noise produced by the electric motors used to power the cutterheads and feed works.

(5) Dust collection system noise.

(6) Noise produced by the vibration of machine surfaces such as feed beds and housings.

(7) Noise produced by the drive train system.

The contribution of each of these sources to the overall planer noise has been studied experimentally and will be discussed in Section 6.4. In order to study the effects of different sources and parameters on planer noise, a series of experiments were conducted using a cabinet type single surfacer installed in a suitable laboratory space. The data acquisition and analysis equipment used is described in the following section.

6.3 Data Acquisition and Analysis

The semireverberant laboratory space where the experimental program was conducted is shown in Figure 6.1. The location of the planer in the room is shown along with microphone positions referenced to the center of the machine cutterhead. The x-y-z coordinate positions correspond roughly to the recommended points on the surface of a hypothetical hemisphere, used to compute the radiated sound power. The substitution method was used to calibrate the room in accord with [11]. Reverberation time measurements were in good agreement with the room constant obtained using the reference sound source method for broadband noise.

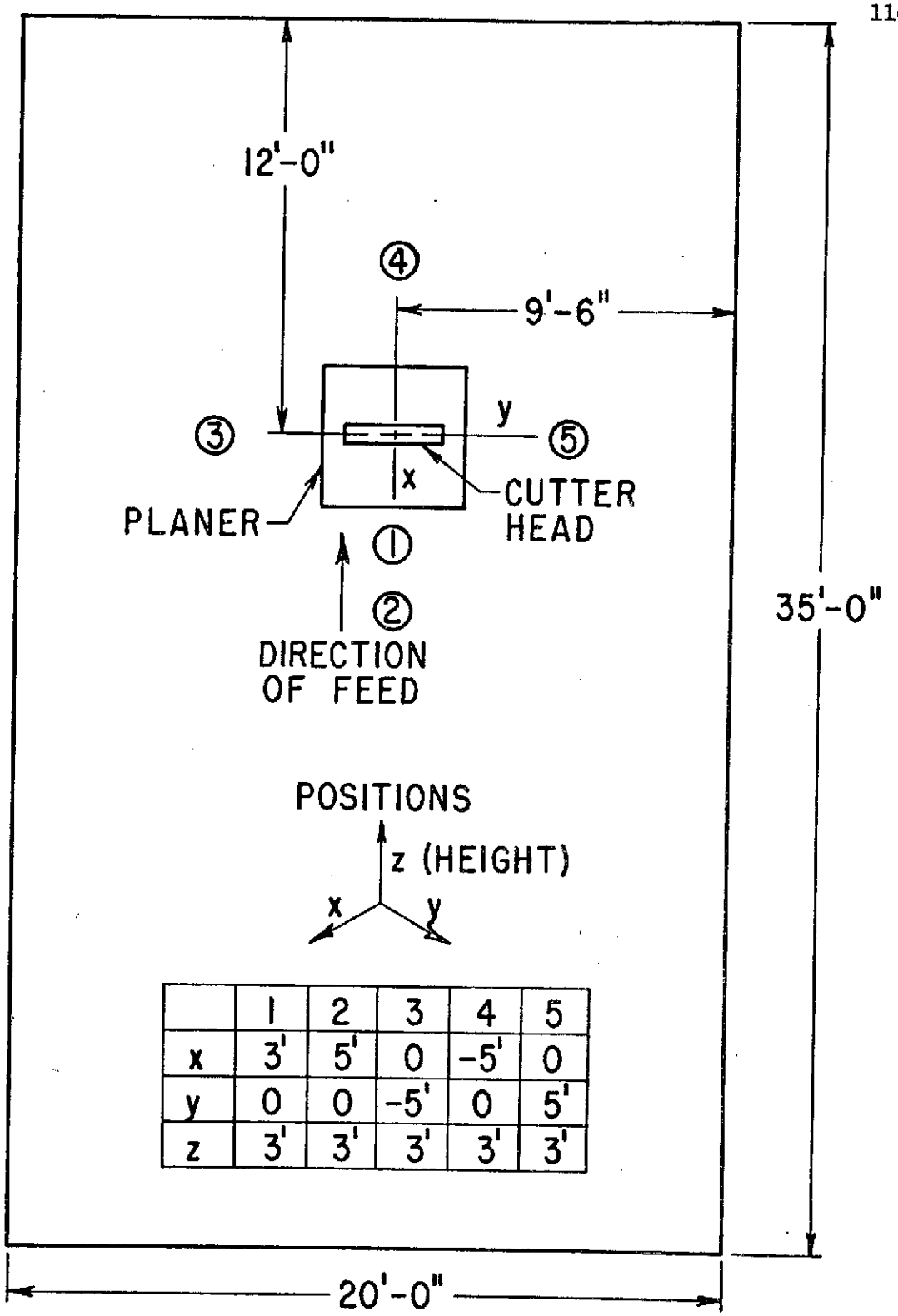

	1	2	3	4	5
x	3'	5'	0	-5'	0
y	0	0	-5'	0	5'
z	3'	3'	3'	3'	3'

Figure 6.1 Diagram of Laboratory Test Positions

Sound pressure level and board acceleration measurements were taken using the experimental arrangement shown in Figure 6.2. The two channel tape recorder was utilized since the simultaneous measurement of sound and vibration was necessary for correlation studies. The data analysis apparatus also shown consisted essentially of a one-third octave real time analyzer, which aided in the analysis of short duration signals, and a one percent narrow band analyzer, which was necessary in the detection of blade passage frequencies and harmonics. Tape loop capabilities were necessary in conjunction with the narrow band analysis of short duration signals.

An experimental setup was also devised to simulate planer noise by mechanically exciting boards. The arrangement consisted essentially of a square wave signal generator, which simulated the periodic impact of cutterhead knives, an amplification unit, and an electro-mechanical shaker. Correlation studies were easily achieved using this arrangement. The apparatus shown in Figure 6.2 was also used in connection with tire-plate suppression system studies, discussed later in this chapter.

6.4 Factors Influencing Planer Noise

Although several of the factors discussed here are interrelated to some degree, the individual effect on the total sound produced can essentially be considered independently. For example, if by tightening the pressure bar a noise reduction of five decibels is obtained and by using sharp knives another five decibel reduction is expected, then a planer operating with a tight pressure bar and sharp knives would be expected to produce ten decibels less noise than its

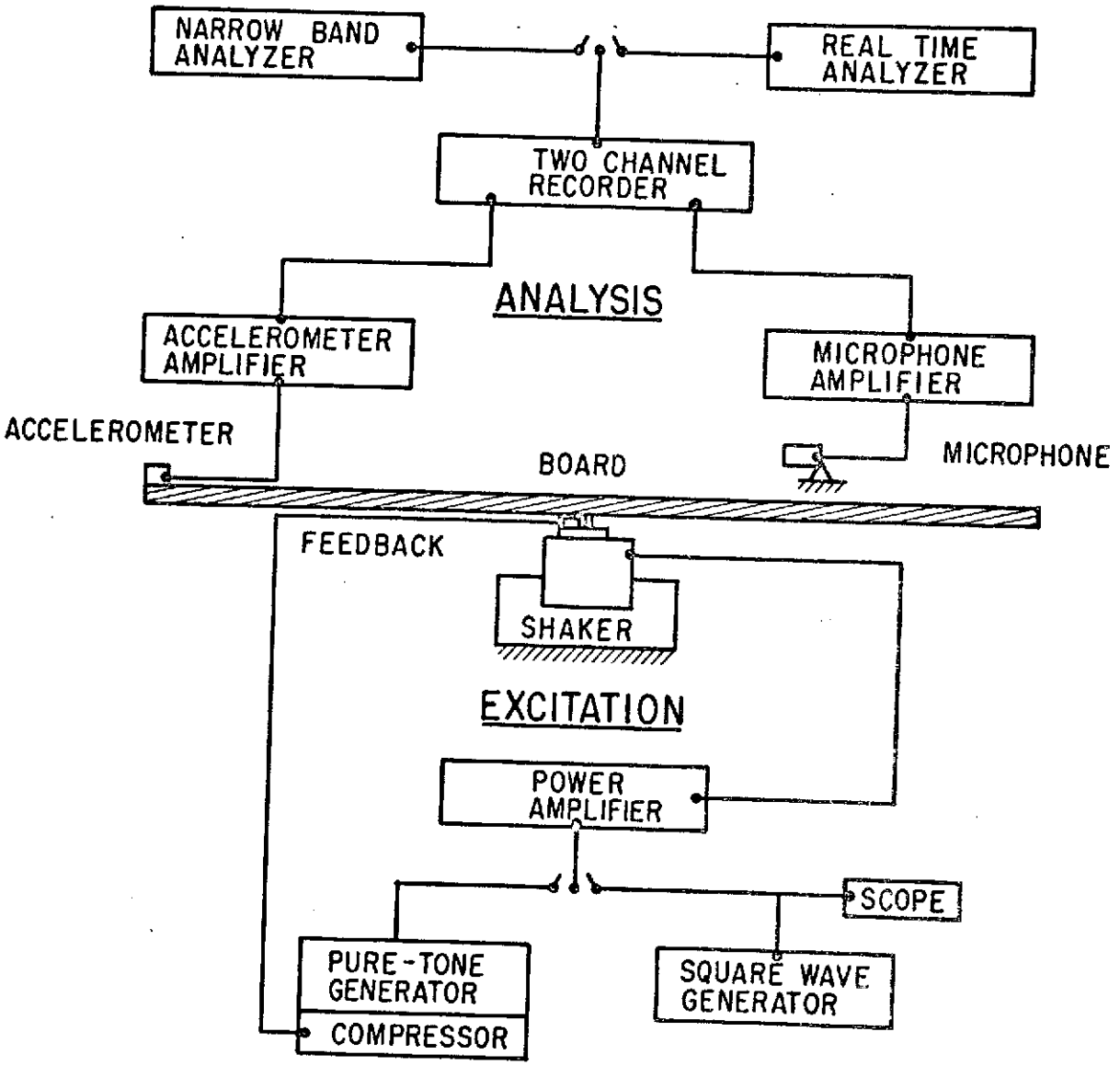

Figure 6.2 Diagram of Experimental Apparatus

counterpart with a loose bar and dull knives. The amount of reduction depends of course on the operating levels, hence the example cited above would be valid only for one particular machine and operating condition.

6.4.1 Board Width

Since board vibration is the major source of noise, board width serves as a measure of the energy input into the board, and thus is an indicator of the resulting sound produced. Since the energy delivered to the board per unit width is constant, the board can be considered to radiate like a series of unit sound radiators, with each unit width radiating a certain amount of the energy that is put into the board. Thus, the total energy input to a wide board is greater than that for a narrow board since more work must be done on the wider board. The power input to the board is a function of the velocity and force of the cutting knives. The power output in the form of sound energy is related to the surface area and transverse velocity of the board. For the case of board vibration, the source strength is related to the board surface area and the board velocity, where the velocity is a space-time average over the surface of the board.

Based on this physical reasoning, a series of tests were conducted to ascertain the variation in radiated sound power with board width. This was accomplished by measuring the sound pressure levels at four locations around the machine for various board widths holding other parameters constant. Using the methods [11], sound power levels were computed from the average sound pressure levels. Figure 6.3 shows

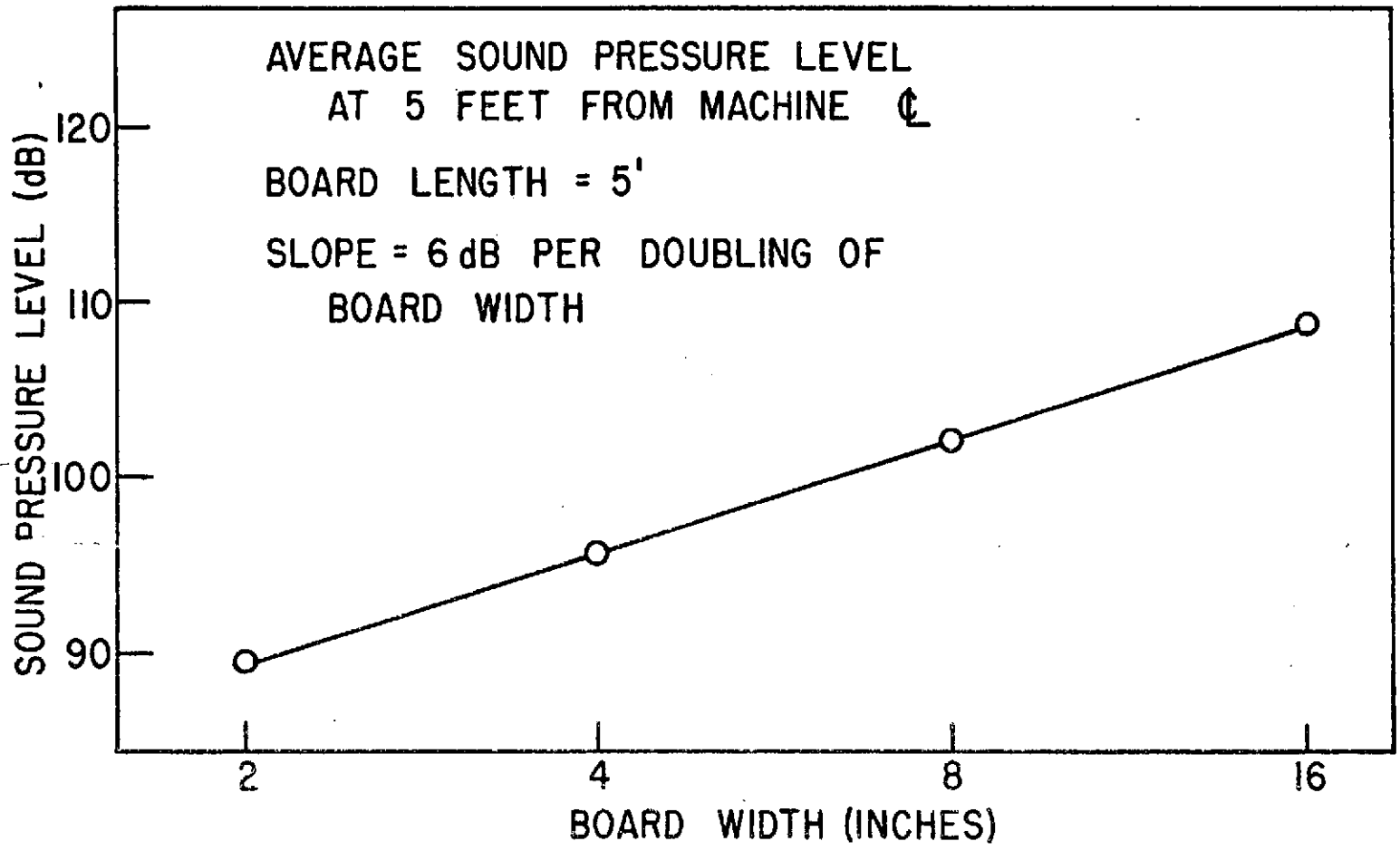

Figure 6.3 Increase in Sound Pressure Level with Board Width

the results of these measurements and indicates a six decibel increase in sound power for each doubling of board width.

6.4.2 Board Length

The length of the board is not so simply related to the resulting sound field since the energy transmitted to the board from the cutterhead tends to be distributed along the board longitudinally. As a result of this spreading out of the vibrational energy, the total sound emission is not dependent on the length of the board, since changes in surface velocity due to variations in length are counterbalanced by a change in the surface area of the board (length times width). Noise level measurements for various length boards, shown in Figure 6.4, indicate that the length of the board, alone, does not influence the sound levels produced. The acceleration levels, however, are significantly increased as board length is decreased. The product of board surface area and acceleration remains essentially constant. The relationship between sound pressure level (noise level), acceleration level (g level), and board length for a double surfacer and the single surfacer studied is shown in Figures 6.5 and 6.6. These figures show that although the acceleration levels are lower for the longer boards, the product of acceleration level and board length remains constant. The decrease in acceleration level of approximately three decibels per doubling of length is shown in Figure 6.7 for both the single and double surfacer.

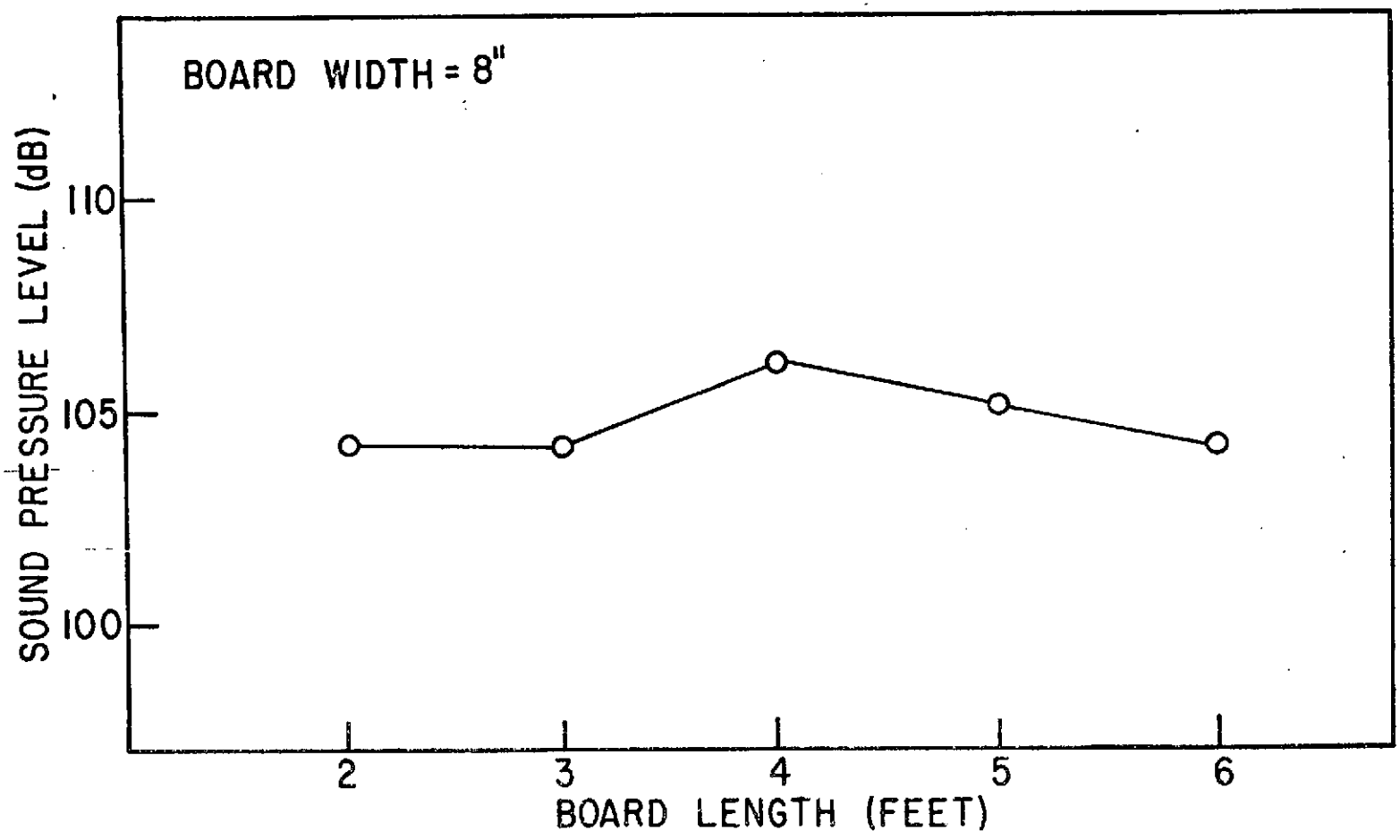

Figure 6.4 Sound Pressure Level Versus Board Length

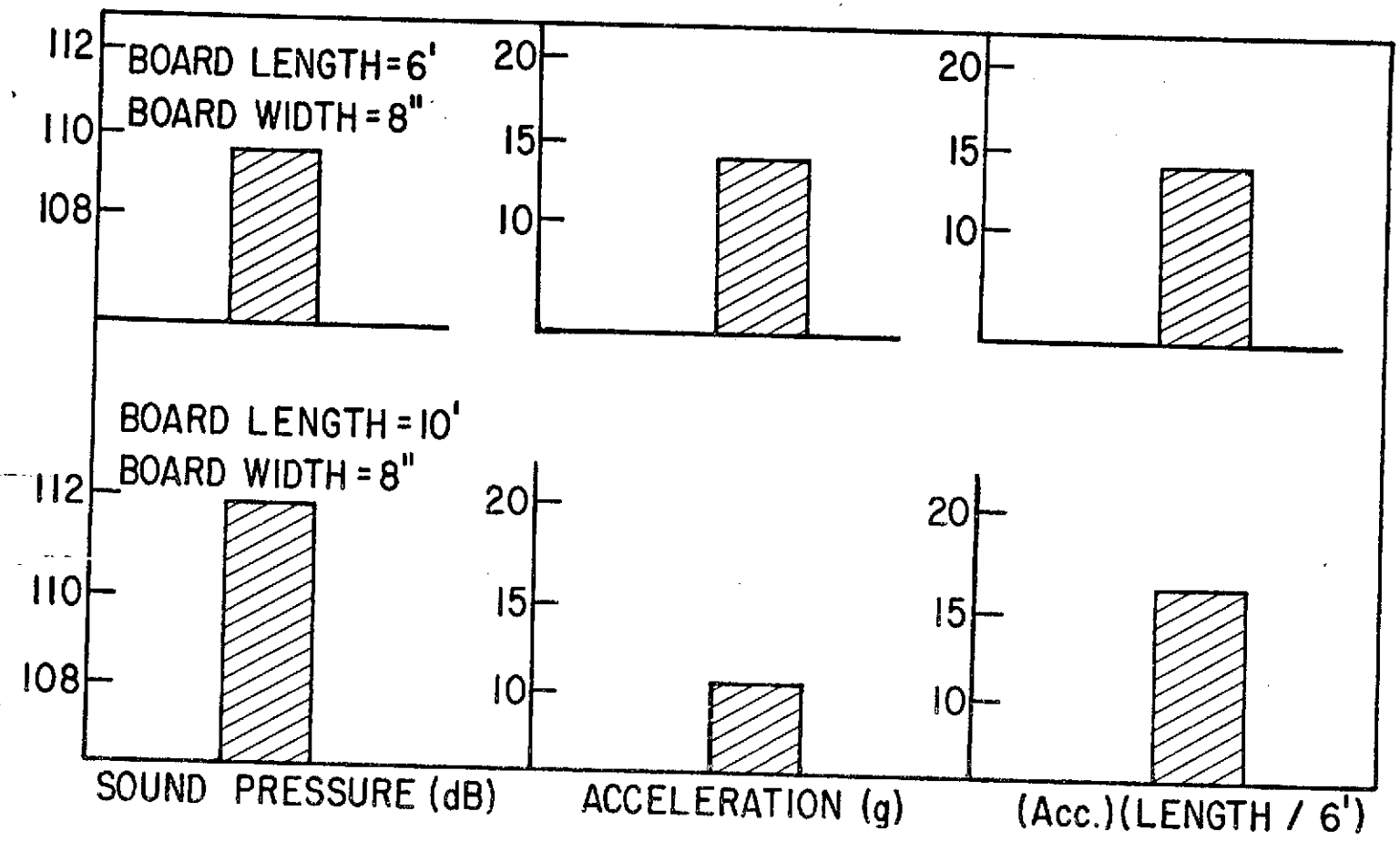

Figure 6.5 Relationship Between Sound Pressure Level, Acceleration, and Board Length for a Double Surfacer

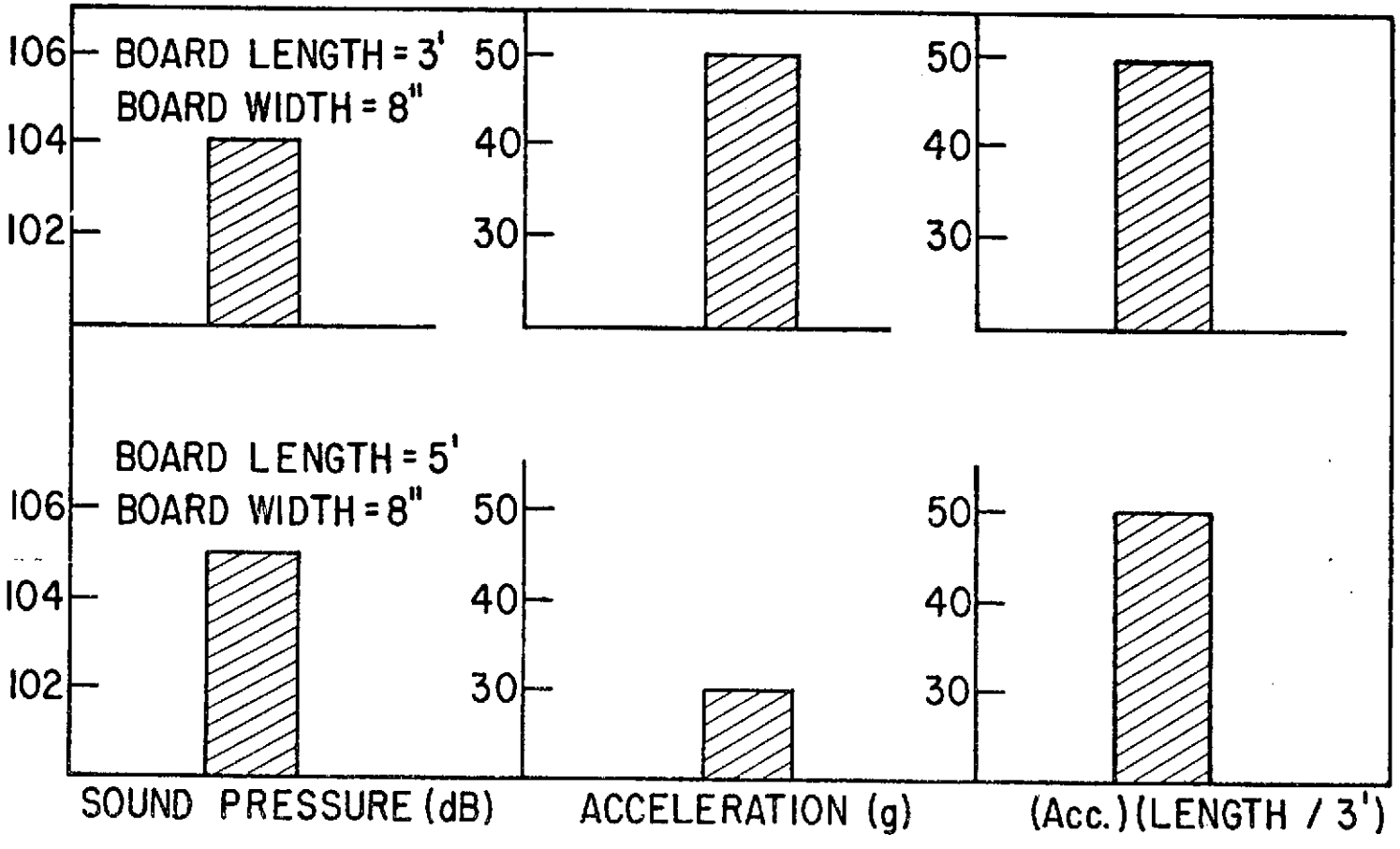

Figure 6.6 Relationship Between Sound Pressure Level, Acceleration, and Board Length for a Single Surfacer

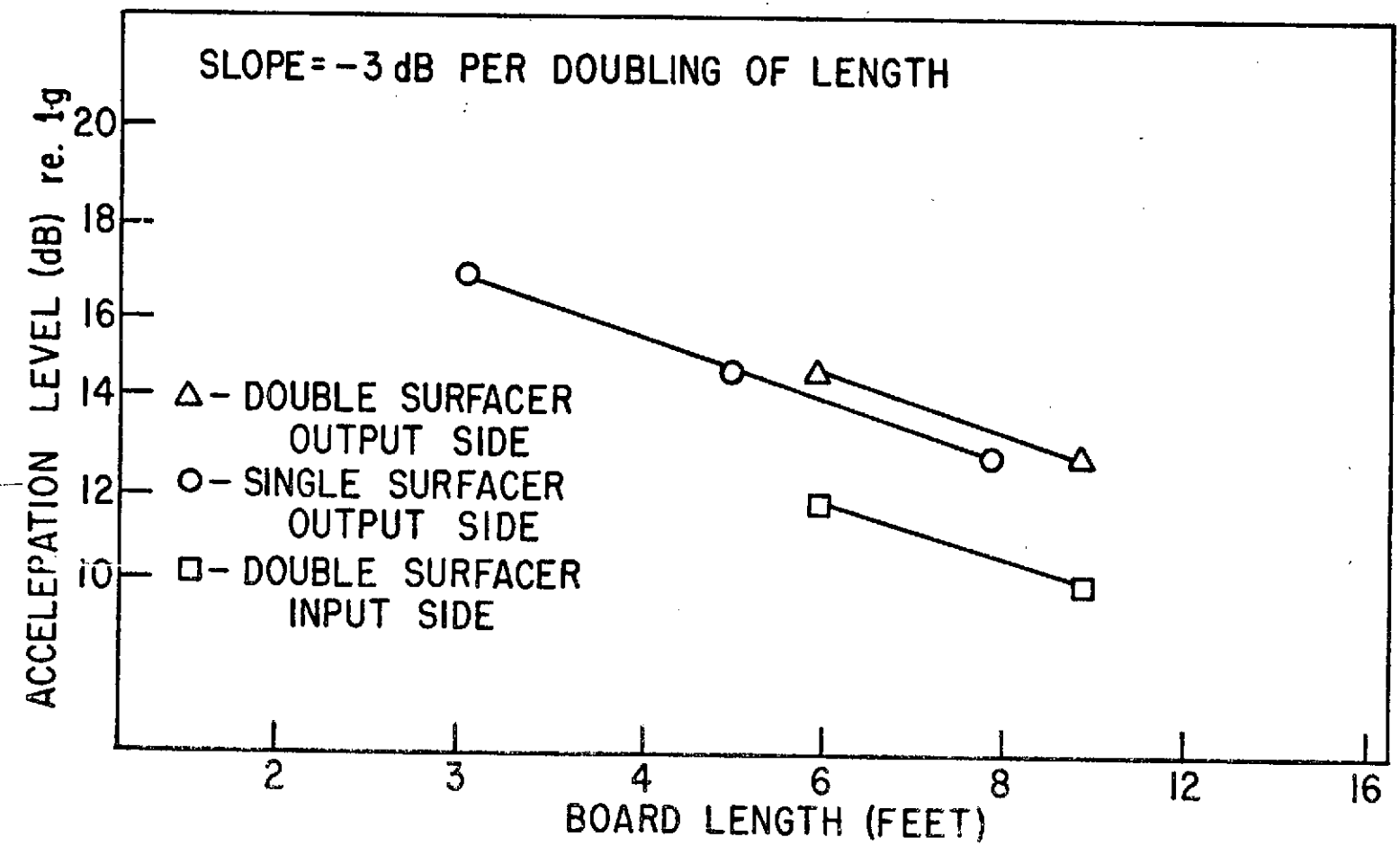

Figure 6.7 Decrease in Acceleration Level with Board Length

6.4.3 Board Species

The species of wood being cut has a marked effect on the frequency range of board response. The board responds to some extent at all forced frequencies and harmonics; however, the frequencies of maximum response, corresponding to strong board resonances, are significantly affected by the type of wood being planed. The natural frequencies for a beam of rectangular cross section can be expressed by

$$\omega = \beta(n)(EIg_c/\rho_b\Omega)^{1/2}$$

where the coefficient β depends on the length, boundary conditions, and mode of vibration (n).

Here,

ω = natural frequency,

E = modulus of elasticity,

ρ_b = density,

Ω = cross sectional area,

I = moment of inertia.

The material properties in the equation above are the modulus (E) and the density (ρ_b). Examining the ratio of E/ρ for several board species provides a means of determining the frequency range of maximum board response. Typical values for the ratio of E/ρ_b, normalized on red oak are given in Table 6.1.

Table 6.1 Ratio of E/ρ_b for Different Wood Species

Material	Normalized $\overline{E/\rho_b}^*$
Red Oak	1.0
Pine (short leaf)	1.2
Cedar	0.6

*Values taken from the Handbook of Chemistry and Physics for dry wood.

The values shown above indicate that pine should have a frequency range of maximum response that is higher than red oak, while cedar would respond better in the frequency range corresponding to the lower harmonics of the blade passage frequency. The ratio of I/Ω is proportional to be board thickness squared and also affects the frequencies at which maximum response can be expected. The effect of board thickness on the sound produced is discussed elsewhere in this section.

An experimental analysis of the sound and vibration levels for pine and oak boards indicates a difference in the frequency content of the spectra. The one-third octave plot of Figure 6.8 shows that the sound energy produced by the pine boards is concentrated at higher frequencies than that corresponding to oak boards. The modulus of elasticity and density, as well as variations in internal damping, stiffness, and energy required to remove a chip, are primarily responsible for these differences. The moisture content of the wood could also possibly affect the degree of internal damping and thus the sound produced.

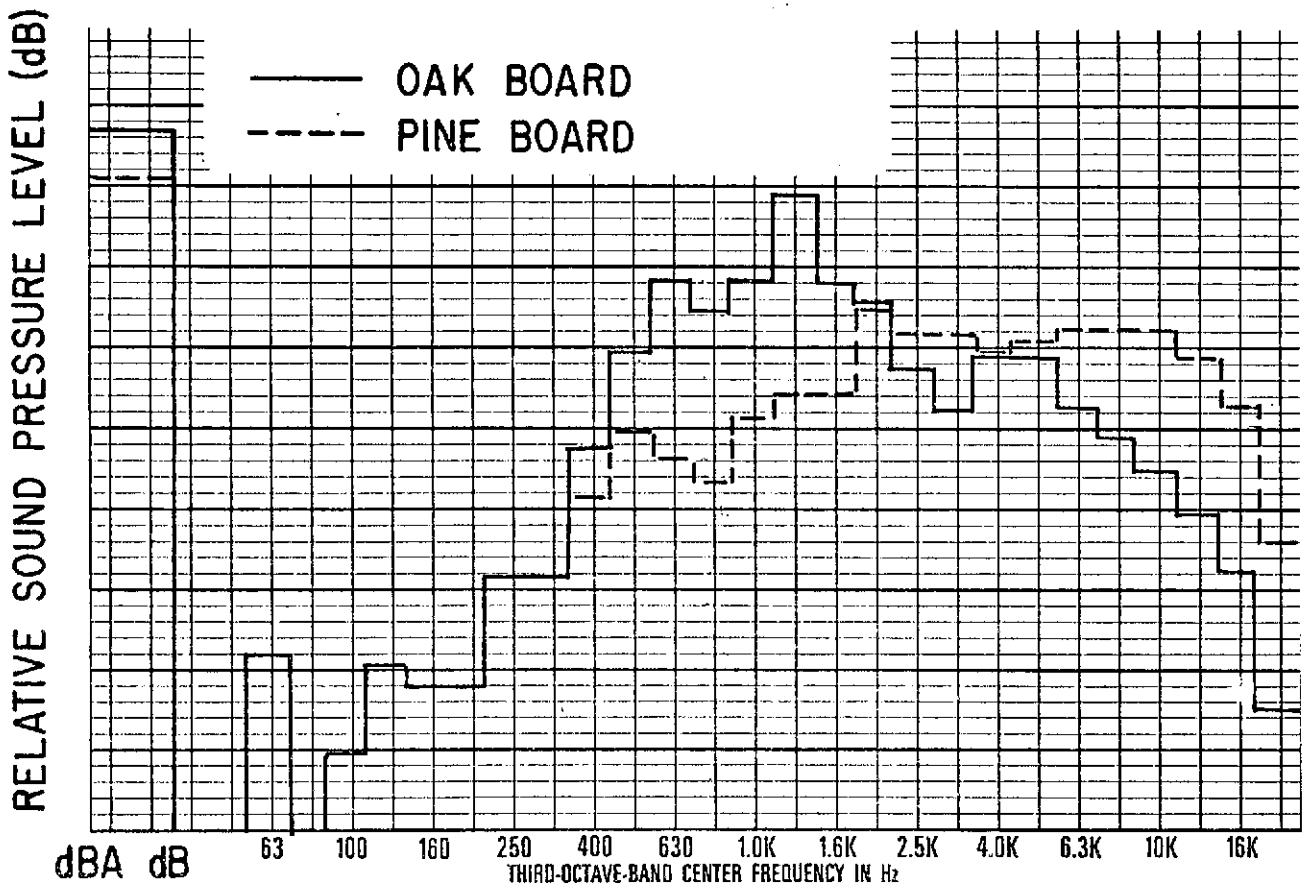

Figure 6.8 Comparison of Sound Pressure Spectra for Oak and Pine Boards

6.4.4 Board Thickness

Although the thickness of the board does not appreciably affect the overall sound pressure level produced, the board thickness does affect the natural frequencies of board vibration. Since the board will respond well only when a natural frequency is close to a forced frequency or harmonic, the effect of board thickness is much the same as that of board species, i.e. it changes the frequency range of maximum board response.

Measurements made on six, eight, and ten inch wide boards having original thickness ranging from 3/8 to 1 and 3/8 inches, indicate no noticeable trend in the overall noise levels produced. The variation in noise level with different board thickness, shown in Figure 6.9, is well within experimental accuracy.

6.4.5 Depth of Cut

The depth of cut does not noticeably affect the vibration or sound spectra for depths ranging from 1/16 to 1/8 of an inch. This result would be expected to apply to any planing operation provided constant blade contact and smooth cutting are maintained. As cut depths are greatly increased or decreased, extraneous factors associated with non-uniform cutting tend to make noise analyses impractical. For an extremely shallow cut, surface irregularities, as well as unequal knife tip radii, result in intermittent cutting and an unsteady sound field.

6.4.6 Sharpness of Knives

Noise levels produced by the planer, for similar cutting operations, increase as the knives become dull, since the force required to

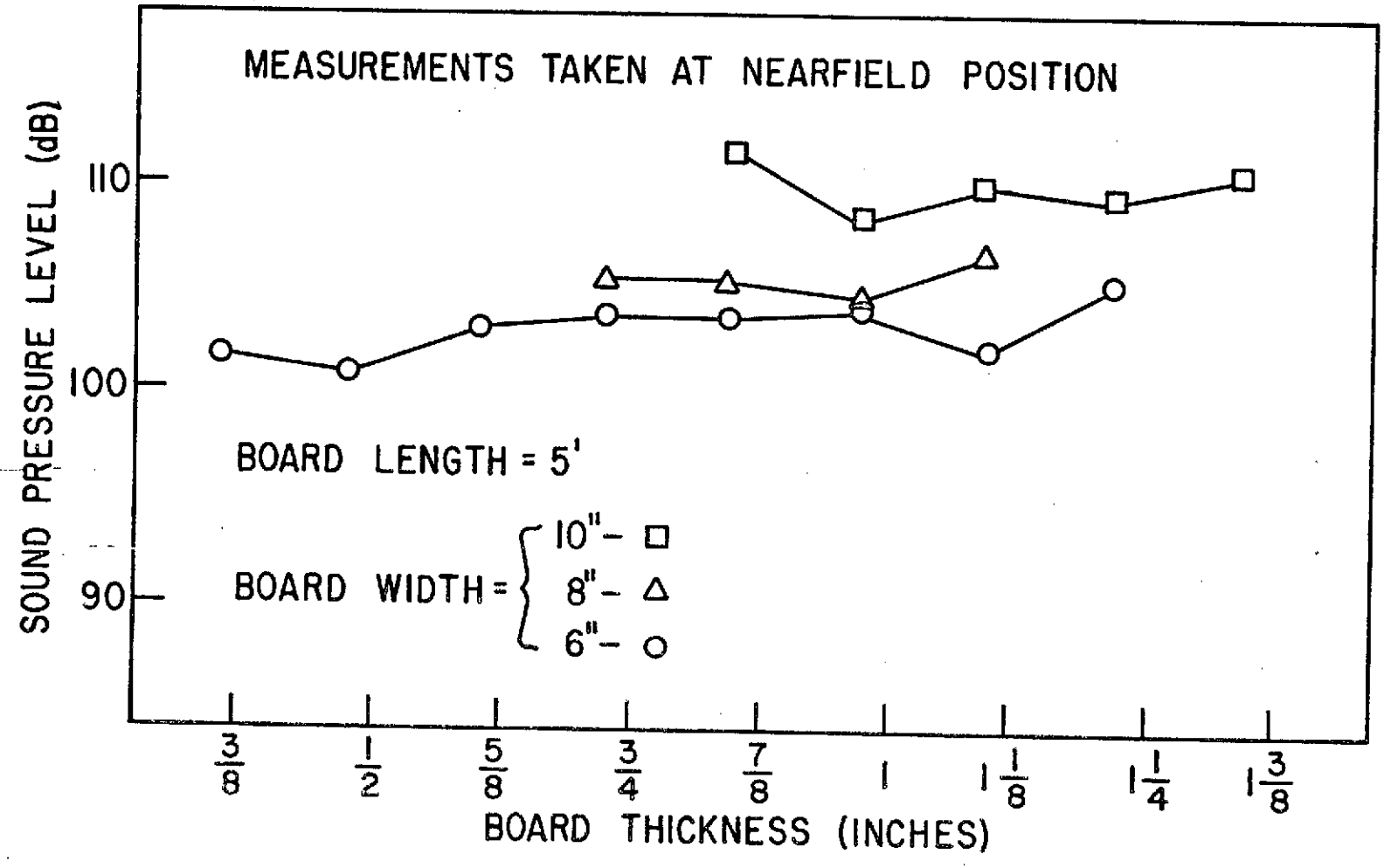

Figure 6.9 Variation in Sound Pressure Level with Board Thickness

remove chips increases and thus the force transmitted to the board is increased. This results in an increased energy input into the board, part of which may be dissipated as sound.

Detailed experimental results relating the variation in noise level to knife sharpness are not available. However, measurements taken over long periods of time have indicated a substantial increase in noise levels as the knives become dull.

6.4.7 Pressure Bar Tightness

The firmness with which the board is held against the anvil structure by the pressure bar greatly affects the magnitude of board vibration and thus the noise produced. The firm contact of the pressure bar on the surface of the board reduces the magnitude of the board response to the periodic impact of the knives. The sound pressure level decrease associated with a tight pressure bar is directly correlated to the corresponding reduction in board acceleration level. The effect of pressure bar tightness on board vibration and the resulting noise level is shown in Figure 6.10.

6.4.8 Machine Feed Speed

The input feed speed does not appreciably affect the noise levels produced for speeds ranging up to several hundred feet per minute. As the feed speed is appreciably increased, however, the sound and vibration signals become transient in nature and are difficult to measure accurately.

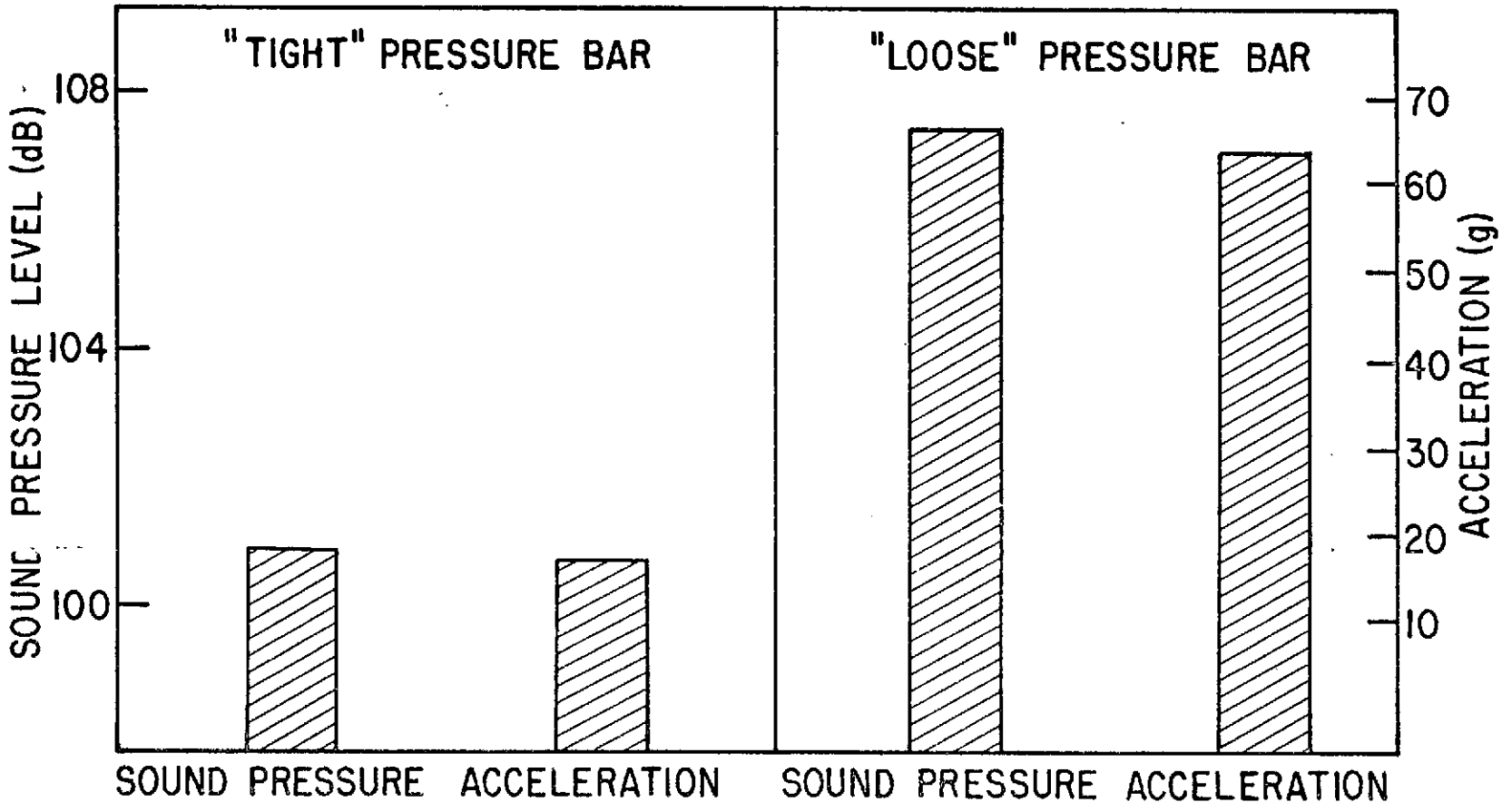

Figure 6.10 Sound Pressure and Acceleration Levels for Operation with the Pressure Bar in the "Tight" and "Loose" Positions

6.4.9 Chipbreaker Mechanism

The chipbreaker mechanism, in addition to its normal function, is observed to act to some degree as a vibration suppressor. The chipbreaker reduces the magnitude of vibrations propagated along the board, and thereby reduces the noise produced by that portion of the board. The mechanism governing this phenomena is believed to be a combination of the chipbreaker acting as (1) a barrier of block of weight added to the board reducing the propagated vibration and, (2) a vibration isolator or absorber at certain "tuned" frequencies. It has also been suggested that the physical effect of the chipbreaking on the mechanism of chip removal contributes to the reduced noise levels. The effectiveness of the chipbreaker as a noise suppressor depends in part on on the pressure exerted on the board, the stiffness of the springs used in the chipbreaker, and the nature of the contact made with the board.

The effect of the chipbreaker on the planer noise level has been investigated experimentally by operating the planer with the chipbreaker completely removed. The noise levels measured, shown in Figure 6.11, increase by approximately ten decibels when compared to a similar operation with the chipbreaker in place.

The chipbreaker, unlike the board, responds well only at frequencies centered around the 500 and 6300 Hz bands. The spectrum of Figure 6.12 shows that 480 Hz is a harmonic of the forcing frequency, while the 6000 Hz component is probably a purely resonant type response. The isolated frequencies of chipbreaker response indicate that a "tuned vibration absorber" effect may be obtained by adjusting the chipbreaker spring stiffness to respond well at certain frequencies. The mechanism

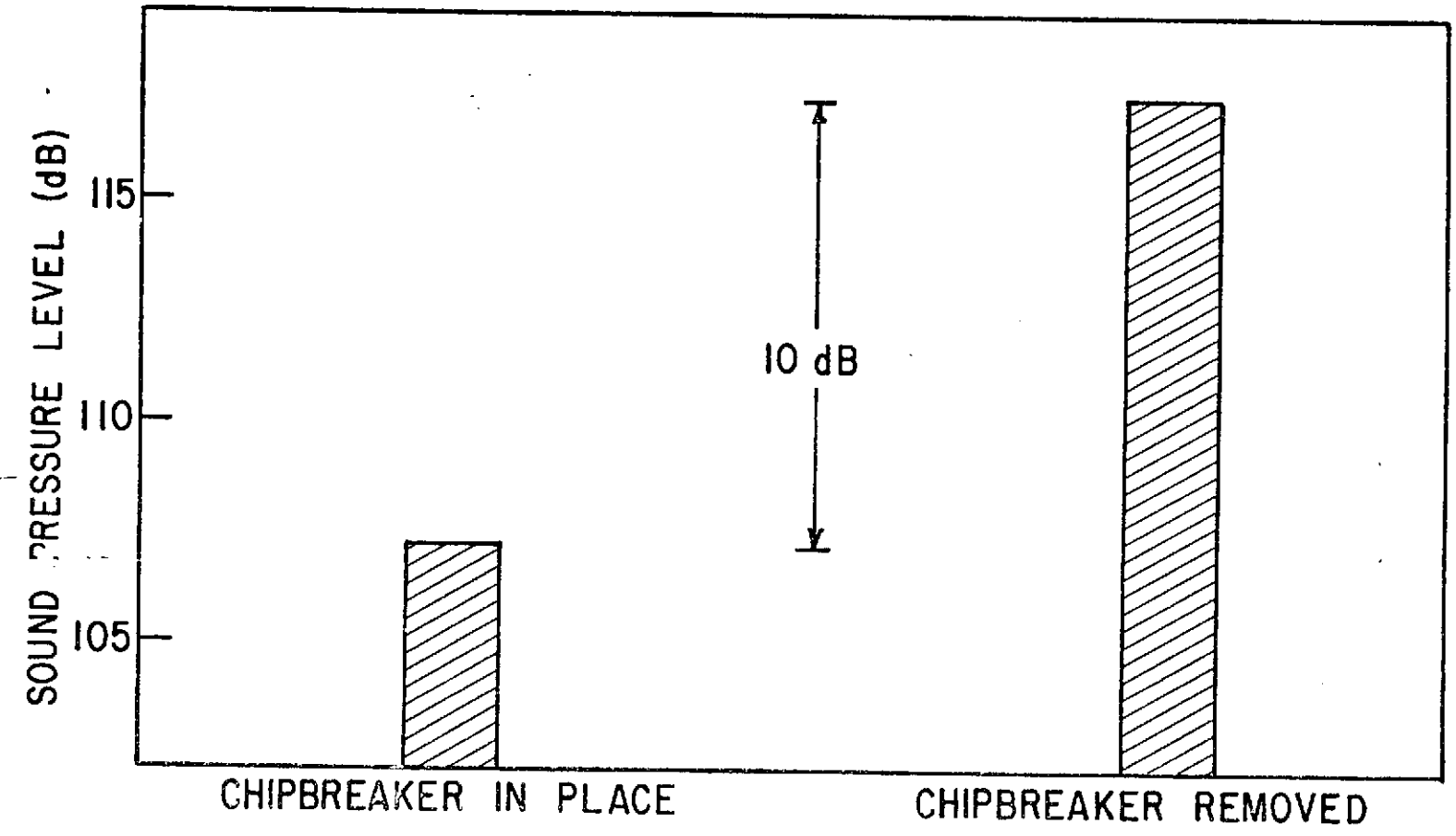

Figure 6.11 Comparison of Sound Pressure Level for Operation with and without the Chipbreaker

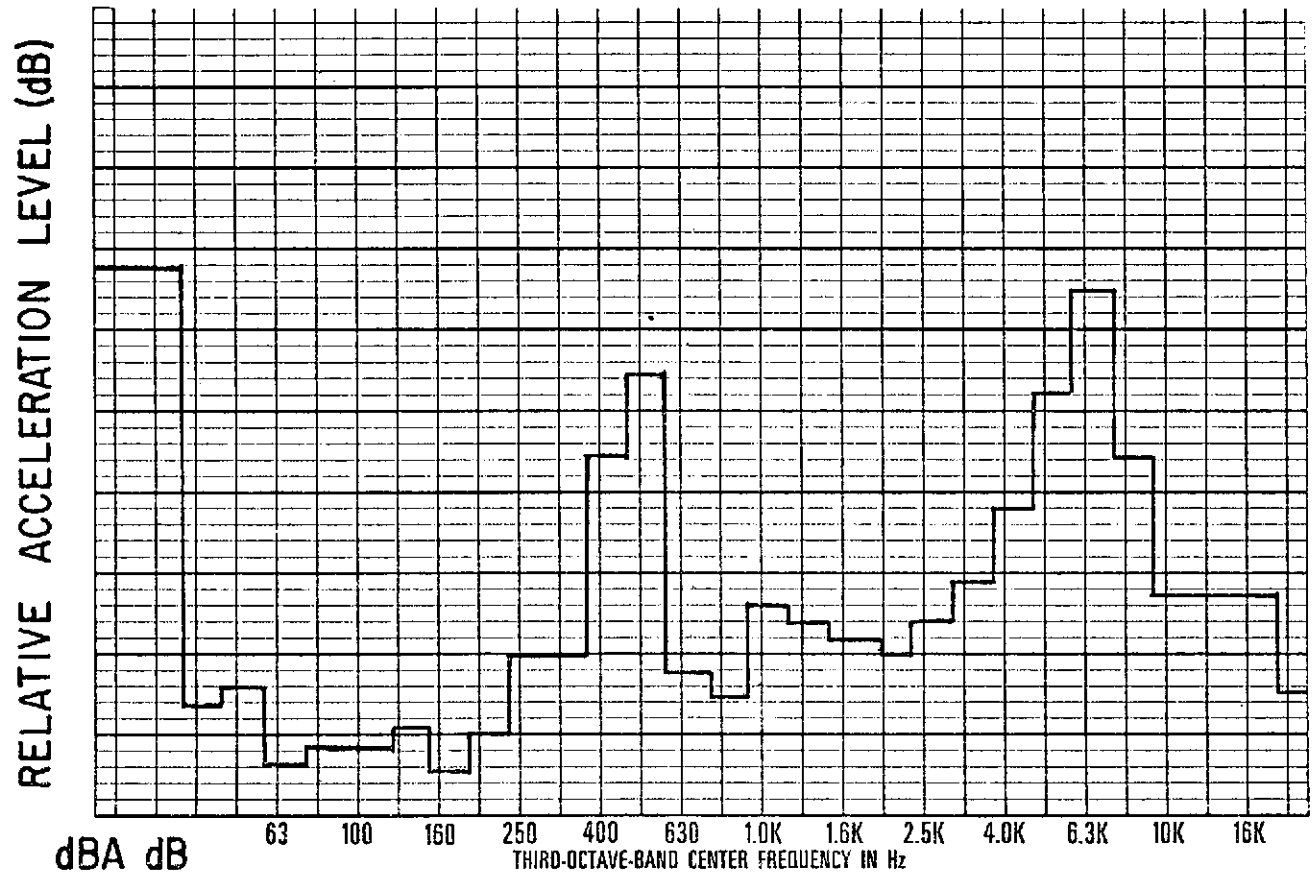

Figure 6.12 Acceleration Spectrum for the Chipbreaker Mechanism

involved in the sound attenuation obtained using the chipbreaker is being studied experimentally in order to optimize chipbreaker design and devise other apparatus to attenuate the longitudinal propagation of vibration along the board.

The chipbreaker has also been utilized to indicate the nature of the force imparted to the board by the knives. Since the chipbreaker responds well at only a few frequencies, the accelerometer readings taken on the surface of the chipbreaker can be used to indicate the duration and frequency of the impulse created upon blade impact. An oscilloscope trace of the chipbreaker acceleration response as a function of time is shown in Figure 6.13. The high frequency oscillation of the signal can be directly related to the observed resonant response of the chipbreaker at 6000 Hz in Figure 6.12. By counting the number of cycles completed per centimeter in Figure 6.13, the resonant frequency of the chipbreaker can be calculated. The pulse duration and spacing can also be obtained from the figure for a given oscilloscope sensitivity. The natural frequency of the chipbreaker is found from:

$$f = \frac{3 \frac{\text{cycles}}{\text{cm}}}{.5 \frac{\text{msec}}{\text{cm}}} = 6 \frac{\text{cycles}}{\text{msec}} = 6000 \text{ Hz}$$

6.4.10 Cutterhead Design

The noise produced by the cutterhead and knives can be grouped into two categories; (1) aerodynamic noise and (2) noise produced by

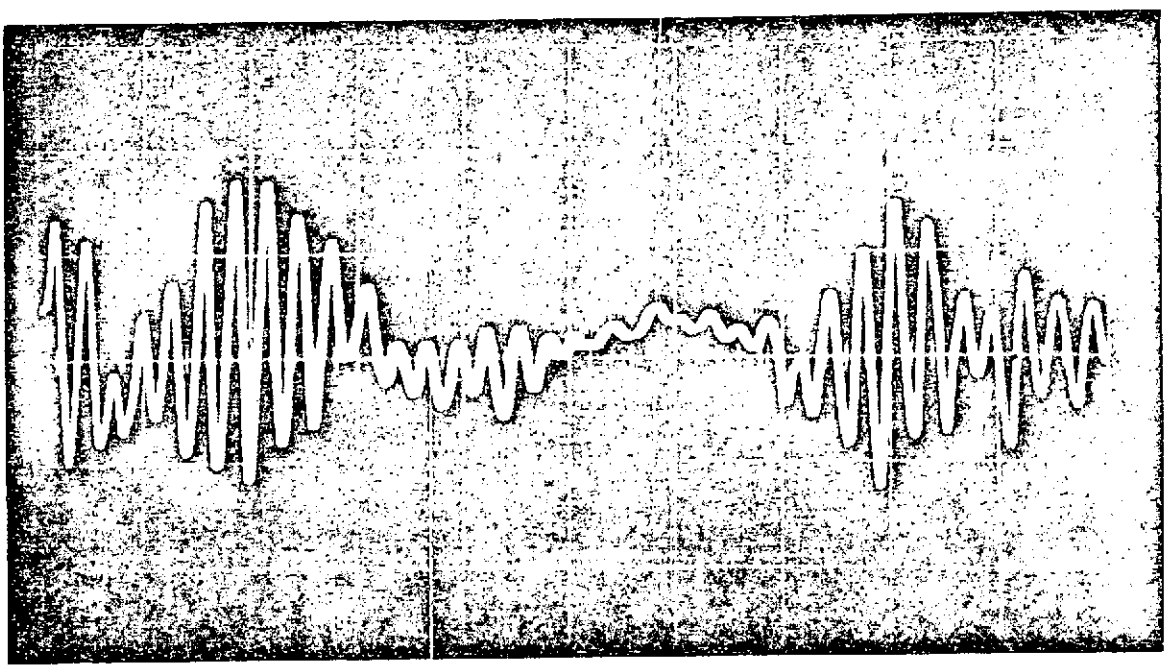

Figure 6.13 Oscilloscope Trace of Chipbreaker Acceleration Response Versus Time

forced vibration of the board. The aerodynamic noise is predominant when the machine is idling, but is usually well below the noise produced due to board vibration when material is being planed.

Aerodynamic Noise

The predominant source of noise when the machine is idling is aerodynamic noise. The mechanism of noise generation is the presence of pressure fluxuations when air is disturbed by the knives in the vicinity of stationary surfaces. Several pure-tone frequencies are usually produced and can be easily correlated with the blade passage frequencies and their harmonics. Usually only the first three harmonics are of importance in the aerodynamic noise. The expected frequencies are integral multiples of the blade passage frequency defined by

$$\text{BPF} = \text{blade passage frequency} = (\text{number of knives})(\text{RPM})/60.$$

The presence of stationary surfaces, such as feed beds and cavities can affect both the frequency and overall level of the radiated noise. The exact proportion by which the noise radiated by planers is affected by surfaces and cavities in the vicinity of the cutterhead has not been established. The idle noise spectras for cutterheads with four and six knives, shown in Figure 6.14, indicate the predominance of the frequency components associated with the blade passage frequency and harmonics.

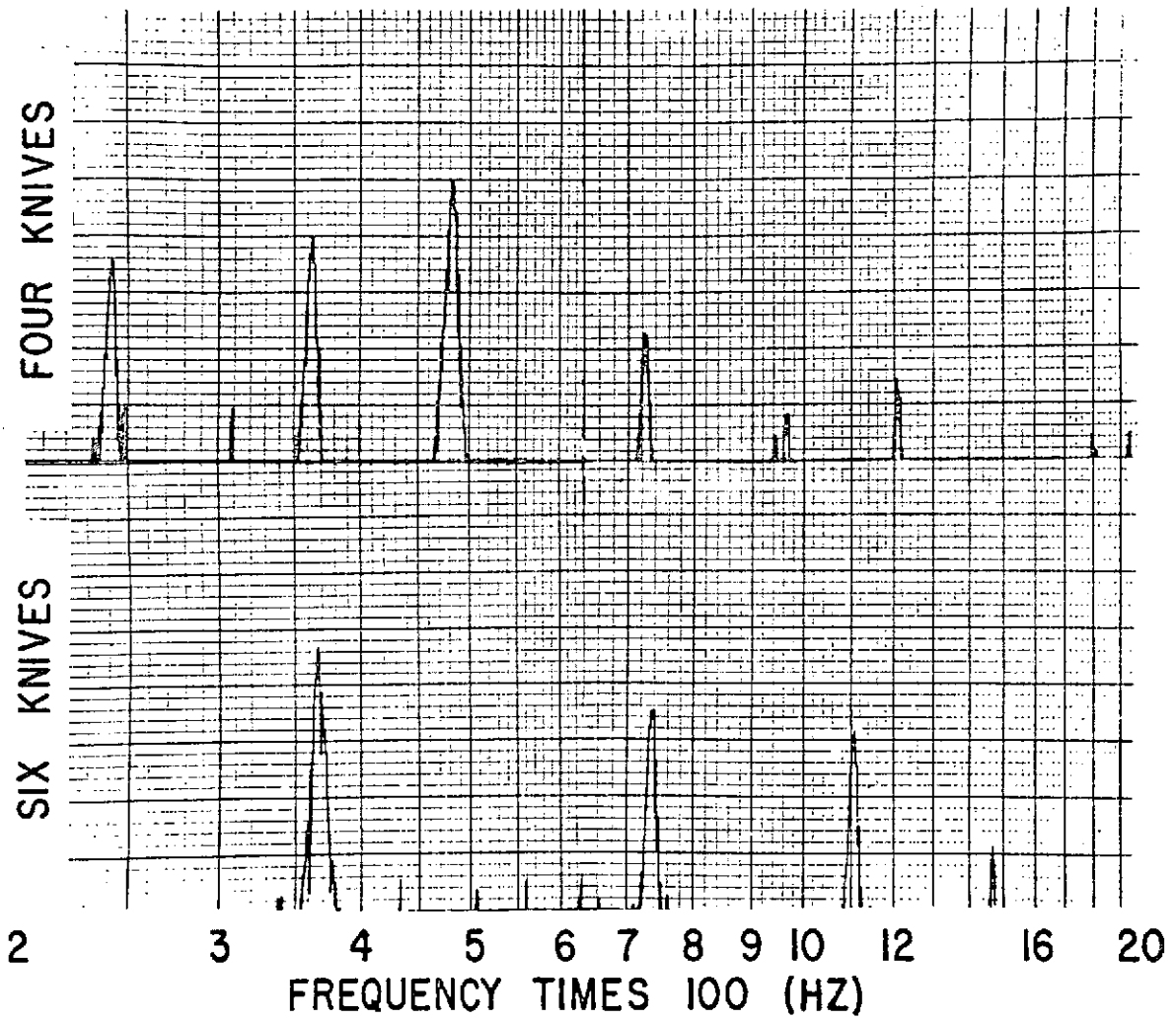

Figure 6.14 Noise Spectra for Planers Idling with Four and Six Cutterhead Knives

Board Vibration Noise

The force imparted to the board by the knives occurs also at the blade passage frequency. For straight knives this force is transmitted to the board periodically and the resulting board vibration occurs primarily at the blade passage frequency and its harmonics which are near natural frequencies of the board. Since the board is supported by the feed rollers and moves across these rollers, there are many natural frequencies associated with the board. For this reason the board responds well at the blade passage frequency and each harmonic frequency of the blade passage frequency.

A narrow band analysis of typical sound pressure level and board vibration, shown in Figures 6.15 and 6.16, indicates the presence of the expected frequency components. As indicated, there is excellent correlation between the board acceleration and the sound spectra.

6.4.11 Dust Hoods

The dust hood, in itself, is not a primary source of noise for the planer. However, if not properly isolated from the machine, vibrations can be transmitted to the hood and cause it to vibrate at or near one of its natural frequencies and thus produce sound. The construction of the standard hood does little to contain the noise produced directly over the cutterhead and in some cases, cavity resonances may contribute to the overall noise problem.

The dust hood does, however, radiate energy when struck by chips being removed from the wood. This radiation is usually of little importance in the total noise problem.

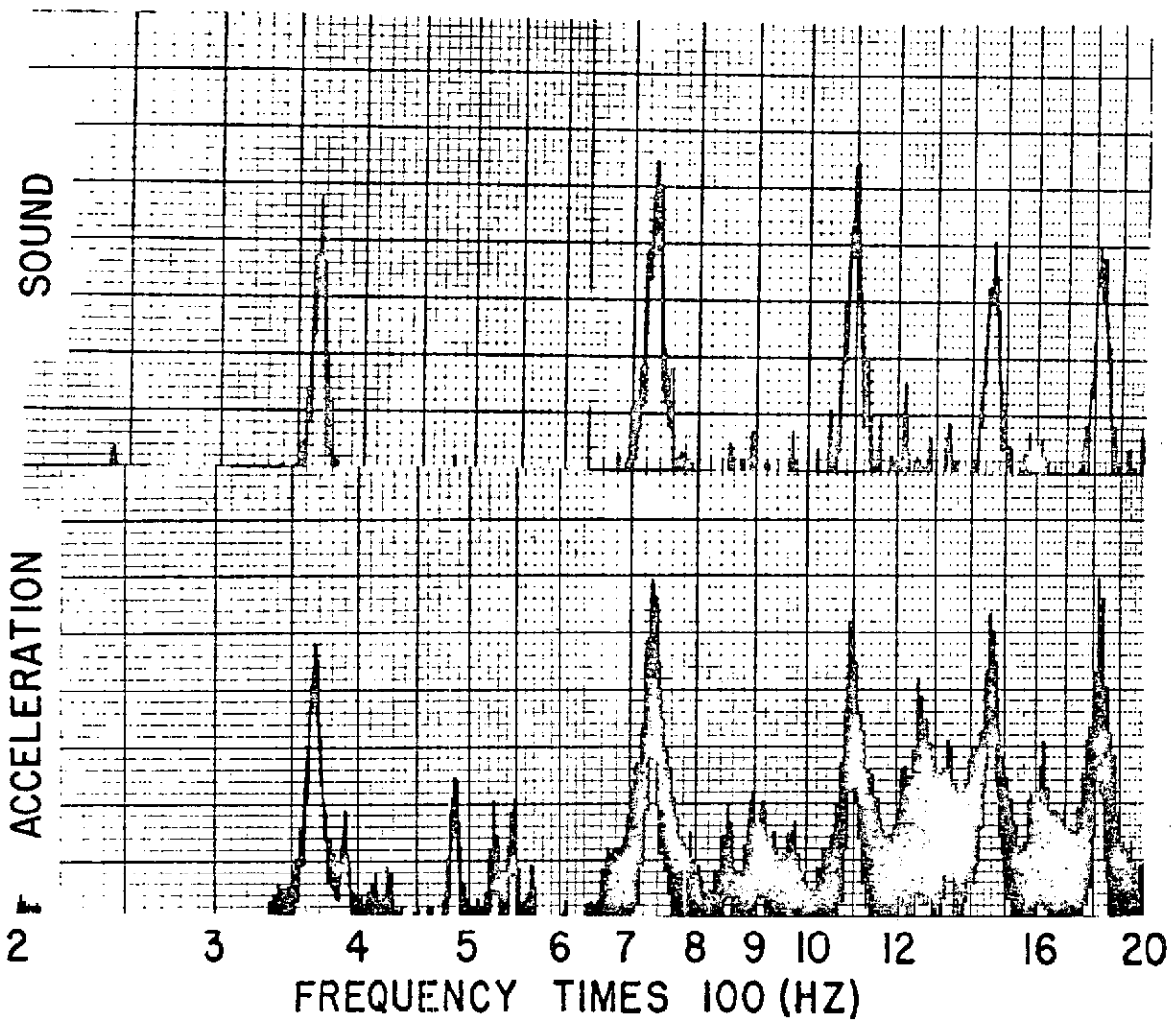

Figure 6.15 Narrow Band Comparison of Sound and Vibration for Cutterhead with Six Knives

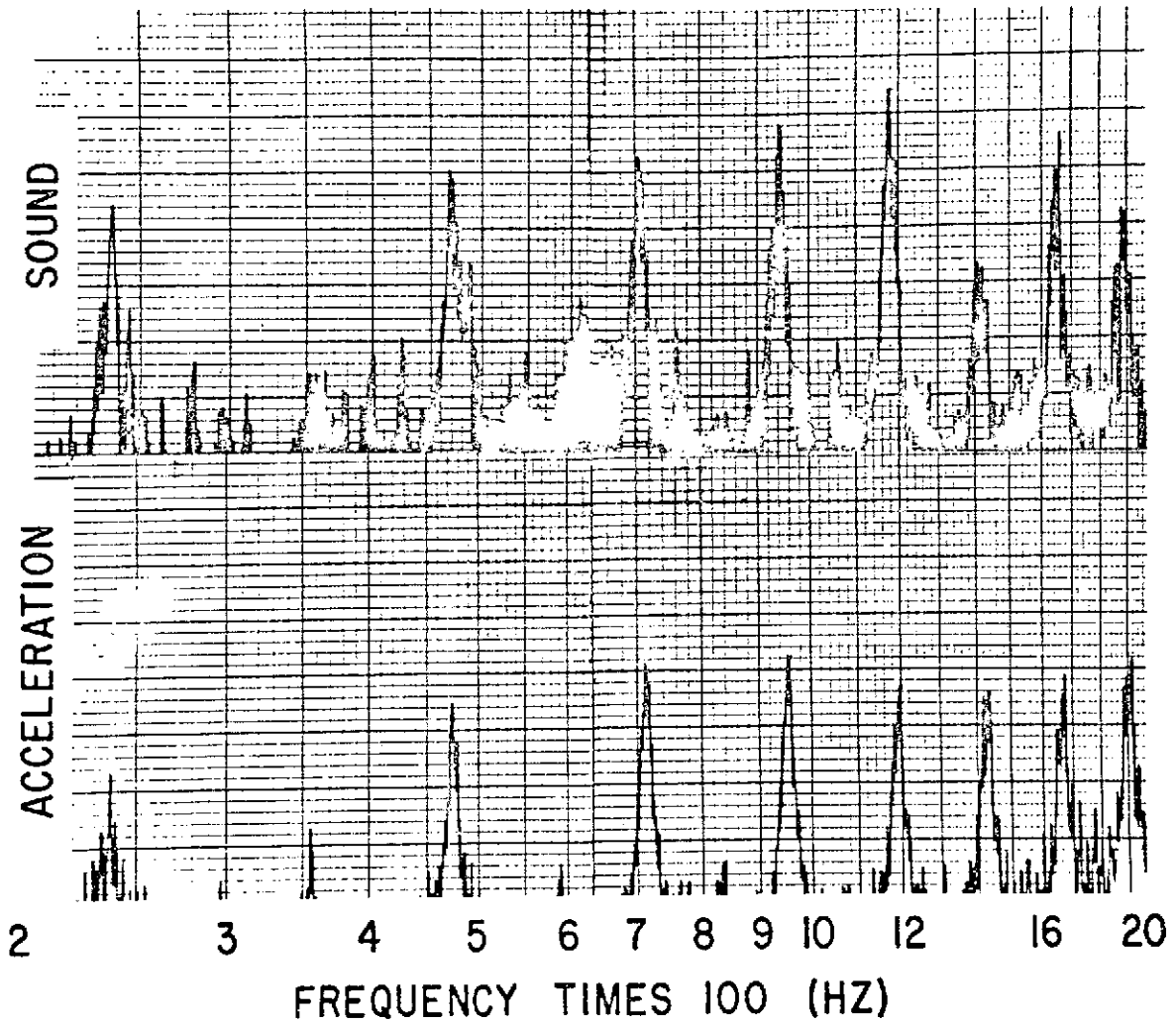

Figure 6.16 Narrow Band Comparison of Sound and Vibration for Cutterhead with Four Knives

Dust hoods could be designed to provide noise reduction by including absorption material in the construction of the hood. It is essential to point out that the hood must not be connected rigidly in any manner to the main body of the machine.

6.4.12 Electric Motors

The three basic sources of electric motor noise are given in [12] as; windage, electromagnetic field, and mechanical parts. High speed electric motors often contribute to the overall machine noise problem and, since windage noise varies approximately with the fifth power of peripheral velocity, can be a major noise source in high-speed machines. Windage noise results from (1) the fundamental fan blade frequency and other fundamental frequencies of rotating parts, and (2) broadband noise.

Broadband windage noise is characteristic of rotating electric machinery and is generally in the frequency range of 150 to 1200 Hz. It is produced by air turbulence as the machine fans circulate air through the complex path of rotor, air gap, coil end turns, stator, and enclosure.

6.4.13 Drive Train Systems

The noise produced by the drive train system associated with the machine feed works does not contribute appreciably to the overall noise problem. This source is usually less than idling or aerodynamic noise provided the machine is in good mechanical condition. The major components of the vibration spectra associated with the operation of the feed works are low frequency with a small amplitude. The feed roll

system may directly affect the noise produced by board radiation depending on the amount of vibratory energy that is absorbed or reflected by the feed rolls.

6.4.14 Machine Component Vibration

During machine operation, vibration due to blade impact is transmitted through the machine as follows:

(1) Direct transmission through the board into the anvil structure and consequently throughout the machine.

(2) Vibration transmitted directly from the board into machine components in contact with the board.

(3) Vibration transmitted back through the cutterhead and throughout the machine.

To determine the manner in which various parts of the machine respond to this transmitted vibration, an acceleration probe was conducted. The accelerometer locations and maximum rms g levels recorded are given along with an evaluation of the possible noise produced by each component.

Anvil Structure (20g)

The portion of the energy from the cutterhead that is transmitted directly through the board into the anvil is dissipated in the anvil or transmitted on to other components of the machine. The mechanisms of energy dissipation for the anvil are much the same as for the board, being internal damping and radiation. Vibration spectra of acceleration on the surface of the anvil correlate well with near field sound pressure level spectra for the area directly beneath the anvil. This

region is one of high sound intensity, resulting from the radiation of sound by both the board and the anvil. The amount of anvil radiation and frequency characteristics are dependent upon the geometry of the anvil as well as the amount of energy transmitted from the board into the anvil.

Feed Beds (2g)

Measurements taken on the surface of the feed beds indicate that the beds respond only slightly to the forcing frequency components and thus do not contribute significantly to the sound emitted.

Input Feed Roller Housing (3g)

The front housing exhibits maximum response at the lower forced harmonic frequencies (240 and 480 Hz). The structure could possibly radiate sound at the lower frequencies and should be isolated from vibration or structurally damped.

Output Feed Roller Housing (2g)

At the frequencies of 1200 Hz and 1900 Hz the housing response is maximum. Although contribution to the total sound emitted is minimal, isolation or damping could be easily effected.

Chipbreaker Mechanism (17g)

The chipbreaker responded well only at the 480 Hz and 6000 Hz frequencies. The limited area of the chipbreaker precludes sound radiation at 480 Hz, however at 6000 Hz radiation is possible. The chipbreaker, as discussed earlier, acts as a noise suppression device.

Pressure Bar (2g)

The pressure bar is quite massive with respect to its radiating area and responds at low g levels. The acceleration response is maximum at 240 Hz. Theoretically, the pressure bar maintains only line contact with the board. By increasing the area of contact with the board, the pressure bar could become effective in noise reduction.

Planer Side Housings (1g)

The right side housing (motor side) exhibits little acceleration response, the maximum being a probable resonance well above 10,000 Hz. The left housing responds well at 240 and 1200 Hz possibly radiating minimal energy.

6.5 Techniques of Noise Reduction

Possible means of noise reduction for the sources identified in Section 6.2 are presented. Special emphasis is placed on the board and anvil structure since these are major noise sources.

6.5.1 Reduction of Noise Produced as a Result of Board Vibration

(1) Physically restrain the board from vibrating. This involves firm contact over the entire surface area of the board.

(2) Cause the board to vibrate at frequencies above or below the audible range.

(3) Add structural or viscous damping to the board to reduce the portion of the energy that is dissipated as sound.

(4) Prevent the longitudinal propagation of vibratory energy along the board by utilizing vibration suppression devices near the cutterhead.

(5) Enclose the area around the radiating surfaces of the board using an acoustic absorption material.

(6) Alter the means by which vibration is induced into the board by changing the manner in which the cutting knives contact the board.

6.5.2 Reduction of Noise Produced as a Result of Anvil Vibration

(1) Physically restrain or structurally reinforce the anvil with due regard paid to the natural resonant frequencies of the anvil.

(2) Add structural damping to the anvil and isolate it from other machine components.

(3) Enclose the vicinity of the anvil using acoustic absorption materials.

6.5.3 Reduction of Noise Resulting from Other Sources

(1) Geometrically altering the cutterhead and (or) nearby surfaces so as to reduce the aerodynamic noise. An acoustic enclosure could be effective in some cases for both idle and operational noise.

(2) Reduce the noise produced by electric motors by redesign or the installation of an acoustic enclosure utilizing forced air or other means of cooling.

(3) Structurally damp and isolate feed beds and housings from other machine components.

(4) Isolate the dust hood from the machine and incorporate the hood into a partial acoustic enclosure.

6.6 Noise Control Study Areas

The three most promising techniques of major noise reduction presented in Section 6.5 from a standpoint of short range solutions

are (1) cutterhead redesign, (2) treatment of vibrating surfaces, and (3) sound absorption techniques. Each of these study areas is discussed in detail and a description of practical applications to production line wood planers is given.

6.6.1 Cutterhead Redesign

Standard cutterheads consist of a cylinder with straight knives equally spaced around the circumference. When material is planed it is acted on by a periodic force delivered by the cutterhead and is consequently set into vibration by these periodic blade impacts occurring at the blade passage frequency. If continuous blade contact with the board could be maintained, the force exerted on the board would no longer be periodic and greatly reduced vibration levels would result. The oscilloscope trace of Figure 6.13 indicates the nature of the force delivered to the board by each blade impact, i.e., the shape, period, and duration of the impact pulse produced by the knives. The oscilloscope trace is complicated by the natural frequency of the chipbreaker appearing as an oscillation imposed on the signal due to blade impact alone. The time interval between the individual pulses is governed by the number of knives and the cutterhead speed. The oscilloscope trace indicates a pulse spacing of approximately eight centimeters, thus the time interval between pulses = 8 cm times (.5) $\frac{\text{msec}}{\text{cm}}$ or 4.0 msec. The frequency of the pulses is found by converting from milliseconds to cycles per second:

$$f = \frac{1000 \frac{\text{msec}}{\text{sec}}}{4 \text{ msec}} = 250 \text{ Hz} \approx 240 \text{ Hz}$$

which is the expected pulse frequency. The pulse duration can also be obtained from Figure 6.13 by estimating the width of each pulse:

$$\text{Pulse duration} \approx 2 \text{ cm times } 0.5 \frac{\text{msec}}{\text{cm}} = 1.0 \text{ msec}$$

which indicates a 1000 Hz waveform. The resulting pulse is seen to resemble a square waveform of one millisecond duration and four milliseconds spacing. This information is useful in arriving at the proper signal to be used in experimental arrangements. The actual force delivered to the board is of the form as shown in Figure 6.17. The applied force is seen to vary with time, resulting in board vibration.

The ideal situation would be the case where the force is applied to the board in a constant manner. The time rate of change of the force would become zero and the board would no longer undergo steady state vibration. The applied force history would then be represented by Figure 6.18. Two methods by which the present situation as shown in Figure 6.17 could be changed to conform more closely with the ideal situation shown in Figure 6.18 are (1) increase the duration of the shock pulses to effectively smooth out the curve of Figure 6.17, and (2) increase the frequency at which the pulses in Figure 6.17 occur to obtain a smoother curve.

These methods may be combined to some degree to obtain a force history that approximates the ideal case of Figure 6.18. The frequency of the pulses is equivalent to the blade passage frequency and may be increased by increasing the number of knives on the cutterhead or the cutterhead RPM. The duration of the pulse shown in Figure 6.17 is

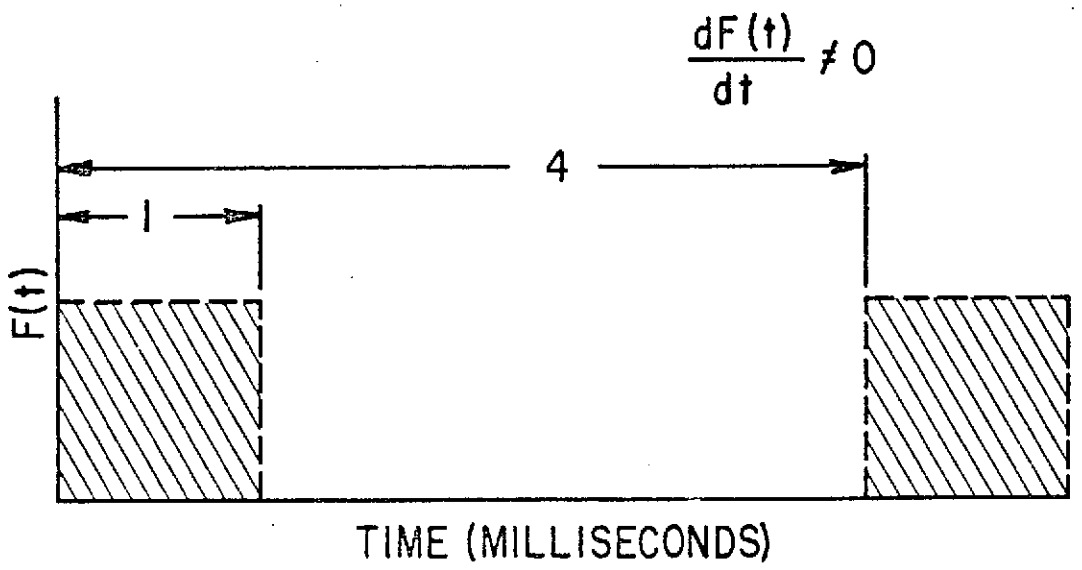

Figure 6.17 Waveform of Force Delivered to the Board for the Standard Cutterhead

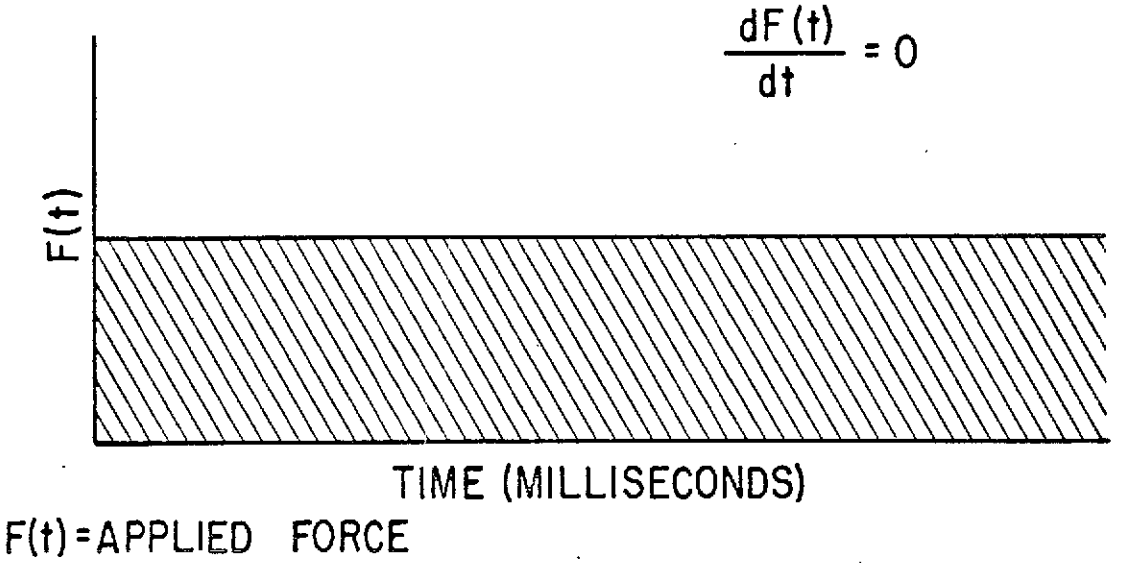

Figure 6.18 Force Delivered to the Board for the Ideal Case

governed by the time span that each blade is in contact with the board. For the special case of a helical or wound blade, blade contact with the board and thus the force input would be maintained constant. For a true helix the force-time history would be that of Figure 6.18 and the ideal case would be achieved.

A semi-helical (segmented) cutterhead, shown in Figure 6.19, consisting of several knives wrapped on the cutterhead forming partial helices, has provided significant noise reduction. This special cutterhead provides a means of more constant contact between the knives and the board. However, the machines tested utilizing the segmented heads produced sound and vibration spectra that indicated the presence of a blade passage frequency, which was due to the deviation of these heads from the ideal true helix. The improvement provided by these heads is evident in both idle (aerodynamic) noise and operating (forced board vibration) noise. Noise level reductions in the neighborhood of ten decibels are possible for machines equipped with the segmented heads. The effectiveness of a particular segmented head design has been evaluated experimentally. A comparison of noise spectra between the four blade semi-helical arrangement and the standard straight knife cutterhead, shown in Figure 6.20 indicates a reduction in the frequency components centered above 500 Hz. A similar reduction in the acceleration spectrum is also observed. The improvement obtained is due primarily to the deviation from the purely periodic excitation, resulting in reduced resonant response of the board.

Although blade impact characteristics are changed somewhat for the segmented cutterhead, a passage frequency is still evident in the noise

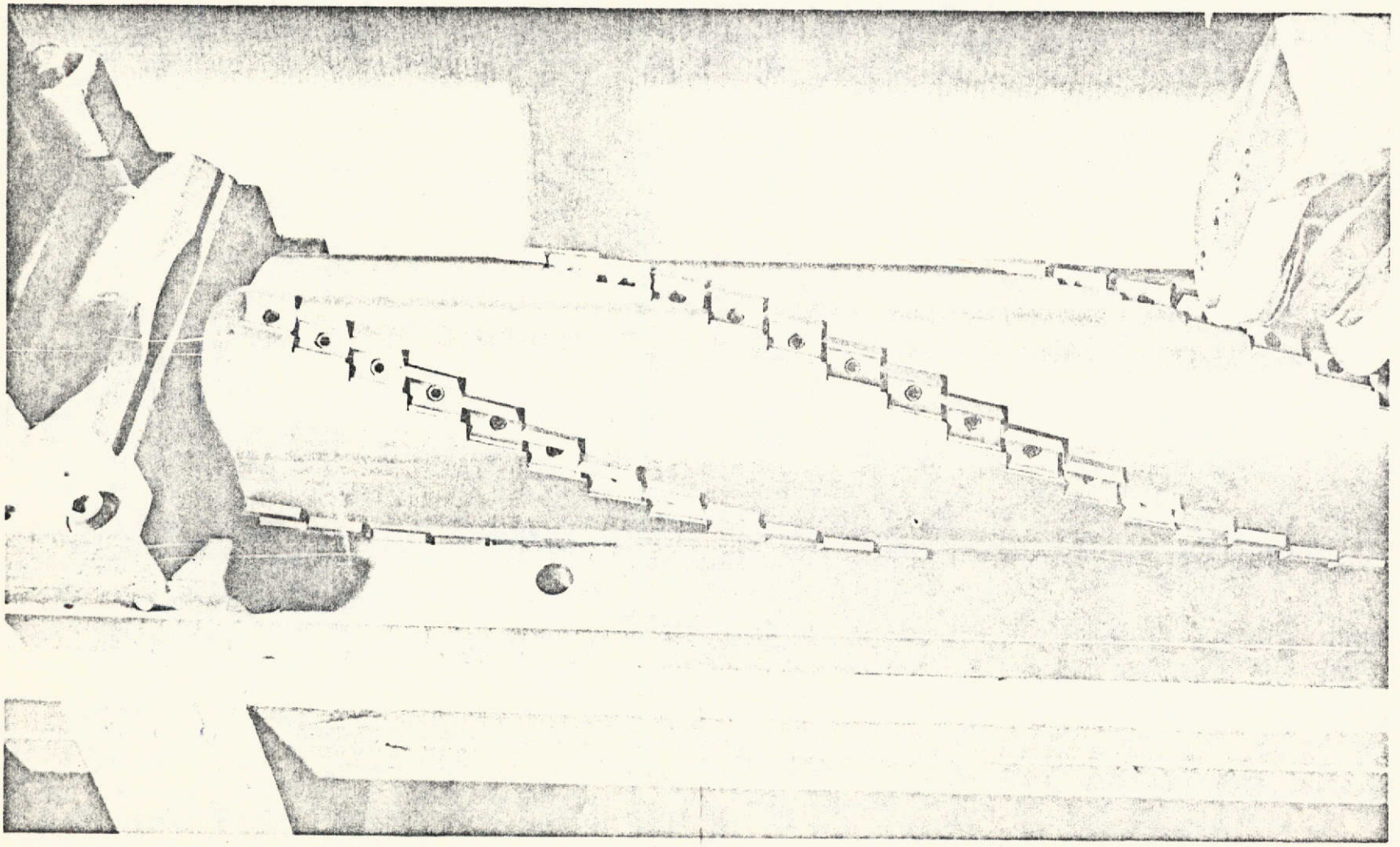

Figure 6.19 Segmented Cutterhead

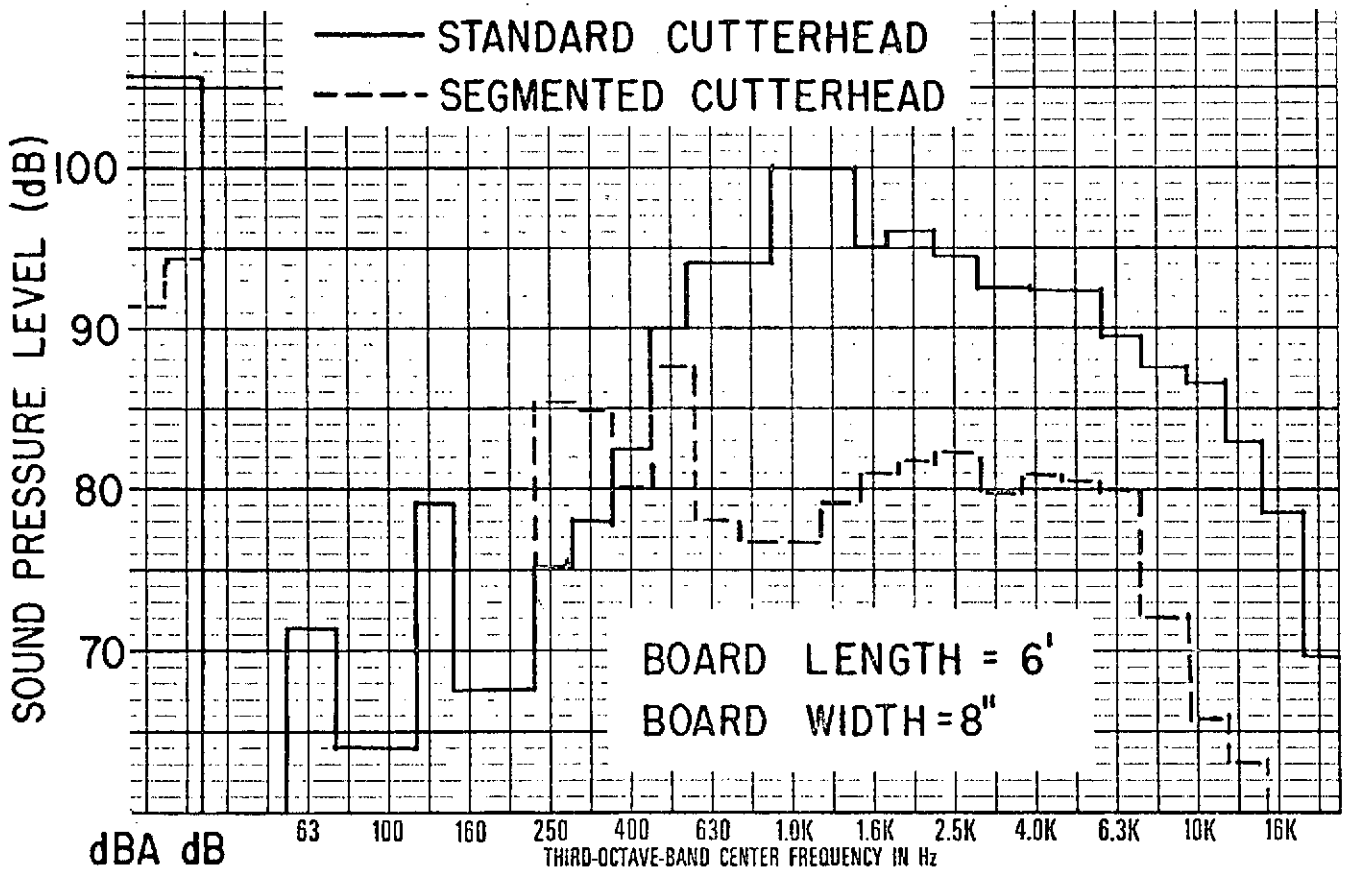

Figure 6.20 Comparison of Sound Pressure Spectra for Operation with Segmented (Helical) and Standard Cutterheads

and vibration spectra. Predominant frequencies for the four blade segmented arrangement were again 240 times n (n = 1,2,3...), since blade contact was not maintained constant over the entire width of the board. The origin of this periodic excitation is a combination of two factors, being (1) the mismatch that occurs when the individual segments are combined to form the cutterhead, representing a deviation from a true helix; and (2) the "loose" helix angle that is utilized and the resultant lack of constant contact.

6.6.2 Treatment of Vibrating Surfaces

The treatment of vibrating surfaces includes techniques for damping, absorbing, and reflecting vibratory energy. Each of these techniques have been studied experimentally.

Structural Damping

Energy dissipation through internal damping of vibrating structures is an important means of energy removal and has been experimentally investigated by (1) adhering a damping agent directly to the surface of the board and (2) applying a damping material to the surface of the feed beds and anvil structure. The addition of a damping material directly to the surface of the vibrating board was accomplished by cementing rubber strips onto the face of the board which was not being planed. The result of providing the board with an alternate means of energy dissipation was a decrease in the radiated noise levels of six to ten decibels. The significant reduction in noise level obtained by structurally damping the board indicated the dominance of board vibration as the mechanism of sound generation. The noise

reduction obtained as well as the frequency range affected by the damping is shown in Figure 6.21 which compares the noise reduction obtained for the treated board with the noise produced by an untreated board. The range of effectiveness of the damping agent (1000 to 3000 Hz) depends upon the thickness and consistency of the rubber damping material.

The effect of structural damping on board radiation led to experiments designed to determine the effectiveness of a damping layer applied directly to the anvil and feed beds to accomplish damping of the board. The addition of damping material to the feed beds and anvil resulted in only slight noise reductions at the operator position. The lack of firm contact between the board and the damping agent was primarily responsible for this limited success. Friction effects made it impractical to perform measurements on the treated side using hold-down mechanisms on the board.

Although the damping agent applied to the machine surfaces had little effect on the sound radiation in the far field, there was a substantial effect on anvil vibration. Acceleration levels were reduced from 20g for the untreated side to 4g for the treated portion, with pronounced reductions at probable anvil resonant frequencies.

Three damping agents were utilized for damping tests made on the anvil structure, the most effective and practical being the constrained layer or sandwich type. This treatment consisted of a layer of viscoelastic polymer covered by a thin sheet of steel mounted on the upper face of the anvil. Structural damping of the anvil, and possible shear type damping of the board, was achieved using the constrained layer damping.

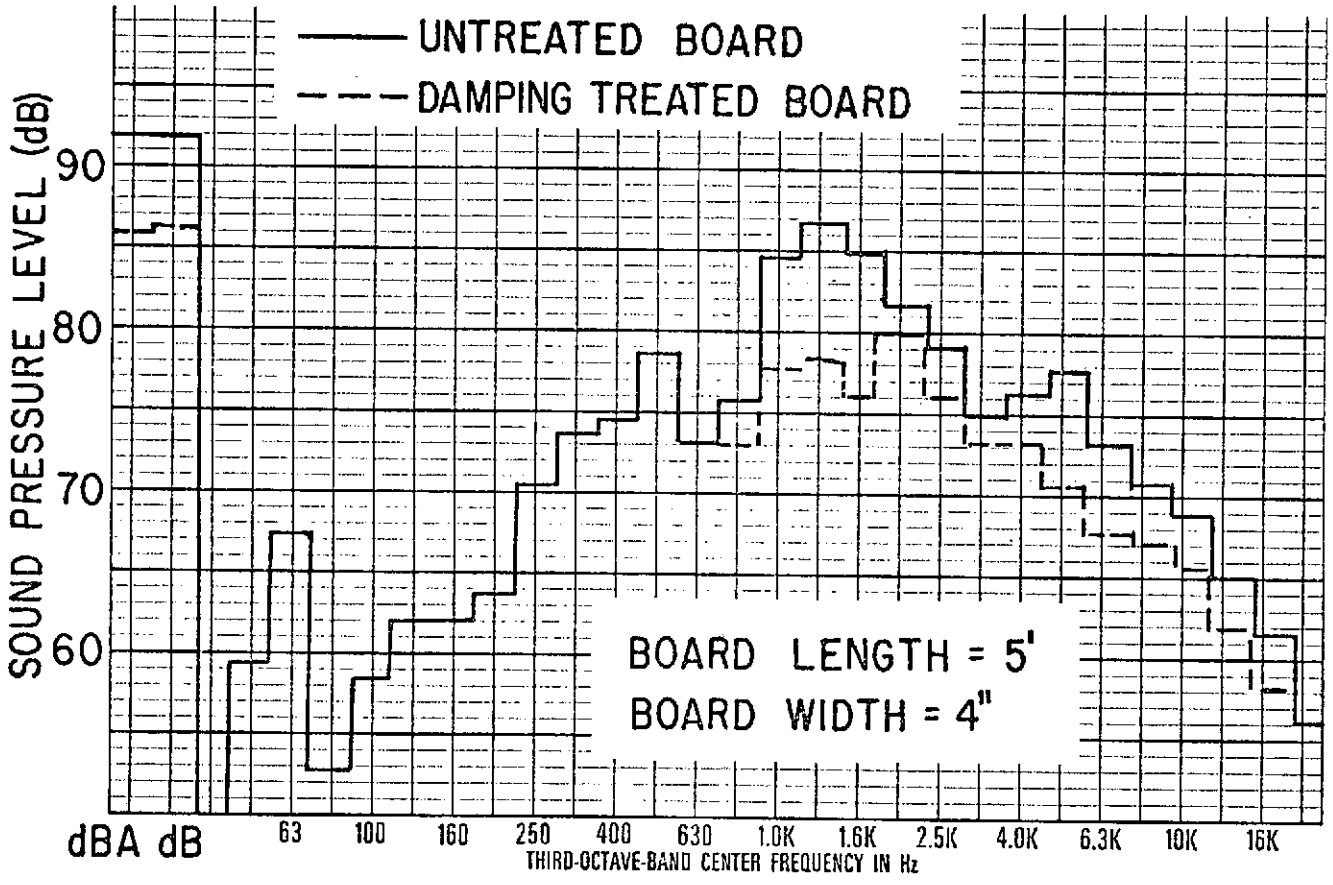

Figure 6.21 Comparison of Sound Pressure Levels for Damping Treated and Untreated Boards

The bar graph of Figure 6.22 shows the effect of each damping agent tested on the resulting anvil vibration (g) level. The neoprene and constrained layer type damping were the most effective, reducing the level approximately 15g from the untreated level. Theoretically, damping treatments are effective methods for reducing board and machine component vibration and the corresponding contribution to the total noise. Friction, excessive sensitivity to temperature, and wear problems make damping treatments difficult to apply in practice.

The effect of adding constraint mechanisms to physically restrain the board from moving (vibrating) at the point of application has been investigated. A constraint, such as a feed roller, may influence board vibration by:

(1) Acting as a simple line constraint having no effect on the magnitude of the vibration transmitted beyond it. The modes of board vibration adjust so that a nodal point situates itself at the point of constraint. A number of constraints placed along the feed beds effectively raise the frequency of vibration and thus the frequency of the sound produced.

(2) Acting as barrier to outward propagating vibration and effectively decreasing the dynamic board length. To achieve this condition a massive contact with the board is required, applied over a large area.

(3) Acting as an energy absorber at the point of contact. The chipbreaker mechanism exhibits this effect to some degree.

The conventional steel input and output feed roller mechanisms used on planers act primarily as a simple line constraint described in

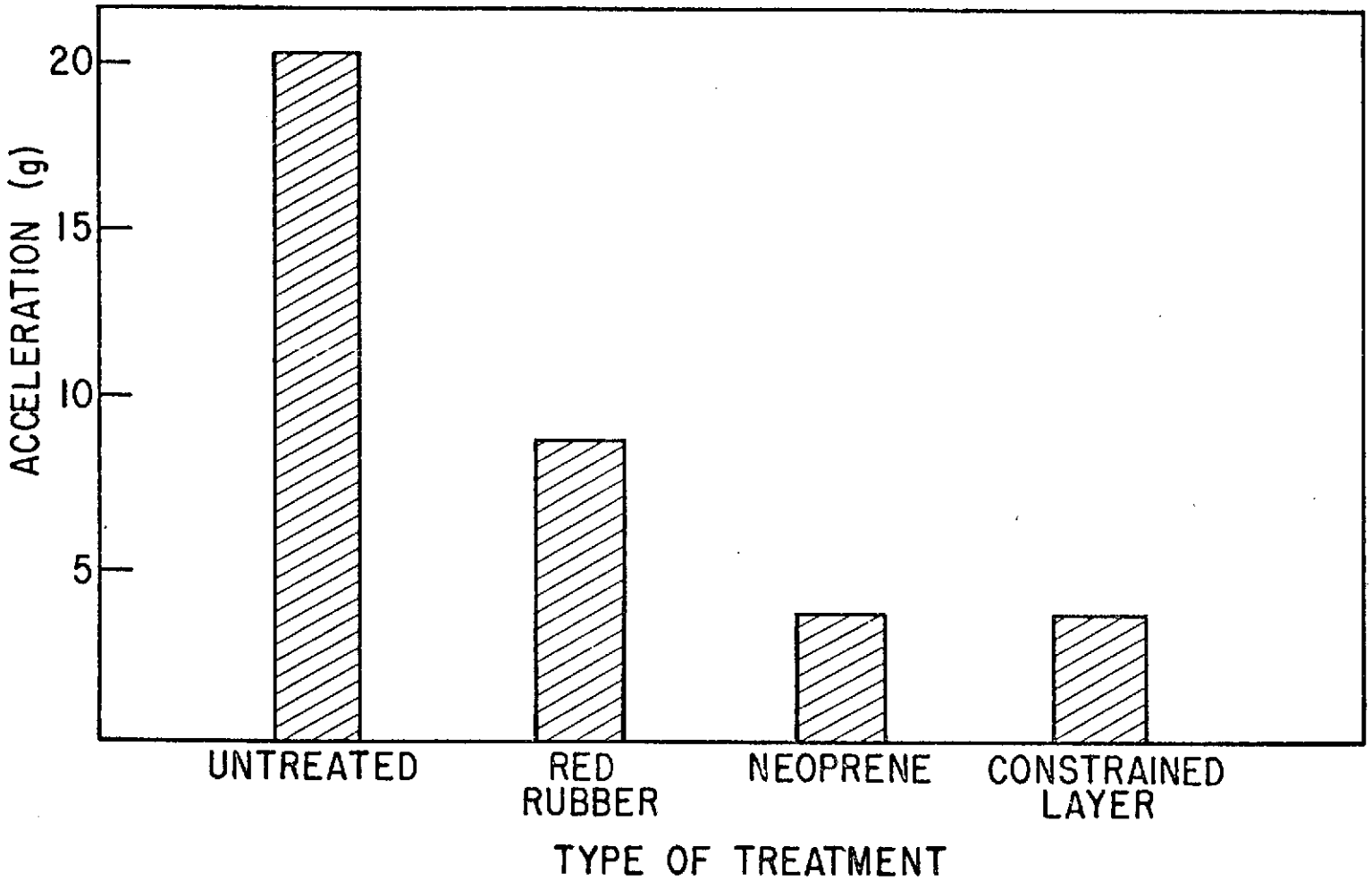

Figure 6.22 Effect of Damping Treatments on Anvil Vibration

paragraph (1). Less conventional feed rollers constructed of rubber could well exhibit the properties discussed in paragraphs (2) and (3) and be valuable in dealing with planer noise.

For experimental purposes, a foam filled rubber tire and steel plate arrangement was designed to perform the previously cited functions to some degree, i.e., tend to (1) attenuate outward propagating vibration by reflecting the vibratory waves, and (2) absorb energy by virtue of the foam filled rubber tire and thus reduce the energy dissipated as sound. With moderate force exerted, the tire deflects forming a tire flatness, which is quite effective in attenuating the spread of vibratory energy beyond the tire-plate. The tire itself also absorbs considerable vibratory energy. Sound pressure level and acceleration measurements were made on the portion of the board extending beyond a particular tire-plate suppressor. An acoustic enclosure was utilized to reduce the sound eminating from the inner portion of the board to levels well below the signal of interest. Figure 6.2, discussed previously, shows the experimental arrangement with the board being excited by a mechanical vibrator with a square wave input. The vibration insertion loss was detected by accelerometers located on either side of the tire-plate system. An 18 dB insertion loss was obtained with moderate loading of the tire and a similar 18 dB reduction in noise level was observed.

Such a tire-plate system can be easily installed on existing roughing and cabinet type planers or incorporated into the feed works. In conjunction with a moderate size acoustical enclosure, a tire-plate suppression system has reduced noise levels in excess of 15 dBA in

industrial applications. Considerable work remains to be done in this area, especially concerning the physical aspects of the tire in regard to energy absorption.

6.6.3 Acoustic Enclosures

One means of obtaining substantial noise reduction for the planer is the installation of a total or partial acoustic enclosure. For most planing operations the acoustic energy radiated is concentrated between 500 and 5000 Hz. In this frequency range, a combination of absorbing material and a housing of moderate stiffness and mass provides excellent attenuation when the source is totally enclosed. The planer, however, must have an area left open for input and output operations. Since these "holes" greatly decrease the effectiveness of an enclosure, the area of the opening must be minimized with respect to the total enclosed area for maximum enclosure benefit. The adverse effect of the opening also depends to a large degree on the frequency of the sound energy being contained and absorbed within the enclosure. A guide to the effectiveness of an enclosure that can be expected with respect to opening sizes and acoustical absorbing surface area is given by [33] and is repeated in Table 6.2.

An enclosure composed of several segments was used to evaluate the maximum noise reduction obtainable for an enclosure having minimal openings for feed purposes. The relative importance of each section of the enclosure was obtained by systematically removing and replacing various sections. Photographs of the enclosure are shown in Figure 6.23. Since the total length of the enclosure was equal to the length of the machine, the board length became increasingly important. The amount of

Table 6.2 Noise Reduction for Acoustically Lined Plywood Enclosures with Untreated Openings

Hole Area (% of Total Area)	Fiberglass Treated Area (%)	Noise Reduction (dBA) Plywood Thickness 1/2"	3/4"	1"
.1%	25%	13.0	18.0	20.0
	50%	16.0	20.0	23.0
	75%	18.0	23.0	25.0
	100%	19.5	24.0	27.0
1%	25%	10.0	14.0	14.0
	50%	13.0	17.0	17.0
	75%	15.0	18.5	18.5
	100%	17.0	20.0	20.0
5%	25%	7.0	9.0	9.0
	50%	10.0	13.0	13.0
	75%	11.5	14.0	14.0
	100%	13.0	15.0	15.0
10%	25%	5.0	5.0	5.0
	50%	8.0	8.0	8.0
	75%	9.0	9.0	9.0
	100%	10.0	10.0	10.0

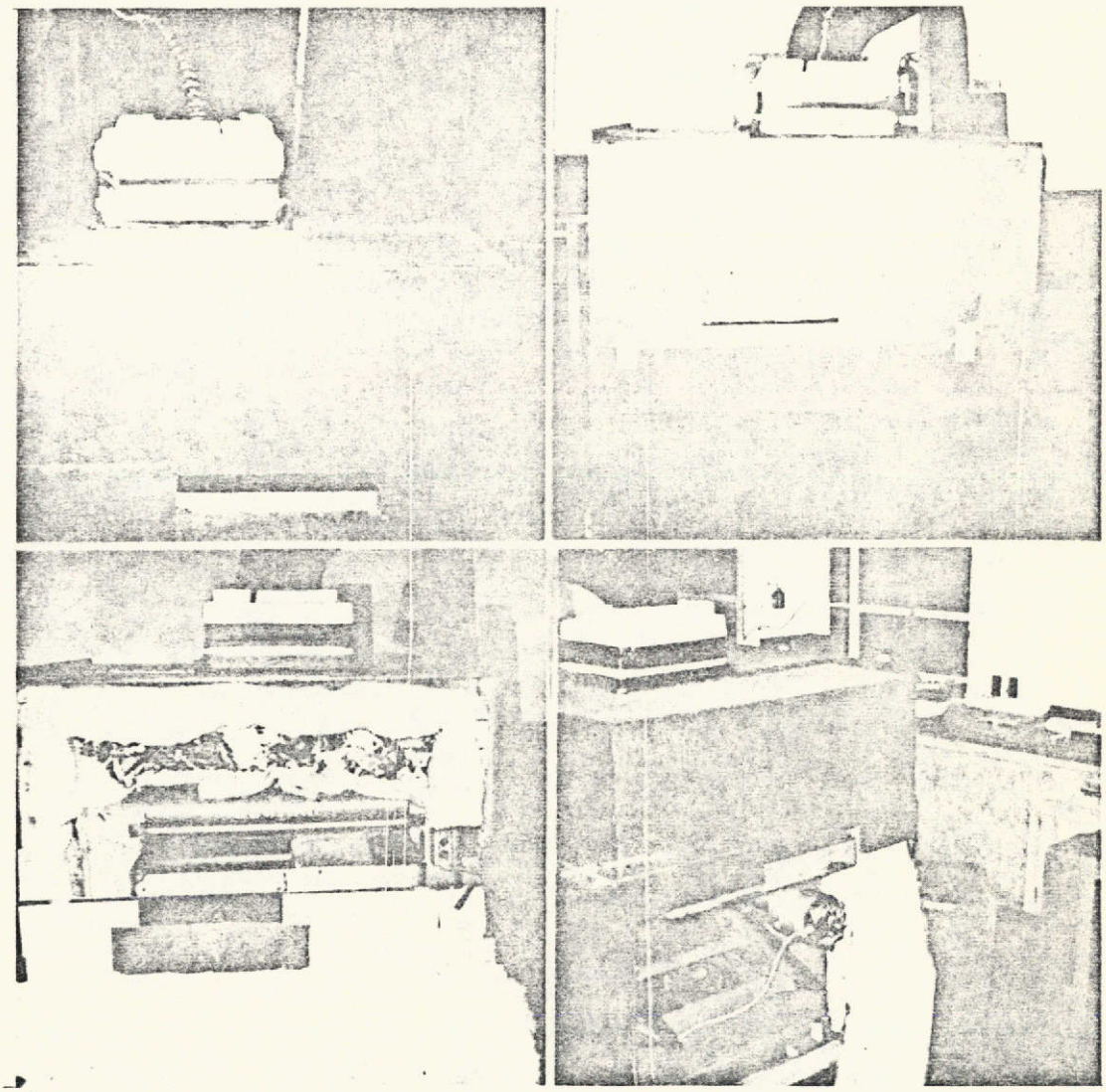

Figure 6.23 Acoustic Enclosure for Single Surfacer

absorption obtainable was dependent upon the portion of the board that was enclosed at any instant of time. Since vibrational energy spreads through the board, the noise level at the operator position is dependent upon the percentage of the board that is within the enclosure. Noise levels for boards of length less than the machine length were significantly reduced, while the reduction for longer boards was considerably less. Boards whose length exceeded the length of the enclosure produced sound levels which varied with the position of the board with respect to the enclosure. The sound levels were noted to steadily decrease as the longer boards submerged into the enclosure until the leading end of the board began to emerge from the output side of the planer.

The effectiveness of the enclosure decreases with increasing board length as shown in Figure 6.24. For boards of length greater than three feet, the noise level varied with position as indicated in Figure 6.25.

In order to evaluate the relative importance of each section of the enclosure, measurements were taken with different sections removed. Figure 6.26 shows the reduction in noise level for two and six feet long boards as the various sections of the enclosure are added. The directivity characteristics, shown in Figure 6.27, remain essentially the same for operation with and without the acoustic enclosure. Directivity characteristics, shown in Figure 6.28, for different board widths would be expected to maintain a similar relationship for operation with the acoustic enclosure.

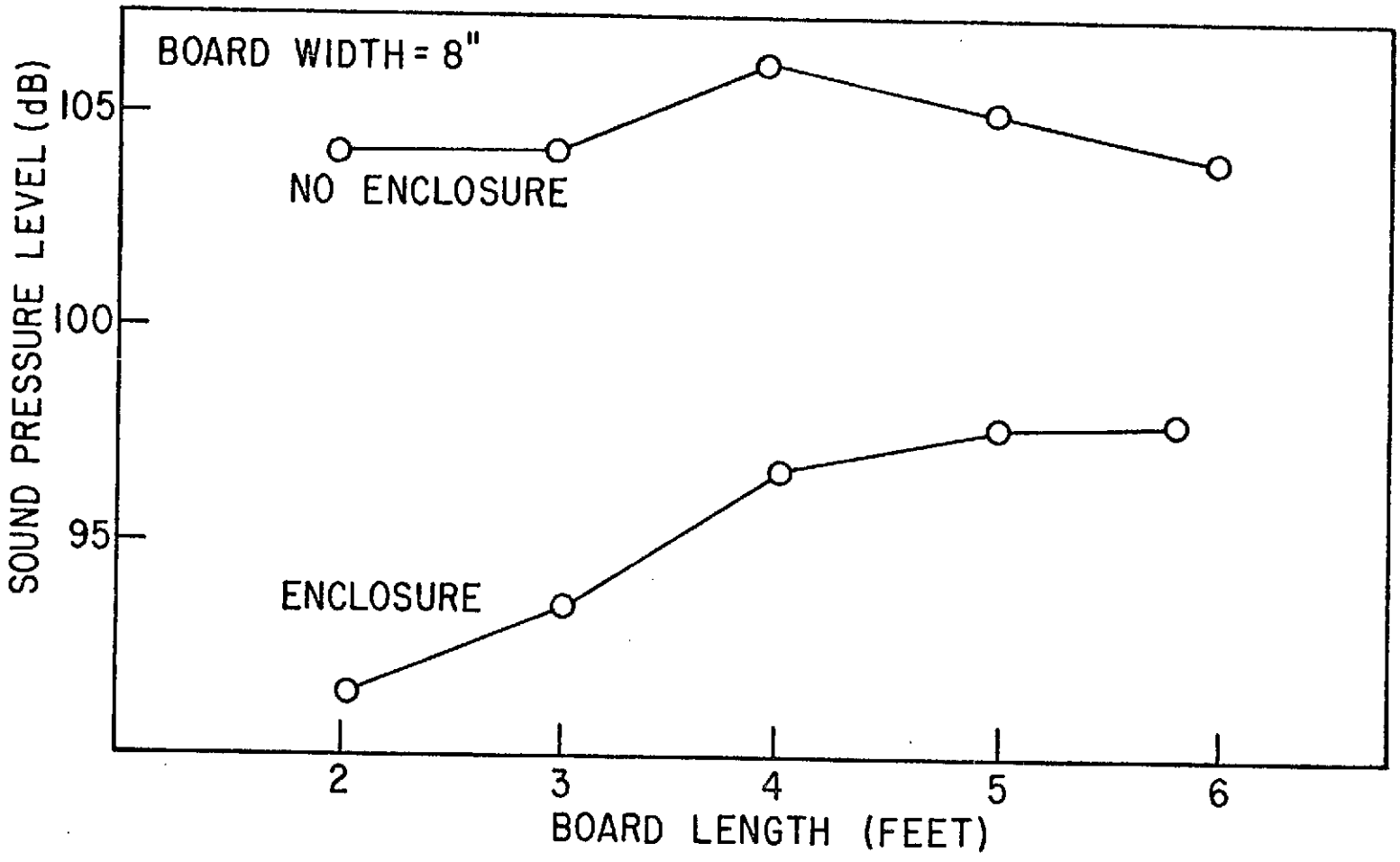

Figure 6.24 Sound Pressure Level Versus Board Length for Operation with and without an Acoustic Enclosure

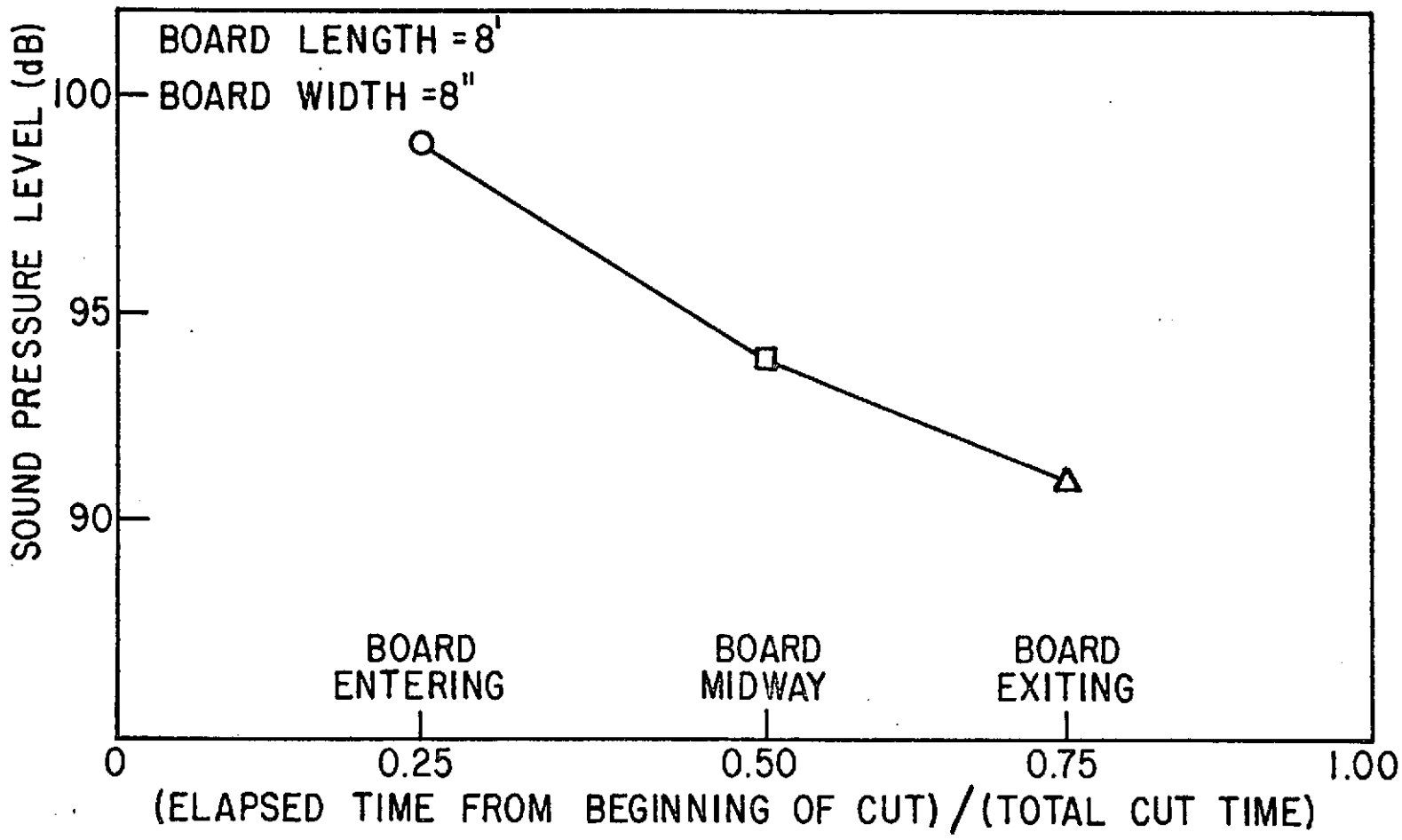

Figure 6.25 Sound Pressure Level Versus Board Position with Respect to the Enclosure

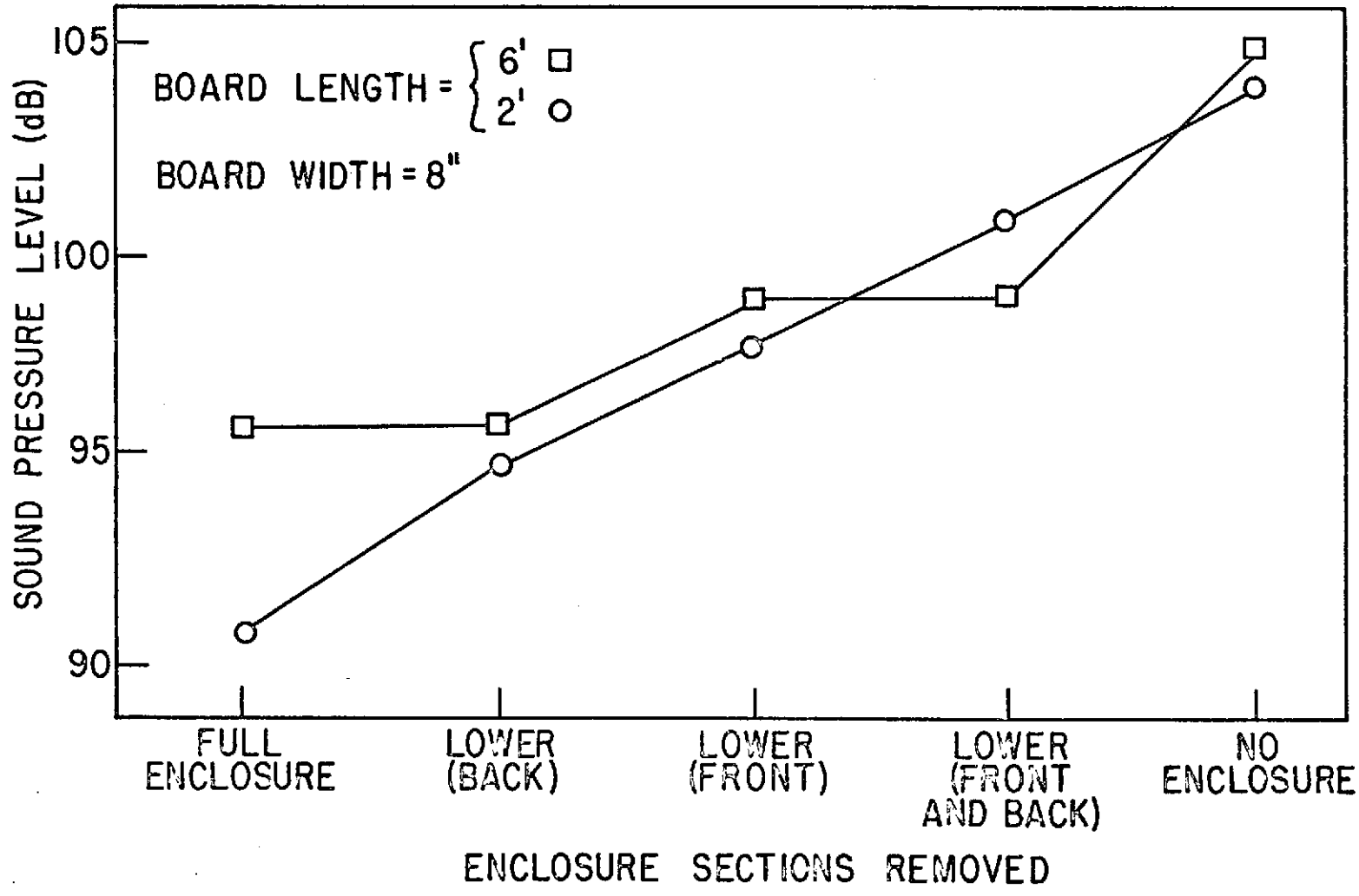

Figure 6.26 Relative Importance of Different Sections of the Acoustic Enclosure

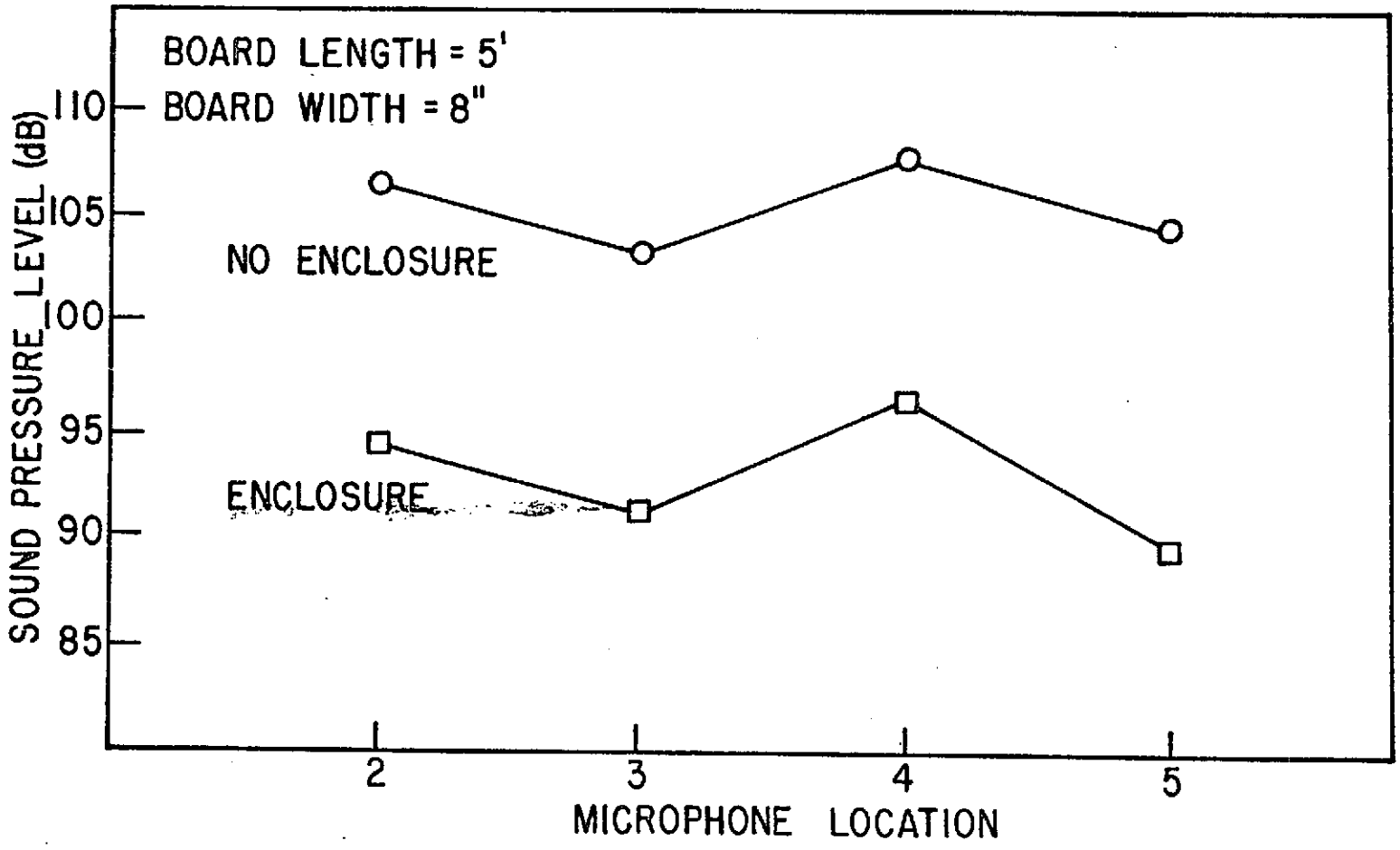

Figure 6.27 Directivity Characteristics for Operation with and without the Acoustic Enclosure

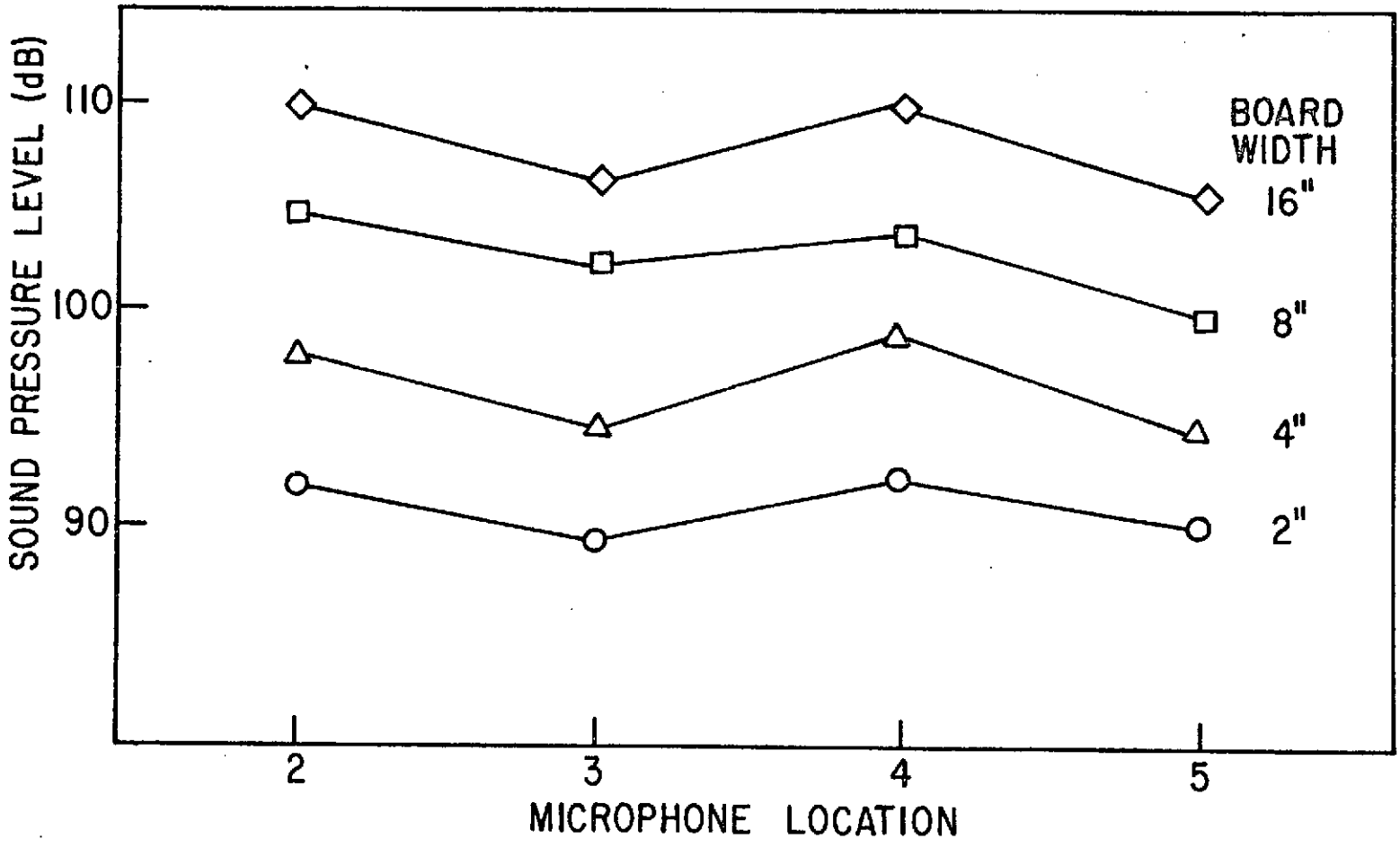

Figure 6.28 Directivity Characteristics for Different Board Widths

7. COMPARISON OF THEORETICAL AND EXPERIMENTAL RESULTS

The important result obtained in the development of a model for board vibration for the special case of a periodic forcing function was given by equation (4.50) as

$$Y(x,\omega) = \frac{2}{\rho_b \Omega \ell} \sum_{n=1}^{\infty} \frac{\sin(n\pi x/\ell)\sin(n\pi x_o/\ell)}{\omega_n^2} \left\{ \frac{1}{(1-(\omega/\omega_n)^2)^2+\delta_1^2} \right\} \cdot \sum_{j=-\infty}^{\infty} A_o(j\omega_o)\delta(\omega-j\omega_o) \quad , \tag{7.1}$$

for the response in the frequency domain. The response at each frequency ($j\omega_o$) is seen to be weighted by the frequency response function of the beam. Thus the frequency spectrum of board vibration for the planer is a discrete spectra with peaks occurring at each harmonic of the blade passage frequency with the amplitude governed by the nearness of these forced frequencies to natural resonant frequencies of the board. Figure 3.6 indicates the close agreement of the vibration spectra of the board with that predicted by equation (4.50). The excellent correlation of the sound and acceleration spectra shown in Figures 6.15 and 6.16, indicates the importance of board radiation as a noise generation mechanism as well as bearing out the theory for cutterheads having four and six knives.

The important experimental result of a six decibel increase in overall radiated sound power per doubling of board width was formulated in terms of a source strength parameter. This source strength was determined to be proportional to board width near the critical frequency

resulting in equation (6.3) for the sound power level proportionality, i.e.;

$$L_W \sim 10 \log (Q_s)^2 \sim 20 \log(W) \tag{7.2}$$

Figure 3.7 illustrated this increase along with experimental values of radiated sound power.

For frequencies near the critical frequency, where the sound radiation is concentrated, the piston model of Chapter 5 gave the sound power output as

$$\begin{aligned} L_W = {} & 10 \log_{10}(W^2) + 20 \log_{10}(f_o) \\ & + 10 \log_{10}(\ell \langle \bar{V}_o^2 \rangle) - 10 \log_{10}(f) \\ & + 10 \log_{10}(\pi \rho_a / 2P_o) \end{aligned} \tag{7.3}$$

In the immediate vicinity of the critical frequency equation (7.3) can be written in terms of the proportionality;

$$L_W(f \simeq f_c) = 20 \log_{10}(W) \tag{7.4}$$

Thus, the theoretical acoustic power produced is also observed to depend primarily on beam width and increases six decibels for each doubling of width.

The experimental values obtained for the radiated sound power level (overall), given in Figure 3.7, were obtained by measuring the

average sound pressure level over a hypothetical hemispherical surface and accounting for the particular environment in accord with [11]. The contributions to the radiated power occur at the blade passage frequency and harmonics, with the major contributions being near the critical frequency.

In Section 5.5.2 the actual radiated power for the four and eight inch beam widths was computed. Contributions from the third, fourth, fifth, and sixth harmonics were totaled to obtain the overall sound power level. These levels were then adjusted according to [11] to give the following values for the average sound pressure level at a five foot radius;

$$L_p \ (W = 4) = 101 \text{ dB}$$

$$L_p \ (W = 8) = 107 \text{ dB} \quad ,$$

which are in good agreement with the experimental results

$$L_p \ (W = 4) = 99 \text{ dB}$$

$$L_p \ (W = 8) = 105 \text{ dB} \quad ,$$

measured five feet from the machine centerline. The theoretical accuracy could be improved by obtaining an exact measure of the quantity $\ell\langle\bar{V}_o^2\rangle$ which was assumed to be unity in this example.

8. SUMMARY AND CONCLUSIONS

Several sources of planer noise have been identified, the major sources being board vibration, rotational noise, and anvil vibration. For most planers the board radiation dominates as evidenced by the six decibel increase in noise level per doubling of board width and the excellent correlation between the sound and board vibration spectra. The board length did not directly affect the radiation since the energy is distributed along the length of the board. The energy input to the board by the cutterhead is independent of board length but increases with increasing board width.

The vibration model developed in Chapter 4 is valid strictly for slender beams. The transition from a beam to a plate is generally defined to occur when $W/\ell > 1/10$. The model is valid for board widths up to about one foot, which is usually the case for roughing planers. Panels ($W/\ell > 1/10$) can be analyzed by a similar modal approach, allowing for vibration parallel as well as perpendicular to the cutterhead. Special attention was given to the case of periodic forces since this is typical of most cutterheads. The vibration model serves as a guide to cutterhead design since the relationship of the forced harmonics to the beam resonances governs sound radiation near the critical frequency. Non-periodic forcing functions obtained by shear type cutterheads can also be compared with standard heads on a vibration basis.

The radiation model developed in Chapter 5 combines the phase cell concept of structural vibration in terms of the critical frequency with the classical radiation theory for rectangular pistons. This rectangular model is simplified to a square piston in most cases. The radiated

power was given by equation (5.13) as $P_a = R_{rad} \langle \bar{V}^2 \rangle$ where the radiation resistance is dependent on the "Ka" factor, the structural area, and constants of the medium. The velocity term is a mean-square space-time average which, in a reverberant vibrational field, is assumed to have the same average properties for each piston element.

In order to represent the radiated power by equation (5.13), the modes are assumed to be excited by a random noise in a narrow bandwidth $\Delta\omega$ centered on frequency ω, and the space-time average transverse velocities of the modes within the band are assumed to be equal. The equation governing the pure-tone response of any single mode can be written as the product $(Z_m V_m)$, where Z_m is the sum of the mechanical and radiation impedances. The mechanical impedance is the impedance of the simple resonator that represents one natural mode of the structure in vacuo. In the derivation of equation (5.13) for the radiated sound power, small forces arising from internal dissipation and from sound radiation pressure that could tend to couple the response of modes were neglected.

The baffled piston radiation properties were extended in an approximate manner to apply to the case of an unbaffled piston by using an analogy with a freely suspended disk. Expressions for the radiation resistance were obtained in three frequency ranges for both baffled and unbaffled beams. The velocity term to be used in equation (7.3) was approximated using energy methods valid for reverberant fields rather than the more complex expressions of Chapter 4.

The radiation model consolidates and extends existing theory by using the radiation properties of a rectangular piston exclusively.

The important result that the major contribution to the radiated sound power is concentrated near the critical frequency for wide boards and spread out for narrower boards is apparent in the simple piston model. The piston model exhibits the important theoretical trends of the complex model of Section 5.4.3, while allowing quite simple computations of the radiated sound power.

The physical parameters such as board width, critical frequency, and board length-velocity product are easily observed from the piston model. The six decibel increase per doubling of width is explained in relation to the power controlling critical frequency. There was good agreement with experimental power measurements.

The experimental study defines the effect of various sources and parameters on the noise emitted in a manner which can be directly applied to future machine design. The major source of planer noise was determined experimentally to be board radiation caused by the periodic impact of the cutterhead knives. Board width was found to affect the sound levels by an increase of six decibels per doubling of board width, which indicates the dependence of source strength upon width.

The length of the board did not directly affect the noise levels but had a pronounced effect on vibration level. The vibration levels decreased with increasing board length indicating a spreading out of vibratory energy. Board length did, however, become quite important when an acoustic enclosure was utilized since an enclosure is effective only for that portion of the board that is contained within the enclosure. Thus, longer boards produced greater noise levels at the

operator position. For this reason enclosures of the type discussed offer only limited noise reduction, the amount depending on the size of the enclosure and the length of the boards being planed.

The most promising means of noise reduction are; (1) cutterhead redesign, (2) vibration suppression, and (3) acoustic enclosures. Each of these areas have been studied in detail and significant improvements realized.

In general there has been excellent agreement between the theoretical and experimental results. Many of the concepts developed have been tested experimentally and successfully implemented on production line machines. The progress that has been made toward understanding the mechanism of noise generation in planing operations can be extended readily to other woodworking machinery.

9. RECOMMENDATIONS

The entire vibration model and phase cell concept of board radiation can be extended to plates, which are typical of panels in the woodworking industry. This study was not pursued since the noise emission from most panels can be controlled by an enclosure in the vicinity of the cutterhead (most panels are less than four feet long).

Additional study is needed in the area of cutterhead redesign, since the exact effect of knife sharpness, helix angle, segmented knife overlap, cutterhead speed, and cutterhead geometry on operational noise levels is not known, although the results indicate that the ideal case is that of a true, tightly wound, helix.

The vibration suppression techniques have not been analyzed in detail in regard to the factors affecting the reflection, transmission, and absorption of vibratory energy. The tire system could possibly be designed to act as a dynamic vibration absorber which would absorb energy over a wide frequency range, and thus substantially reduce the noise output from the board. Modern day, high energy absorbing, polymers could possibly be used in an energy absorbing capacity, or incorporated into tire construction.

Long range study areas include such revolutionary changes as the use of laser beams to do many of the noisy and unsafe operations in the woodworking industry with a significant reduction in waste and waste products.

10. LIST OF REFERENCES

1. Barnoski, R. L. 1965. Response of Elastic Structures to Deterministic and Random Excitation. Technical Report AFFDL-TR-64-199. Air Force Flight Dynamics Laboratory, Research and Technology Division Air Force Systems Command, Wright-Patterson Air Force Base, Ohio.

2. Beranek, L. L. 1971. Noise and Vibration Control. McGraw-Hill Book Company, Inc., New York, New York.

3. Beranek, L. L. 1960. Noise Reduction. McGraw-Hill Book Company, Inc., New York, New York.

4. Bramer, T. P. C. 1969. Literature Survey: Noise Generation in Wood Planing and Moulding Machines. Contract No. KJ/4M/107/CB 78A, Technical Report No. C/C. 311 for The Ministry of Technology, Sound Research Laboratories, Eastgates Colchester, Essex.

5. Chizherskiu, M. P., and S. I. G. Shkalenko. 1968. Experiments on Noise Reduction in Planers. Derev. Prom., No. 1, pp. 26-27.

6. Churchill, R. V. 1958. Operational Mathematics. McGraw-Hill Book Company, Inc., New York, New York.

7. Cox, J. R. 1955. Quieting Wood Planers. Liberty Mutual Insurance Co., Research Center, Boston, Massachusetts.

8. Crandall, S. H., and W. D. Mark. 1963. Random Vibration. Academic Press, New York, New York.

9. Cremer, L. 1953. Calculation of Sound Propagation in Structures. Acustica, Vol. 3, No. 5, pp. 317-335.

10. Greenwood, J. H. F. 1968. Noise Reducing Enclosures for a Planer and a Moulder. Woodworking Industry, Vol. 25, No. 11, pp. 19-20.

11. Hart, F. D., and J. S. Stewart. 1971. Noise Level Prediction for Simple and Complex Sources in the Industrial Environment. Presented and published in the proceedings of the IEEE Annual Meeting, Cleveland, Ohio, pp. 731-737.

12. Hollowood, H. B. 1971. Electric Equipment Noise. Presented at the Thirty-third Annual Meeting of the American Power Conference, Chicago, Illinois.

13. Hurty, W. C., and M. F. Rubinstein. 1964. Dynamics of Structures. Prentice-Hall, Inc., Englewood Cliffs, New Jersey.

14. Johnston, R. A., and A. D. S. Barr. 1968. Acoustic and Internal Damping in Uniform Beams. Journal of Mechanical Engineering Science, Vol. 11, No. 2, pp. 117-127.

15. Kinsler, L. E., and A. R. Frey. 1962. Fundamentals of Acoustics. John Wiley and Sons, Inc., New York, New York.

16. Koch, Peter. 1964. Wood Machining Processes. The Ronald Press Company, New York, New York.

17. Kozyakov, A. F. 1966. Noise Control in Woodworking Machines. Izvestiya Vysshikh Uchebniykh Zavedeniy, Lesnoy Zhurnal, No. 12, pp. 124-129.

18. Kuleskov, L., and V. Grirkov. 1966. Influence of Knife Form on the Level of Noise while Planing. Woodworking Industry, Vol. 2, No. 5, pp. 11-12.

19. Liegman, E. 1956. Noise Research on a Planer. Holz als Roh-und Werkstoff, Vol. 14, No. 4, pp. 121-135.

20. Lyon, Richard H. 1962. Sound Radiation from a Beam Attached to a Plate. J. Acoust. Soc. of America, Vol. 34, No. 9, pp. 1265-1268.

21. Lyon, Richard H., and Gideon Maidanik. 1962. Power Flow between Linearly Coupled Oscillators. J. Acoust. Soc. of America, Vol. 34, No. 9, pp. 623-639.

22. Maidanik, Gideon. 1962. Response of Ribbed Panels to Reverberant Acoustic Fields. J. Acoust. Soc. of America, Vol. 34, No. 6, pp. 809-826.

23. Mazur, V. F., and O. K. Kurtun. 1966. Noise Production in Rotary Cutters. Derev. Prom., No. 12, pp. 34-39.

24. Morse, P. M., and K. U. Ingard. 1968. Theoretical Acoustics. McGraw-Hill Book Company, Inc., New York, New York.

25. Pahlitzsch, G. 1956. Research on Noise Formation in Wood Planing Machines. Holz als Roh-und Werkstoff, Vol. 14, No. 4, pp. 90-95.

26. Richards, E. J., and D. J. Mead. 1968. Noise and Acoustic Fatigue in Aeronautics. John Wiley and Sons, Inc., New York, New York.

27. Schmutzler, W. 1967. Noise Abatement in Woodworking. Holz als Roh-und Werkstoff, Vol. 25, No. 4, pp. 130-131.

28. Smith, J. Howard. 1971. Noise in the Woodworking Industry - A Review of the Literature. Forest Products Journal, Vol. 21, No. 9, pp. 82-83.

29. Smith, P. W., Jr. 1962. Response and Radiation of Structural Modes Excited by Sound. J. Acoust. Soc. of America, Vol. 34, No. 5, pp. 640-647.

30. Smith, P. W., Jr., and Richard H. Lyon. 1965. Sound and Structural Vibration. NASA Contractor Report CR-160, National Aeronautics and Space Administration, Washington, D. C.

31. Smith, P. W., Jr. 1964. Coupling of Sound and Panel Vibration Below the Critical Frequency. J. Acoust. Soc. of America, Vol. 36, No. 8, pp. 1516-1520.

32. Sneddon, I. N. 1951. Fourier Transforms. McGraw-Hill Book Company, Inc., New York, New York.

33. Stewart, J. S. 1972. Noise, Enclosures and the Woodworking Industry. National Hardwood Magazine, Vol. 46, No. 4, pp. 40-51.

34. Stewart, J. S., and F. D. Hart. 1972. Analysis and Control of Wood Planer Noise. Sound and Vibration, Vol. 6, No. 3, pp. 24-27.

35. Volterra, E., and E. C. Zachmanoglou. 1965. Dynamics of Vibrations. Charles E. Merrill Books, Inc., Columbus, Ohio.

36. Thomson, W. T. 1965. Vibration Theory and Applications. Prentice-Hall, Inc., Englewood Cliffs, New Jersey.

37. Thunnell, B. 1957. On Noise Problems with Woodworking Machinery. Stockholm, Sweden.

11. LIST OF SYMBOLS

A	Radiating surface area of vibrating structure
Acc.	Acceleration
A_o	Fourier coefficient in series expansion of waveform
A_r	Area of reflecting room surfaces
a	Characteristic dimension of radiator
a_o	Reference acceleration
$\langle\bar{a}\rangle$	Space-time averaged acceleration
BPF	Blade passage frequency
b	Dimension of radiator
$\bar{b}$	One-half the vector distance between monopole sources located on each piston face
C_a	Speed of sound in air
C_B	Transverse bending wave velocity
C_n	Generalized damping coefficient for the nth mode of beam vibration
c(x)	Viscous damping coefficient
d	Length of rectangular piston element
dB	Decibel
E	Modulus of elasticity
E_T	Total stored vibrational energy
F(x,t)	Beam excitation function
$F(x,\omega)$	Fourier transform of F(x,t)
$F_e\{\ \}$	Denotes Fourier transform operation
$F_e^{-1}\{\ \}$	Denotes inverse Fourier transform operation

F_R	Beam radiation loading function
f	Frequency in Hertz
f_c	Critical beam frequency
f_h	Harmonic frequencies present in excitation signal
$f_n(x)$	Mode shape of beam vibrating in the nth mode
g	Unit of measure for acceleration
g_c	Acceleration due to gravity
$H_n(\omega)$	System frequency response function
H_z	Hertz (cycles per second)
h	System response to a unit impulse
I	Area moment of inertia of beam cross section
i	$\sqrt{-1}$
J_o	Zero order Bessel function
J_1	First order Bessel function
j	Integer
K	Acoustic wave number = ω/C_a
Ka	Dimensionless product governing radiation
Kb	Dimensionless product governing radiation
K_d	Structural wave number = ω/C_B
K_n	Generalized stiffness coefficient for nth mode of beam vibration
$L_n(x,t)$	Generalized force corresponding to the nth mode of beam vibration
$L_n(x,\omega)$	Fourier transform of $L_n(x,t)$ with respect to time
L_p	Sound pressure level, referenced to 0.0002 μbar
$\bar{L}_p$	Space average of sound pressure levels

L_W	Sound power level, referenced to 10^{-13} watts
ℓ	Beam length
M	Total mass of beam
M_n	Generalized mass corresponding to the nth mode of beam vibration
mv	Millivolts
N	Number of knives on cutterhead
N_p	Number of contributing piston elements
n	Integer
P_a	Acoustic power radiated to the far field
P_o	Reference acoustic power, taken as 10^{-13} watts
$Q_n(\omega)$	Fourier transform of $q_n(t)$
Q_s	Acoustic source strength
$q_n(t)$	Generalized coordinate corresponding to the nth normal vibrational mode
R	Room constant
Re{ }	Denotes real part of quantity to be taken
RPM	Revolutions per minute
R_{rad}	Radiation resistance
r	Radius of radiating disk
S	Surface area of baffled beam = $W\ell$
S_f	System input power spectral density
S_H	Surface area of test hemisphere
S_y	System output power spectral density
T	Period of signal
t	Real time

t_b	Beam thickness
t_{bo}	Reference beam thickness
t_o	Instant of time
V	Transverse beam velocity
V_o	Reference beam velocity
$\langle \bar{V}^2 \rangle$	Mean-square transverse beam velocity
W	Width of beam or piston element
W_o	Reference width of beam or piston element
x	Coordinate along beam length
x_o	Specific position along x coordinate
$Y(x,\omega)$	Fourier transform of $y(x,t)$ with respect to time
y	Coordinate perpendicular to beam length
$y(x,t)$	Transverse displacement of beam
Z	Radiation impedance
$\bar{\alpha}$	Acoustic absorption coefficient
β	Coefficient typical of particular type of boundary conditions
δ	Dirac delta function
δ_i	Internal damping coefficient
ξ	Damping factor
ξ_n	Damping factor for the nth vibrational mode
η_a	Acoustic loss factor
η_d	Dissipation loss factor
θ_o	Radiation efficiency function for square piston
$\theta_\square$	Radiation efficiency function for rectangular piston

λ_a	Acoustic wavelength
λ_{ns}	Modal structural wavelength
λ_s	Structural wavelength
ρ	Mass density
ρ_a	Mass density of air
ρ_b	Mass density of beam
ρc	Specific acoustic impedance
σ	Radiation efficiency
τ	Time variable used in conjunction with convolution integral
Ω	Cross sectional area of beam
ω	Angular frequency
ω_n	Natural vibrational frequency
$\Delta\omega$	Small frequency increment centered on frequency ω
$(\dot{})$	Denotes differentiation with respect to time
$(\ddot{})$	Denotes second derivative with respect to time
$(\,)'$	Denotes differentiation with respect to x
$(\,)''$	Denotes second derivative with respect to x
$*$	Denotes convolution operation
$\begin{Bmatrix}1\\2\end{Bmatrix}$	Indicates the radiation resistance should be multiplied by a factor of one for the baffled radiator and a factor of two for the unbaffled radiator